AD-A184 054 LASER PROBES OF PROPELLANT COMBUSTION CHEMISTRY(U) SRI INTERNATIONAL MENLO PARK CA D R CROSLEY ET AL. AUG 87 ARO-21443.7-CH DAAG29-84-K-0092 1/2

UNCLASSIFIED F/G 21/2 NL

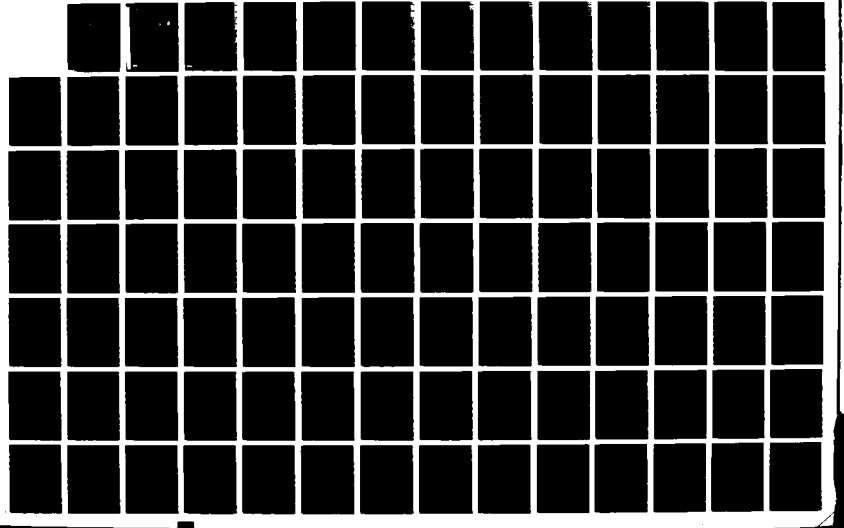

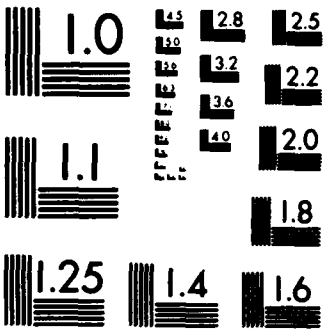

ARO 21443.7-CH

(2)

LASER PROBES OF PROPELLANT COMBUSTION CHEMISTRY

August 1987

Final Report

By: David R. Crosley, Gregory P. Smith,
and David M. Golden

Prepared for:

U.S. ARMY RESEARCH OFFICE
P.O. Box 12211
Research Triangle Park, NC 27709

Attention: Dr. Robert G. Ghirardelli

ARO Contract No. DAAG-29-84-K-0092
SRI Project PYU-7416
MP 87-207

SRI International
333 Ravenswood Avenue
Menlo Park, California 94025-3493
(415) 326-6200
TWX: 910-373-2046
Telex: 334486

SRI International

LASER PROBES OF PROPELLANT COMBUSTION CHEMISTRY

August 1987

Final Report

By: David R. Crosley, Gregory P. Smith,
and David M. Golden

Prepared for:

U.S. ARMY RESEARCH OFFICE
P.O. Box 12211
Research Triangle Park, NC 27709

Attention: Dr. Robert G. Ghirardelli

ARO Contract No. DAAG-29-84-K-0092
SRI Project PYU-7416
MP 87-207

Approved by:

D. C. Lorents, Director
Chemical Physics Laboratory

G. R. Abrahamson
Vice President
Physical Sciences Division

SRI International®

ADA184854

UNCLASSIFIED
SECURITY CLASSIFICATION OF THIS PAGE (When Data Entered)

MASTER COPY - FOR REPRODUCTION PURPOSES

REPORT DOCUMENTATION PAGE		READ INSTRUCTIONS BEFORE COMPLETING FORM
1. REPORT NUMBER: ARO 21443.7-CH	2. GOVT ACCESSION NO.: N/A	3. RECIPIENT'S CATALOG NUMBER: N/A
4. TITLE (and Subtitle): LASER PROBES OF PROPELLANT COMBUSTION CHEMISTRY		5. TYPE OF REPORT & PERIOD COVERED: Final Report 1 Jun 84 - 31 May 87
		6. PERFORMING ORG. REPORT NUMBER
7. AUTHOR(s): D. R. Crosley, G. P. Smith, and D. M. Golden		8. CONTRACT OR GRANT NUMBER(s): DAAG-29-84-K-0092
9. PERFORMING ORGANIZATION NAME AND ADDRESS: SRI International, 333 Ravenswood Avenue, Menlo Park, CA 94025		10. PROGRAM ELEMENT, PROJECT, TASK AREA & WORK UNIT NUMBERS
11. CONTROLLING OFFICE NAME AND ADDRESS: U. S. Army Research Office, Post Office Box 12211, Research Triangle Park, NC 27709		12. REPORT DATE
		13. NUMBER OF PAGES: 125
14. MONITORING AGENCY NAME & ADDRESS (if different from Controlling Office)		15. SECURITY CLASS. (of this report): Unclassified
		15a. DECLASSIFICATION/DOWNGRADING SCHEDULE

16. DISTRIBUTION STATEMENT (of this Report)

Approved for public release; distribution unlimited.

17. DISTRIBUTION STATEMENT (of the abstract entered in Block 20, if different from Report)

NA

18. SUPPLEMENTARY NOTES

The view, opinions, and/or findings contained in this report are those of the author(s) and should not be construed as an official Department of the Army position, policy, or decision, unless so designated by other documentation.

19. KEY WORDS (Continue on reverse side if necessary and identify by block number)

laser-induced fluorescence/free radicals/propellant combustion/ combustion chemistry/reaction rates/flame diagnostics

20. ABSTRACT (Continue on reverse side if necessary and identify by block number)

Laser-induced fluorescence (LIF) can be used to measure the small (diatomic and triatomic) free radicals and other transient species that are intermediates in combustion chemistry. LIF can be coupled with detailed computer models of the chemical reaction networks that incorporate a consistent set of reaction rate constants. Doing so leads to an understanding

DD FORM 1 JAN 73 1473 EDITION OF 1 NOV 65 IS OBSOLETE

UNCLASSIFIED
SECURITY CLASSIFICATION OF THIS PAGE (When Data Entered)

of that chemistry, of predictive value to describe the combustion under conditions difficult to probe experimentally. This report describes the development of LIF techniques, their applications to flames and laser/pyrolysis (LP) kinetics experiments, and rate constant estimation studies for detailed combustion chemistry modeling. The systems studied were those of hydrocarbons burning in nitrous oxide. These contain some of the chemical networks, individual reactions, and intermediate species present in the gas-phase combustion of nitramine propellants such as HMX and RDX.

Described are experiments investigating the spectroscopy of the triatomic free radical NCO in flames, and spectra and collisional quenching of NCN in a low-pressure flow system. Transition probability measurements were made on the CH free radical in flames. Also developed was a method of multiple species detection, using a single tunable laser wavelength to measure simultaneously as many as four free radicals having overlapping absorption lines but spectrally resolvable fluorescence. State-specific fine structure transfer and quenching in $3p^4D$ nitrogen atoms was investigated. Rate constant formulations for unimolecular and bimolecular chemical reactions were established, and the technique of laser pyrolysis/laser fluorescence was developed for application to controlled combustion chemical networks.

This report consists of a background description of nitramine combustion chemistry and the pertinence of free radical measurements, followed by a brief description of results in each research area. Further details can be found in the ten corresponding publications reproduced as part of the report.

CONTENTS

I INTRODUCTION

Knowledge of the detailed chemistry that occurs in a combustion process can be useful in several ways in understanding and thus controlling the system that includes that combustion. The first are those aspects in which the chemical kinetics itself dominates (e.g., ignition processes in many cases). Secondly, the effects of additives or modifiers can be understood and ultimately tailored for beneficial purposes. The third is establishing the relationship between some observable that is readily measured in a complex system (such as the emission of light in a particular spectral region) to the behavior and progress of the overall process.

To understand such details of the combustion chemistry at a microscopic level, it is necessary to measure and relate to one another the concentrations of the free radical intermediates that are formed and converted during the course of those chemical reactions. This information can be used quantitatively, by comparing with the results of a computer model of the reaction network, or qualitatively, to draw insight into the mechanism from an examination of the relative rates of appearance and disappearance of key intermediate species.

During the past six years, we have performed research, under Army Research Office support, on intermediate species and chemical reactions expected to be found in the gas phase chemistry of the combustion of nitramines. This comprises two closely related parts: the development and use of the method of laser-induced fluorescence (LIF) detection of reaction intermediates, and the formulation of chemical models and rate constant estimation techniques for the reaction networks involved. Particular focus has been given to flames of hydrocarbons and formaldehyde burning in oxides of nitrogen.

Several important findings have resulted from this research. A key early finding was the first observation of NH radicals in CH_4/N_2O flames, raising significant questions (not yet answered) about their role in the chemistry of flames in oxides of nitrogen. Quantitative experiments were refined, using

absorption measurements in atmospheric pressure burners at the Ballistic Resear.h Laboratory (BRL), where copious quantities of NCO, CN, and NH radicals were found. Part of the SRI research consisted of spectroscopic studies of NCO, NH_2, and CH in flames, including a successful search for wavelengths at which 2, 3 or 4 radicals could be detected simultaneously, a technique that could prove very useful in probes of actual propellant flames. Collisions of radicals, including the important OH molecule, have been studied for the purpose of establishing quantitative LIF measurements, at the same time yielding new insights into the dynamics of molecular collisions. Two-photon LIF detection of the oxygen and nitrogen atoms was first accomplished on this project, and has led to flame detection experiments in many laboratories including a series of experiments at BRL. Reaction rate constants needed in the modeling of combustion chemistry have been formulated and codified within a reliable theoretical framework. In particular, these studies have now resulted in the proper incorporation, into flame models, of the combined temperature and pressure dependence of reactions proceeding through bound intermediates.

In the following Background section, we describe some aspects of nitramine chemistry, indicating the potential importance of some of the reactions and species to be studied, together with some comments on how these laser probes and chemical models might be used to infer some understanding about the experimentally difficult problem of actual nitramine combustion. Next, we detail the progress made during the last three years of this project, that covered by the contract DAAG-29-84-K-0092.

II BACKGROUND: NITRAMINE COMBUSTION CHEMISTRY

The class of propellants known as nitramines (cyclic nitroorganic compounds, in particular HMX and RDX) possesses several desirable qualities, such as high energy release coupled with low vulnerability. However, they also have disadvantages, including low burn rates and marked breaks in the slopes of curves of the burn rate versus pressure. Ideally, modifiers could be added to ameliorate these undesirable characteristics without degrading the positive attributes.

The selection of possible modifications is very difficult, for the mechanisms by which the propellants ignite and burn is not well understood. The global chemical approaches useful to describe overall combustion in typical ballistic models are not helpful for detailed chemical kinetic and mechanistic questions. Part of the experimental problem is the high pressure and hostile environment under which actual propellants burn, making detailed experiments extremely difficult. For example, the distance scales involved pose special problems. The fizz (or flame) zone near the propellant surface is thought to be some tens of micrometers thick at the lowest pressures at which the propellants burn. Although this is in principle amenable to measurement by high resolution laser methods, the surface irregularities are larger than the flame thickness, in effect rendering undefinable the appropriate length scales. Consequently, information on propellant ignition and combustion mechanisms at a fundamental, molecular level must come from a variety of separate sources not entailing the direct burning of propellants under conditions found in guns.

Many experiments on actual propellants are of course, most valuable; these include final or intermediate stable product determinations by gas chromatography or molecular beam mass spectrometric sampling. In flames at lower pressure, reactive intermediates have been detected. Fitting such observations into a detailed chemical description of the gas-phase propellant combustion requires separate experiments to develop and validate the flame chemistry itself; such experiments are the subject of this proposal.

The gas-phase part of nitramine flames forms an important part of the propellant combustion. Simple chemical considerations show that the majority of the heat release occurs in the gas phase. It is this energy, fed back to the surface, that controls the initial vaporization and decomposition processes that take place in the condensed phase, on the solid (liquid) surface, or immediately below it.

Gas-phase processes are probably crucial in the ignition of the propellant, particularly when convective heating is involved. At BRL, the ignition of RDX was studied in a flow of hot nitrogen.[1] The results showed that ignition occurred in the gaseous wake, probably from reactants that formed from pyrolysis of gaseous species evolved from the solid. The flame then propagated back to the surface. In convective flow experiments at much higher temperature, ignition was also found to occur in the gas phase.[2] LIF imaging was used very recently to study ignition following laser heating of solid HMX at the Naval Weapons Center.[3] Radical species such as NH and CN were first created in the gas phase well above the solid, and then "snapped back" to the solid surface, continuing the flame.

What are the constituents of these gas-phase flames? Although many experiments have been performed on the thermal decomposition of nitramines, the results using different measurement techniques and under different conditions are often in disagreement. Schroeder[4] has reviewed the literature in this area and concludes that the point(s) of bond cleavage in the cyclic compounds are not known. Various decomposition products have been found. Early molecular beam mass spectrometric sampling methods[5,6] indicated considerable quantities of CH_2O and N_2O present in decomposition. Infrared measurements[1,7] were performed at BRL, in the wake of convectively heated but unignited RDX; these showed NO_2, N_2O, HCN and some CO_2 (CH_2O was not detectable in this experiment). Results from LCWSL[8] obtained using coherent anti-Stokes Raman scattering (CARS) in the dark zone of an atmospheric pressure flame of RDX are in partial conflict with those findings. In the flame, CO, CO_2, H_2 and HCN were found near the surface and CH_4, CH_2O and NO were observed in minor quantity. Neither NO_2 nor N_2O were observed. (However, as pointed out by Parr,[9] later unsuccessful attempts to measure NO_2 in static cells indicate this is very difficult.) Early HMX pyrolysis experiments[10] in the Department of Chemical Kinetics at SRI showed that the

molecular elimination of HONO was a major pathway. Recent experiments from this group[11] on dimethyl nitramine using an improved apparatus indicate that the nitroso compound is a major product, but formed very rapidly through secondary reactions.

In view of this array of results, it is impossible to select a single particular system that will fully mimic gas-phase ignition and combustion of nitramines. Clearly[4,11] a variety of pathways are present in the modes of decomposition, and these are likely to vary in importance with pressure and temperature. A sound description of the fundamental chemistry, validated by measurements of key intermediate species, is needed to sort out the actual situation(s) under the experimentally untractable conditions where propellants burn. In this regard, it is important to try to examine species and hypothetical mechanisms which differ upon different modes of breakup of the nitramine.

We have chosen to examine the chemistry and intermediate reactive species found in flames of hydrocarbons and mixed H-C-N-O compounds, burning in oxides of nitrogen. Flames of CH_4/N_2O and CH_2O/N_2O contain pertinent and representative species and chemical sequences; the most experimentally tractable flames in this class, they have been the subject of study in the first six years of this project. CH_4N_2O flames have also been studied at BRL and LCWSL using CARS, Raman scattering, and LIF.

Interesting questions posed by other flames studies can be addressed. Flames of $CH_4/O_2/NO_2$ have been studied recently at the University of Colorado,[12] showing many the same species (OH, NH, CN, CH and C_2) found in the N_2O-based flames studied at SRI and the Army laboratories. A two-stage flame was clearly established, and it was suggested that this was due respectively to oxidation by O_2 and later NO_2. Many of these same reactive species were found in emission (together with OH and CN using LIF) in flames of HMX burning at high pressure, in studies at the Air Force Astronautics Laboratory.[13] Two formulations of HMX were used, differing only by the amount of and type of binder. One had no dark zone; the other had a dark zone plus a much more extended reaction zone (as distinguished by CN LIF signals). Clearly, small variations in the formulation chemistry can have large effects on the mode of combustion. For a proper description, that chemistry will also have to be considered; with a large array of possible formulations, it is essential to have a sound, validated, fundamental understanding of the chemical mechanism involved.

III RESULTS

The research during the six-year overall duration of this project has been concerned with species detection and chemical reaction rates and mechanisms in flames of CH_4/N_2O and CH_2O/N_2O. In this section we describe the progress and findings thus far. A short synopsis of the work performed in the first three years (Section A) is followed by a more detailed description of that in the last three-year period (Sections B, C, and D). Reprints of articles from 1984 to present are included.

A. Results from 1981 to 1984

In early studies[14] of flames of CH_2O/N_2O at BRL, emissions from the radicals NH, CN, and NH_2 were seen, suggesting breakage of the N-N bond and a possible role for these radicals in the chemistry. Therefore, at the onset of the project, a flame of CH_4/N_2O was examined for the presence of the NH molecule in the chemically important ground state.[15] Finding it at significant levels raised new and interesting questions concerning radical chemistry in such flames. Subsequently, probes of such flames at BRL[16] showed not only NH but also CH, C_2, CN and NCO. At SRI, we studied the NCO radical in a discharge flow system, including spectroscopic and lifetime measurements.[17]

Oxygen and perhaps nitrogen atoms are also important participants in flames burning in N_2O. A new method of two-photon LIF was developed[18] to detect these species in flames and plasmas. It has since been used extensively in laboratories around the world, including a series of experiments at BRL concerned with possible photochemical effects accompanying two-photon flame diagnostics.[19]

The OH radical is unquestionably the most important reactive molecular species and is therefore the subject of most LIF flame measurements. Quantitative detection requires knowledge of collisional quenching of the electronically excited state. Measurements for several colliders in a laser pyrolysis system at ~1100 K showed for the first time that OH quenching cross

sections decrease with increasing temperature,[20] and were the first in a series of investigations of hydride quenching collisional dynamics in this laboratory.

Modeling of the isothermal high temperature chemistry of the CH_2O/N_2O system was performed, with special emphasis on understanding the origin of the NH radical. This remains unsatisfactorily explained in 1987, despite its observation in many flame systems in our laboratory and elsewhere. In such combustion chemistry models, it is necessary to have rate constant expressions valid over a wide range of temperature, including the pressure dependence for unimolecular decomposition as well as the large number of bimolecular reactions proceeding through bound intermediates. Parameterization of the rate constants within the proper theoretical framework has been an important aspect of this part of the project; during this period the reactions $H_2CO \rightarrow H + HCO$ and $N_2O \rightarrow N_2 + O$ were studied.[21]

B. Flame Species Spectroscopy

1. NCO and NH_2 visible excitation in flames. Both the NCO and NH_2 radicals are present in significant amounts in flames burning in oxides of nitrogen. They are of imputed importance in certain aspects of flame chemistry pertinent to NO_x production. These triatomic radicals, with three vibrations and (in the cases of NCO) Renner-Teller split states, have a considerably more complex laser spectroscopy than the diatomics previously studied. A comprehensive survey[22] of the LIF spectrum in a CH_4/N_2O flame, and the NH_2 molecule in NH_3/O_2 and NH_3/N_2O flames, all burning rich at one atmosphere, was made. NCO was excited in both the $A^2\Sigma^+ - X^2\Pi_i$ and $B^2\Pi_i - X^2\Pi_i$ systems; the former is much more intense and can be more easily made free of strong interfering transitions due to diatomics. NH_2 was excited in the $\tilde{A}^2A_1 - \tilde{X}^2B_1$ transition. It was found that use of excitation and fluorescence wavelengths farthest to the red minimize background interferences for this molecule.

2. Transition probabilities in CH. An experimental study[23] was made of relative intensities of different vibrational bands of the $A^2\Delta - X^2\Pi$ and $B^2\Sigma^- - X^2\Pi$ systems of the CH molecule, using LIF in atmospheric pressure methane flames. The results were compared with theoretical calculations using

Morse vibrational wavefunctions and a variety of previously computed ab initio electronic transition moments. This relatively easily detected diatomic is present in many hydrocarbon and hydrocarbon-fragment flames; although its high temperature chemistry is not yet well known, it appears to be a good candidate for LIF probing to follow combustion chemical mechanisms.

3. Spectroscopy of vibrationally excited $X^2\Pi_i$ NCO. LIF excitation spectra at 0.3 cm^{-1} resolution were performed for the A-X system of NCO in an atmospheric pressure CH_4/N_2O flame.[24] This combination of selectively detected LIF and a hot flame environment provided high resolution investigation of many levels inaccessible in conventional spectroscopy. Spin-orbit splittings, rotational and vibrational constants have been determined for ten vibrational levels. The results agree well with theoretical predictions of Renner-Teller interactions, when one takes into account Fermi resonance to explain variations in the spin-orbit splitting and rotational constants for four levels with $v_1 = 1$.

4. Multiple species flame diagnostics. We undertook a search for tunable laser wavelengths suitable for the detection of two or more radical species at the same time.[25] Understanding the chemistry of something as complex as nitramine combustion requires knowledge of the concentration of more than one reactive molecule. This is difficult in a flame whose burning varies with time, such as a propellant combusting on a strand burner. Even if two or more lasers are used in an attempt to simultaneously measure two or more species, it is very difficult to ensure that the beams will be probing the same volume in the flame. The concentrations will vary over short distances just as they will over short periods of time. In a complex, turbulent environment, effects such as beam steering exacerbate the problem.

By using one laser, however, to excite more than one radical, we can obtain relative concentrations on a single laser shot, for the exact same spatial volume within the flame. Such relative concentrations are much more meaningful indicators of the flame chemistry than ratios taken from concentrations averaged over many different conditions (i.e., from a series of laser shots, each measuring one species at a time). The idea, then, was to find wavelengths at which two or more radicals could be excited by the laser;

each species would then be distinguished by its fluorescence spectrum, which would be distinct for each molecule.

Excitation of $CH(C^2\Sigma^+)$, $NCO(X^2\Pi_i)$, $CN(B^2\Sigma^+)$, $OH(A^2\Sigma^+)$ and $NH(A^3\Pi_i)$ occurs in the wavelength region near 315 nm and was studied in flames of CH_4/N_2O. Many places were found at which pairs of these radicals could be excited. At one wavelength, 312.2 nm, an overlap among resonant transitions of OH, NH, CH and CN was found; by tuning the laser here, all four radicals could be measured simultaneously in space and time.

Several interesting collisional effects were also observed. Following laser excitation of $OH(A^2\Sigma^+)$, emission was observed from both $NH(A^3\Pi_i)$ and $CN(B^2\Sigma^+)$, and attributed to a surprisingly efficient collisional energy transfer from OH(A) to the other radicals. Collisional energy transfer from the $C^2\Sigma^+$ state of CH to its $A^2\Delta$ and $B^2\Sigma^-$ states was observed and exploited to detect CH LIF in a spectral region free from NH, OH and CN interference.

5. Quenching of nitrogen atoms. The quenching of electronically excited nitrogen atoms was studied in a low pressure discharge flow system.[26] These results were designed to provide an understanding of collisional quenching of the highly excited levels of atoms involved in two-photon LIF. N atoms in the $2p^23p\ ^4D^o$ state were prepared in a low pressure discharge flow with two-photon excitation[18] at 211 nm. Time-resolved fluorescence of the $^4D \rightarrow {}^4P$ transition at 869 nm was used to monitor the upper state population. The radiative lifetime was determined to be 43 ns, and quenching cross sections were measured for all five rare gases. There is a surprisingly large variation, going from $<0.5\text{Å}^2$ to 95Å^2 for He to Xe, respectively. This was interpreted in terms of a mechanism involving long-range attractive forces and curve-crossing in the rare gas collider.

6. LIF spectra, lifetimes and quenching of the NCN radical. The NCO radical is now known to be present in large quantity in CH_4/N_2O flames, and hence may well be of chemical signficance. The presence of other triatomic radicals such as NCN in this or other flames could also provide important signals concerning as yet unknown aspects of the combustion chemistry mechanism. LIF of NCN has been detected for the first time,[27] via the $A^3\Pi_u - X^3\Sigma_g$ transition near 329 nm. It was produced in a flow discharge in He containing a trace of

CF_4 and N_2. Excitation and fluorescence spectra and radiative lifetimes were determined for the strong 000-000 band as well as several previously unobserved, weak off-diagonal bands. (Not all spectroscopic features have been identified with certainty yet.) Quenching cross sections were obtained for 13 different colliders, and vary more than a hundredfold, from $<0.1Å^2$ for He and N_2 to $>50Å^2$ for NO, Xe and CCl_4. This cannot be correlated with an attractive forces calculation, which was relatively successful for $OH(A^2\Sigma^+)$ quenching.[20]

C. Modeling and Rate Constants for CH_4/N_2O Flames

A general approach has been developed for addressing the combined temperature and pressure dependence of hydrocarbon decomposition rate constants.[28] The procedure involves the calculation of nine parameters, which can then be easily incorporated into computer combustion models to obtain the correct rate constants for a wide variety of conditions. This approach was subsequently extended[29] to bimolecular reactions that proceed through a bound intermediate. The theoretical framework was applied to the important reactions $CH_3 + CH_3 \rightarrow C_2H_6 + H$, and in particular, to $H + N_2O \rightarrow NH + NO$ or $OH + N_2$, which may help determine the ignition behavior and extent of NO product in CH_4/N_2O combustion systems.

More recently, the formulation of rate constants for bimolecular reactions proceeding through a bound intermediate has been more fully addressed, by extending our previous RRKM and 9-parameter approach from two exit channels to a more realistic N-channel computer code. This has been applied to the reaction of H atoms with N_2O noted above.

Computer models of both flames and our laser pyrolysis-LIF experiments have been assembled and run. These proceed from the Sandia laboratory CHEMKIN code, which has been implemented on our local computer, and more recently, we have set up the Sandia flame code PREMIX on the same computer system. Our approach thus far has been to use the model to examine the chemistry, comparing with experimental results where available, but not to attempt quantitative fits to flame (or laser pyrolysis system) profiles until more of the fundamental chemistry is well established.

IV PUBLICATIONS

Journal articles supported by this contract (see Section V for reprints) are listed below.

1. G. P. Smith, "Laser pyrolysis techniques: application to catalysis, combustion diagnostics and kinetics," Proceedings of the Society of Photoinstrumention Engineers, 458, 11 (1984).
2. C. W. Larson, R. Patrick and D. M. Golden, "Pressure and temperature dependence of unimolecular bond fission reactions: an approach for combustion modellers," Combustion and Flame 58, 229 (1984).
3. R. A. Copeland and D. R. Crosley, "Spin-orbit splittings and rotational constants for vibrationally excited levels of NCO($X^2\Pi_i$)," Canadian Journal of Physics 62, 1488 (1984).
4. N. L. Garland and D. R. Crosley, "Relative transition probability measurements in the A-X and B-X systems of CH," Journal of Quantitative Spectroscopy and Radiative Transfer 31, 591 (1985).
5. D. M. Golden and C. W. Larson, "Rate constants for use in modelling," Twentieth Symposium (International) on Combustion, The Combustion Institute, Pittsburgh, 1985, p. 595.
6. R. A. Copeland, D. R. Crosley and G. P. Smith, "Laser-induced fluorescence spectroscopy of NCO and NH_2 in atmospheric pressure flames," Twentieth Symposium (International) on Combustion, The Combustion Institute, Pittsburgh, 1985, p. 1195.
7. R. A. Copeland, D. R. Crosley and J. B. Jeffries, "State-specific collision dynamics of OH radicals and N atoms," American Institute of Physics Conference Proceedings 146, 545 (1986).
8. D. R. Crosley, "Laser-induced fluorescence measurement of combustion chemistry intermediates," High Temperature Materials and Processes 7, 41 (1986).
9. R. A. Copeland, J. B. Jeffries, A. P. Hickman and D. R. Crosley, "Radiative lifetime and quenching of the 3p $^4D^o$ state of atomic nitrogen," Journal of Chemical Physics 86, 4876 (1987).

10. J. B. Jeffries, R. A. Copeland, G. P. Smith and D. R. Crosley, "Multiple species laser-induced fluorescence in flames," Twenty-First Symposium (International) on Combustion, The Combustion Institute, Pittsburgh, 1987, in press.

Conference presentations (published abstracts) supported by this contract include the following:

1. N. L. Garland and D. R. Crosley, "Energy transfer pathways for CH $A^2\Delta$ in atmospheric pressure flames," Paper WG'2, Symposium on Molecular Spectroscopy, Columbus, Ohio, June 1984.
2. R. A. Copeland and D. R. Crosley, "Laser-induced fluorescence measurement of spin-orbit splittings in excited vibrational levels of NCO($X^2\Pi_i$)," Paper RF5, Symposium on Molecular Spectroscopy, Columbus, Ohio, June 1984.
3. R. A. Copeland, D. R. Crosley and G. P. Smith, "Laser-induced fluorescence spectrocopy of NCO and NH_2 in atmospheric pressure flames," Twentieth Symposium (International) on Combustion, Ann Arbor, Michigan, August 1984.
4. D. M. Golden and C. W. Larson, "Rate constants for use in modelling," Twentieth Symposium (International) on Combustion, Ann Arbor, Michigan, August 1984.
5. N. L. Garland and D. R. Crosley, "Energy transfer processes in CH $A^2\Delta$ and $B^2\Sigma^-$ in an atmospheric pressure flame," Paper 84-61, Western States Meeting of the Combustion Institute, Stanford, California, October 1984.
6. D. R. Crosley, "Collisional quenching of electronically excited diatomic radicals," American Chemical Society Meeting, Chicago, Illinois, September 1985.
7. R. A. Copeland, J. B. Jeffries and D. R. Crosley, "Collision dynamics of the $^4D^o$ nitrogen atom," Meeting of the Division of Atomic, Molecular and Optical Physics, Eugene, Oregon, June 1986 [Bull. Amer. Phys. Soc. 31, 939 (1986)].
8. D. R. Crosley, "Laser-induced fluorescence measurement of free radical intermediates," XVII Informal Conference on Photochemistry, Boulder, Colorado, June 1986.

9. J. B. Jeffries, R. A. Copeland, G. P. Smith and D. R. Crosley, "Multiple species laser-induced fluorescence in flames," Twenty-First Symposium (International) on Combustion, Munich, Germany, August 1986.
10. J. B. Jeffries, R. A. Copeland, A. P. Hickman and D. R. Crosley, "Collisions of nitrogen atoms in the 3p ^{4}D state," American Physical Society Meeting, New York, New York, March 1987 [Bull. Amer. Phys. Soc. 32, 736 (1987)].
11. G. P. Smith, R. A. Copeland and D. R. Crosley, "Electronic quenching and energy transfer of the triatomic radical NCN ($A^3\Pi_u$)," Conference on the Dynamics of Molecular Collisions, Wheeling, West Virginia, July 1987.
12. J. B. Jeffries and D. R. Crosley, "Collisional quencing of diatomic hydride radicals," Symposium on Chemistry and Photophysics of Energetic Materials, Los Angeles, California, September 1987.
13. G. P. Smith, R. A. Copeland and D. R. Crosley, "Electronic quenching and energy transfer of the triatomic radical NCN ($A^3\Pi_u$)," Third International Laser Science Conference, Atlantic City, New Jersey, November 1987.

V REPRINTS

Reprinted from SPIE Vol. 458—Applications of Lasers to Industrial Chemistry

Laser pyrolysis techniques: Application to catalysis, combustion diagnostics, and kinetics

Gregory P. Smith

Department of Chemical Kinetics, Molecular Physics Laboratory
SRI International, Menlo Park, California 94025

Abstract

A pulsed laser pyrolysis method has been developed to study kinetic processes at high temperatures. A CO_2 laser is used to irradiate a 100 torr mixture of an infrared absorber (SF_6), bath gas (N_2), and reactants. Rapid heating to 700-1400 K occurs, followed by two-stage coooling. Unimolecular reactions are studied by competitive kinetics with a known standard, using mass-spectrometric or gas-chromatographic analysis. Bimolecular processes are examined using laser-induced fluorescence (LIF). The technique offers great advantages in reaching reactive temperatures in a fast and time-resolved manner, without the complications of hot surfaces. It is thus an ideal tool for analyzing and measuring some of the basic processes occurring in more complicated, real, hot systems. Our recent applications of the laser pyrolysis method in the areas of catalysis and combustion are summarized here. Several transition metal-carbonyl bond dissociation energies have been measured, and catalysis by the hot metal particulate products was observed. Since the use of LIF as a flame diagnotic requires some knowledge of the fluorescence quenching rates at high temperatures, the laser pyrolysis method was used to measure these rates for the important OH radical. Its reaction rate with acetylene was also measured, with implications for flame modeling and the mechanism of soot formation. Finally, this method can be used to ignite low concentrations of fuel and oxidant, and then study the time-resolved evolution of the flame chemistry by LIF and chemiluminescence observations.

Introduction

Most chemical processes are accomplished by the application of heat, whether they involve synthesis, catalysis, materials processing, or combustion. Applied externally or internally, this heating is gradual and continuous, and most often involves contact of the system with hot surfaces. The use of a pulsed laser as a heat source offers several advantages: it is localized and controlled; surfaces may be kept cold to avoid unwanted catalytic complications; rapid heating to a high temperature is possible, permitting the use of a high energy chemical pathway without losing the reactants to lower energy products during heating; and the timing of the process is well defined and controllable. Laser welding and surgery are practical examples. We have helped develop a new technique for rapidly heating gas mixtures up to 1500 K using a pulsed infrared CO_2 laser. Many applications of this method relating to chemical synthesis production of solids and generation of catalysts remain to be explored. Assessments of practical applications are still premature. The laser pyrolysis method has to date proven to be an excellent analytical tool for determining the chemistry occurring in more complex systems. In addition to presenting the basic technique for further consideration, several experimental results will be described. These directed basic research efforts include: a study of organometallic bond energies and the catalytic activity of the hot aerosol of metallic particulates created by laser pyrolysis; an examination of fluorescence quenching at high temperatures to permit more quantitative use of laser-induced fluorescence as a remote analytical diagnostic in varied environments; and the determination of high temperature reaction pathways and ignition chemistry.

The pulsed laser pyrolysis technique

A full, detailed description of the method, which was first proposed by Shaub and Bauer,[1] is published elsewhere.[2] This includes the chemical, physical, and computational diagnostics which have aided and substantiated our understanding of the technique. A schematic of the apparatus is given in Figure 1. A gas mixture at 30-100 torr containing SF_6, bath gas M (usually nitrogen), and small amounts of the chosen reactant molecules R flows through a 1-cm thick cell with KCl windows. The mixture is irradiated by a uniform 1-cm diameter portion of a pulsed-CO_2 laser beam at 10.6 μm. The SF_6 absorbs the infrared radiation, and by energy-transfer collisions with the bath gas, the entire irradiated volume of gas is heated to a true and elevated temperature in a few microseconds. The temperature reached depends upon the laser power and the fraction of SF_6 (2-10% for our 2 J/cm^2 laser and 20-100% for our 1 J/cm^2 laser). A mirror reflects the laser beam back through the same volume to insure even heating across the thin cell despite 30% total absorbances. Temperatures are currently limited to roughly 1500 K by thermal SF_6 decomposition, but in theory, more stable sensitizers should allow hotter operation. Two modes of detection are possible. Product and reactant concentrations can be sampled from the flow beyond the cell by mass

spectrometer or gas chromatograph. Real time optical detection can be accomplished through a monochromator with photomultiplier tube, coupled to a boxcar integrator and recorder. This system can measure chemiluminescence, or by adding a dye laser can measure ground state radical concentrations via laser-induced fluorescence. A variable time delay between the CO_2 and dye lasers permits the probing of radical concentrations as a function of time. By scanning the laser through various lines, rotational level populations of the ground-state radical, and thus the temperature, can be determined. As shown in Figure 1, the two lasers and monochomator are mutually perpendicular, providing spatially-resolved detection.

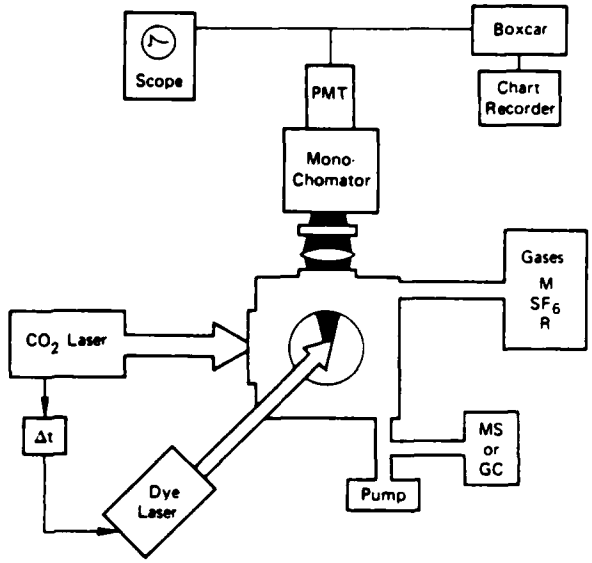

Figure 1. Schematic of laser pyrolysis apparatus

Consideration of the gas dynamics involved is necessary to understand and quantify the chemistry occurring under laser pyrolysis conditions. The initially heated volume, now at a higher pressure than the surrounding gas, will expand against this gas and slightly compress it. This is accomplished by an expansion wave propagating inward to the center and then outward again at the local speed of sound. Concurrently, a compression wave moves outward. Once the expansion is finished, the pressure is equal across the hot and cool region boundary at roughly its initial value, the hot region has cooled typically several hundred degrees from T to T' ($T'/300 \sim (T/300)^{1/\gamma}$), where γ is the heat capacity ratio), and the heated volume has expanded considerably by ~ T'/300. This cooling takes ~ 15 μs for our geometry. The above values then stay relatively steady for longer time periods, since further cooling only occurs slowly by thermal conductivity across the interface between heated and unheated regions (~ 1K/μs). Meanwhile, the outward-going compression wave, followed by the expansion wave, produces negligible heating. If allowed to reflect off the walls of a small and symmetrical cell, however, it can reheat the irradiated region, and thus complicate the kinetics. High activation energy unimolecular decomposition reactions will occur during the hottest, short, initial time-period before expansion cooling. Low activation energy bimolecular reactions occur predominantly during the longer steady temperature period, which is when they will be studied.

Transition metal carbonyl pyrolysis, bond energies, and catalysis

Catalytic reactions are central to many important industrial processes. Transition metals are usually involved, many times CO is a reactant, and for homogeneous catalysis, transition metal carbonyl compounds are often used or are intermediates in the mechanism. To understand and improve these reactions and predict new ones, accurate values of the strengths of the bonds broken and formed are needed. While very few organometallic bond dissociation energies are available from conventional kinetic methods due to surface decomposition reactions, laser pyrolysis is ideally suited for their measurement. We have recently measured[3] the first bond dissociation energy for $Fe(CO)_5$, $Cr(CO)_6$, $Mo(CO)_6$, and $W(CO)_6$.

The essence of the experiment is to add two reactants that will decompose to the gas mixture, and sample their concentrations beyond the cell by mass spectrometer with the laser on and off. From the gas flow rate, laser repetition rate, cell volume, and irradiated volume, one can calculate (and vary) the number of heating pulses a typical molecule receives, and hence its single-shot reaction rate, kt. One compound will be the unknown, a carbonyl. The other, our chemical thermometer or standard has known Arrhenius parameters ($k = A \exp(-E/RT)$). We used dicyclopentadiene, which decomposes to the monomer by a reverse Diels-Alder reaction. The slope of a plot of log (kt) for the unknown versus the standard, is just the ratio of activation energies. Thus the unknown E, which should be close to the bond energy, can be determined. The pre-exponential A-factor is then calculated from the relative rates and t = 10 μsec.

The Arrhenius parameters for $Cr(CO)_6$ decomposition were measured relative to dicyclopentadiene, and those for the other carbonyls relative to $Cr(CO)_6$. An example of the data and results for iron relative to chromium is shown in Figure 2. To determine whether the measured parameters, given in Table 1, correspond to scission of the first metal-ligand bond, excess CO or PF_3 was added. If some later bond cleavage is rate-determining,

Table 1. Metal Carbonyl Bond Energies (kcal)

Compound	Log A	E_a	BDE	Average
$Cr(CO)_6$	17.2	45.5	35	26
$Mo(CO)_6$	15.4	38.9	39	36
$W(CO)_6$	15.5	44.3	44	43
$Fe(CO)_5$	15.7	39.6	40	28

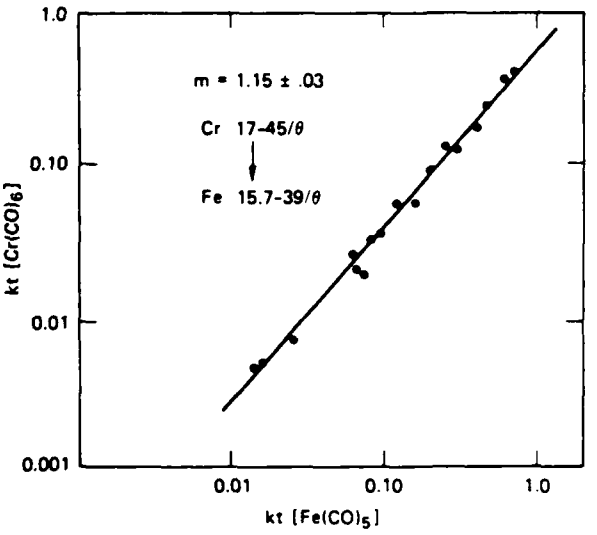

Figure 2 Logarithmic relative rate plot for chromium and iron carbonyl

earlier dissociations must be in a partial equilibrium, which will then be affected by the added concentrations of ligands. This was observed only for $Cr(CO)_6$, which one might expect, given the unusually high A-factor measured. The more complicated kinetics of $Cr(CO)_6$ decomposition can be deconvoluted[3] to give a first bond energy of 35 kcal/mole. Average bond energies for all CO ligands, derived from calorimetric data, are also given in Table 1. Particularly for the first transition metal series, the bond dissociation energy is larger than the average value. Thus such averaged values should not be used in estimating kinetics. Finally, if heats of formation have been measured for substituted carbonyls, $M(CO)_nL$, bond energies can be derived for other ligands L. Pyridine bonds, for example, are roughly 6 kcal/mole weaker than CO, and ethylene bonds are 4 kcal weaker than CO for iron.[3] This last value is particularly relevant since coordinatively unsaturated fragments from $Fe(CO)_5$ photolysis catalyze olefin isomerization and hydrogenation reactions,[4] and because such bonds are important in the mechanism of hydroformylation, by which commercial metal carbonyl catalysts transform alkenes into aldehydes and alcohols.

Except for chromium, the carbonyls rapidly lose their remaining ligands following the initial rate-determining bond scission. After laser pyrolysis of $Fe(CO)_5$, for example, we could easily detect gas-phase iron atoms by laser-induced fluorescence excitation of the $y^5F_4^o$ - a^5D_4 transition at 293 nm. These atoms rapidly nucleate to form an aerosol of small metallic particles, which can be detected by light-scattering of a He-Ne laser beam. They persist for ~ 1 msec, and then coalesce to larger particles and condense at the cell walls. The resulting dark powder is ferromagnetic and contains little carbon or oxygen. While suspended and heated in the gas phase, the iron system was observed to catalyze the decomposition of tert-butyl iodide to HI and isobutene, and the decomposition of paraldehyde, the cyclic trimer of acetaldehyde. Laser pyrolysis of $Mn_2(CO)_{10}$ shows similar behavior, and catalytically produces C_2Cl_6 from CCl_4. These observations suggest a potential use of laser pyrolysis for producing catalytic particles of refractory metals, and in vapor deposition technology. Carefully controlled mixtures including non-metal additives, are possible. (Such methods are being used now to create uniform ceramics by pyrolysis of SiH_4, NH_3, and C_2H_4.) In addition, this in situ generation of hot metallic particles with a large surface area provides an ideal method for studying heterogeneous catalysis by convenient gas-phase techniques.

Quenching of laser-induced fluorescence at high temperatures

Laser-induced fluorescence is one of the most sensitive diagnostic techniques.[5] It is particularly well suited for the remote analysis of reactive radical intermediates in chemical networks; important examples include OH in combustion systems and atmospheres, and atomic species in plasmas. To use this technique, one tunes a laser to the proper wavelength to electronically excite molecules from level c, and then detects the fluorescence F. The amount of signal is related to the radical concentration N by $F = cA\Phi N_e$, where A is the Einstein coefficient (τ^{-1}), c contains all the detection efficiency factors, and $\Phi = A/(A + Q)$ is the fluorescence quantum yield. Quantitative analytical application of LIF requires knowledge of the collisional quenching rate Q, and thus of the composition of the medium and the appropriate quenching rate constants. Values of k_Q vary with temperature in a poorly understood manner, and values at high temperature are particularly needed, and absent, for application of LIF analytics to combustion processes. We have therefore used the laser pyrolysis technique to measure quenching rate constants for the important OH radical at ~ 1100 K for many flame gases, and presented a theoretical framework for temperature extrapolation of quenching rate constant data.[6]

The following variation of the laser pyrolysis experiment was used. A few millitorr of H_2O_2 was added in a bubbler (0°C) to a flow of SF_6 (~ 40 torr) and varying amounts of the

quenching gas. Heating by the CO_2 laser produced OH by thermal decomposition of H_2O_2. At a 30 μsec delay, after the expansion cooling, the dye laser was fired to excite the OH, and the resulting fluorescence decay was photographed from the oscilloscope. The temperature was determined from OH rotational level populations by scanning the laser through several spectral lines. The partial pressure of the added quencher was deduced from mass flowmeter measurements, the total pressure read on a gauge, and a computer calculation of the expansion gas dynamics. It roughly equals the initial pressure. The measured fluorescence decay rate, $1/\tau$, is the result of several factors: radiative decay (A), quenching by SF_6 (slow), quenching by H_2O_2 and H_2O from the bubbler, and quenching by the added gas. Figure 3 is a plot of τ^{-1} versus pressure of added CO_2, where the contributions of radiative decay and SF_6 quenching have been subtracted from the data. The intercept shows the background H_2O quenching and the slope gives the rate for CO_2 quenching of OH (A-X)(0,0) fluorescence. The temperature was 1250 K at 40 torr total pressure, and $k_Q(CO_2) = 1.9 \times 10^{-10}$ cm^3 s^{-1}. For various gases, several such experiments were done, the results expressed as cross-sections ($k = \sigma \bar{v}$), and averaged.

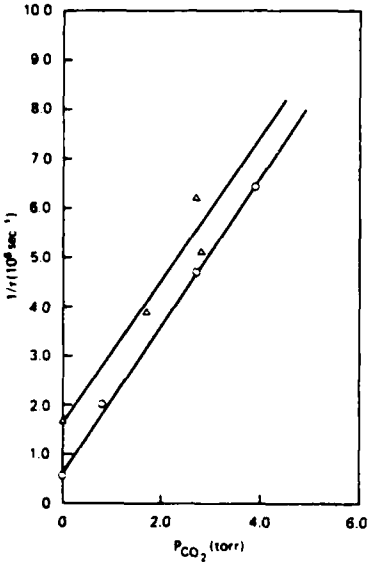

Figure 3. OH(A) quenching rate versus CO_2 pressure

The results are summarized in Table 2. Typical uncertainties are 20%. The values are generally smaller than those at 298 K (by up to 50%), and thus illustrate the importance of such high-temperature measurements, rather than simply using the room-temperature cross-sections. With the exception of SF_6 and N_2, these quenching cross-sections are large. This suggests long-range, attractive forces between OH(A) and the quencher are responsible for the mechanism. We have used a simple collision complex model to predict σ. The long-range interaction was given by a sum of attractive multipole interactions (dipole-dipole, dipole-quadrupole, dipole-induced dipole, and dipersion) and a repulsive centrifugal barrier. From the position and height of the barrier in the total effective potential, σ can be calculated.[6] The resulting ratio of experimental to theoretical values given in the table generally vary from .3 to .45. This can be interpreted as the probability for quenching once a complex has been formed.

Table 2. OH Quenching Cross Sections 1100 K (A^2)

Gas	SF_6	N_2	CO_2	H_2O	CO	CH_4	H_2	NH_3	O_2	NO	N_2O
σ	0.14	0.7	13	26	20	15	10	39	11	26	30
σ/theory	0.002	0.14	.20	.29	.35	.32	.28	.45	.27	.49	.46

Finally, this theory predicts a decline (of ~ 40%) in quenching cross-section when the temperature increases from 300 K to 1100 K. The general agreement of experiment and theory in trend and size suggests that this theoretical approach can be used to extrapolate quenching cross-sections to different temperatures.

High-temperature kinetics

A good deal of effort in recent years has gone toward detailed modeling of combustion systems. Two of the goals are to predict the effects of various mixtures and additives on combustion and pollutant formation, and to correlate certain observables (e.g., NH LIF) to the flame chemistry so that they may be used knowledgably to monitor the conditions of real processes. Such modeling requires a detailed chemical mechanism and values for many high-temperature rate constants. Laser pyrolysis with LIF detection offers a new method for measuring some bimolecular rate constants above 1000 K. We have recently examined the reaction between OH and acetylene.[7]

The apparatus and procedure is similar to the previous quenching experiment. The boxcar integrator, however, is now used to measure the amount of OH laser-induced fluorescence, and hence determine the relative OH density as a function of delay time, Δt, between the CO_2 and dye lasers. This was done at various C_2H_2 pressures, and without C_2H_2. A logarithmic plot of the ratio of these signal levels versus time gives as its slope the OH ground-state decay rate due to reaction with a certain pressure of C_2H_2. This data can then be reduced to a rate constant in the same manner as was done for the OH(A) quenching just described. An example is illustrated in Figure 4 for OH + C_2H_2 at 1170 K. The measurements at various

rate constant was measured between 25 and 100 torr total pressure, indicating no third-body pressure dependence for this reaction. We have previously reported similar experiments for the OH-methane reaction.[2]

At lower temperatures where it had previously been studied,[8] the OH-acetylene reaction is known to proceed by OH addition to an acetylene π-bond to form an adduct. Collision with a third body is needed to remove energy and stabilize this adduct, and at pressures below 100 torr the reaction rate thus depends upon the total pressure. Our 1200 K measurements show no such pressure dependence, and give a lower rate constant than the typical 300 K values. This suggests the adduct is no longer stable at high temperatures, and that a new direct reaction channel, endothermic hydrogen abstraction, becomes dominant. We have performed RRKM-type calculations on the pressure-dependence data at low temperatures. The results are described elswhere,[7] but do fit the data and predict a lower addition rate constant and rapid adduct dissociation at 1200 K. The theory also predicts some pressure dependence due to the addition channel at 900 K, which we have now observed in laser pyrolysis experiments at these lower temperatures. The mechanistic transition from addition to abstraction for this reaction (and many others) occurs near 1000 K. It is very important to include the correct products and rate constants in models of combustion chemistry, but high-temperature kinetics experiments and the sound application of theoretical understanding are necessary to do this successfully. The acetylene reaction is a prime example, since the C_2H product is considered a precursor of soot while the C_2H_2OH adduct is not.

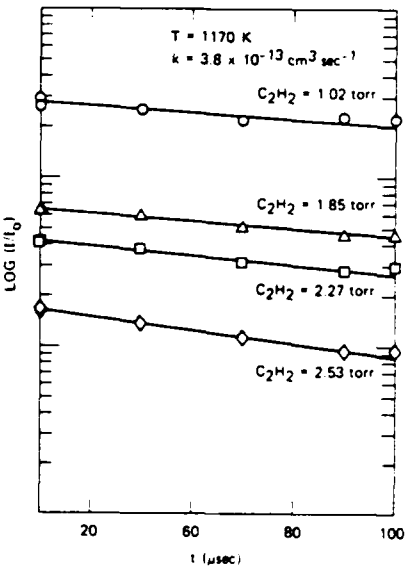

Figure 4. OH decays from reaction with acetylene

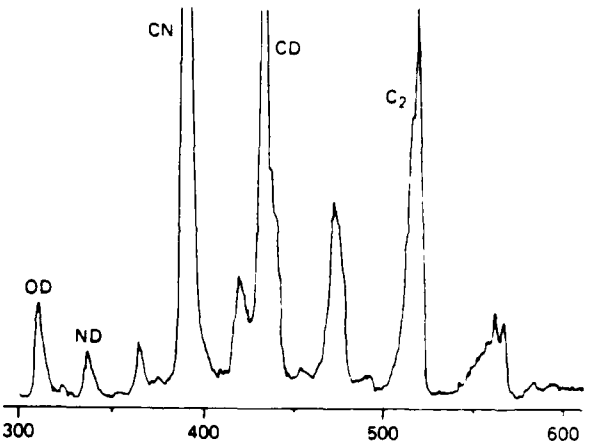

Figure 5. Chemiluminescence from laser pyrolysis of CD_2O and N_2O

Pulsed laser oxidation chemiluminescence

The rapid and temporally well-defined heating of laser pyrolysis can also be used to study the more complicated networks of reactions involved in flame chemistry. We recently used CO_2-laser irradiation to heat to ~ 1500 K a mixture of 35 torr SF_6 with 2 torr N_2O and 0.5 torr deuterated formaldehyde. This flame is considered a model for certain propellant systems. At the temperatures attained, some fuel and oxidizer decomposition to form H and O atoms will occur, and a typical radical chain oxidation mechanism will ensue. (Some F-atoms from SF_6 pyrolysis may also participate.) Post-irradiation mass-spectral analysis of the mixture showed CD_2O and N_2O consumption and the production of N_2, CO (deduced from isotopic peak ratios), and D_2O. In addition, a bright blue glow appears in the irradiated region. Under these particular conditions, the chemiluminescence rises within 10 μsec, peaks at a 0.5 msec delay, and is over in 2 msec. It requires the presence of both reactants. Figure 5 is a spectrum of this light emission, made by scanning the monochromator. The characteristic spectra of C_2, intense CN and CD, and minor OD and ND emission are identified. (The smaller $\Delta v = \pm 1$ features for C_2 and CN are unlabeled.)

This luminescence suggests two approaches to assist in efforts to analyze flames. Significant concentrations of these radicals in their ground states probably exist for probing

by LIF. By time-resolved probing at various reactant concentrations, one can deduce portions of the flame chemistry and correlate this with the LIF (and chemiluminescence) observables. Because of the temporally-resolved nature of the experiment, it may be a particularly suitable tool for studying ignition phenomena. Secondly, flame chemiluminescence may yet prove to be a useful diagnostic itself. Although it is very easily observable, this emission arises from trace concentrations of excited states, not the ground state radicals of chemical significance. If the kinetics by which emission arises, about which little is known, can be determined, it should be possible to link luminescence observations to the flame chemistry. This laser pyrolysis experiment, with its time resolution and various subsets of the flame chemistry, should prove of great help in this effort.

Conclusions

As with most new experimental techniques, many potential uses of laser pyrolysis remain to be explored. Most of our efforts to date, as describe in this paper, have concentrated on understanding the physics and chemistry of the process, and on utilizing it as a tool for analyzing the kinetics of high-temperature environments. Uses in developing analytical methods and producing catalytic materials are suggested by this work, and other applications will, perhaps, be found in the future. In this regard, the main advantageous features of laser pyrolysis to consider are its rapid heating to high temperatures, the localized and controlled nature of this heating, and the time resolution achievable with the pulsed technique. In addition, it should be mentioned that the original continuous laser pyrolysis method,[1] using a CW CO_2-laser, can also be applied to many of the same purposes, but at lower temperatures due to the longer reaction time.

Acknowledgements

The author wishes to thank his coworkers on these experiments at SRI, Karan E. Lewis, Drs. Paul Fairchild, David Crosley, Donald McMillen, David Golden, and Richard Laine. The research summarized in this paper was supported by the National Science Foundation, the U.S. Army Research Office, and the U.S. Department of Energy.

References

1. W. M. Shaub and S. H. Bauer, Int. J. Chem. Kinetics, 7, 509 (1975); W. M. Shaub, Ph.D. Thesis, Cornell University, 1975.
2. D. F. McMillen, K. E. Lewis, G. P. Smith, and D. M. Golden, J. Phys. Chem., 86, 709 (1982); P. W. Fairchild, G. P. Smith, D. R. Crosley, Nineteenth Symposium (International) on Combustion, p. 107 (1982).
3. K. E. Lewis, D. M. Golden, G. P. Smith, J. Am. Chem. Soc., to be published.
4. R. L. Whetten, K.-F. Fu, E. R. Grant, J. Chem. Phys., 77, 3769 (1982).
5. D. R. Crosley, G. P. Smith, Opt. Eng., 22, 545 (1983).
6. P. W. Fairchild, G. P. Smith, D. R. Crosley, J. Chem. Phys., 79, 1795 (1983).
7. G. P. Smith, P. W. Fairchild, D. R. Crosley, J. Chem. Phys., submitted.
8. R. A. Perry, D. Williamson, Chem. Phys. Lett., 93, 331 (1982).

COMBUSTION AND FLAME 58: 229–237 (1984)

Pressure and Temperature Dependence of Unimolecular Bond Fission Reactions: An Approach for Combustion Modelers*

C. WILLIAM LARSON, ROGER PATRICK,** and DAVID M. GOLDEN

Department of Chemical Kinetics, SRI International, Menlo Park, CA 94025

There exists a well recognized need for a critical overview of the rate data that go into combustion modeling. Modelers should be able to consult tables of parameters for combustion-relevant reactions that would enable the calculation of relevant rate constants as a function of temperature and pressure over the entire range of interest. A complete tabulation would include both uni- and bimolecular reactions; in this paper we focus on the analysis of unimolecular reactions. The approach is illustrated with unimolecular "falloff" calculations for formaldehyde, methane, ethane, butane, hexane, octane, and the ethyl radical

I INTRODUCTION

There is seeming agreement in the combustion literature with the premise that combustion must be understood through the successful modeling of this complex process from elementary considerations of chemistry and physics. The usual definition of elementary for chemical purposes involves the rate constants for individual chemical steps that make up the "mechanism" of the chemical transformations affected by the combustion event. A practical goal might be the production of a continually updated handbook of reaction rate constants that modelers could use as input data. (This goal has been achieved for some time now in the modeling of chlorfluoromethane effects on stratospheric chemistry.)

The current understanding of chemical kinetcis allows us to break elementary reactions into two major groups: unimolecular and bimolecular reactions. In this paper we offer a suggestion as to the form in which unimolecular rate data should be presented to combustion modelers.

The unimolecular pyrolysis reactions of hydrocarbon molecules and radicals that occur in combustion depend on temperature and pressure in a complex manner dictated by (1) the complexity or size of the molecule or radical, (2) the threshold energy for reaction, and (3) the details of the intermolecular energy-transfer processes.

In the simplest model of unimolecular reactions, the Lindemann–Hinshelwood reaction scheme, energization by collisions is followed by reaction of energized species, A^*:

$$A + M \rightleftarrows A^* + M,$$

$$A^* \rightarrow \text{products}.$$

Solution of the differential rate equations in the steady-state approximation produces a particularly simple expression relating the reduced unimolecular rate constant, k_r, to the reduced pressure, P_r:

$$k_r = P_r/(1 + P_r). \tag{1}$$

Here, k_r is the ratio of the unimolecular rate constant at pressure M to its value as $M \rightarrow \infty$: k_r

* This work was supported by the Army Research Office, Contract No. DAAG29-80-K-0049

** Current address: LSI Logic Corporation, 3105 Alfred Street, Santa Clara, CA 95050

0010-2180/84/$03.00

$= k/k_\infty$. Also, $P_r = (k_0/k_\infty)[M]$, where $k_0[M]$ is the value of the unimolecular rate constant as $M \to 0$.

Since the Lindemann-Hinshelwood model neglects the pressure dependence of the relative populations of the manifold of energy eigenstates of A^*, as well as the differential depletion of these populations by reaction of A^*, it predicts that k_r will "fall off" from its high-pressure limiting value more slowly than is observed. The quantum statistical RRKM theory corrects this deficiency.

Troe [1] has developed an approach for modeling the pressure and temperature dependence of unimolecular reactions of ethane and smaller molecules based on use of a "corrected" Lindemann-Hinshelwood model. In the Troe approach, the corrected reduced umimolecular rate constant is defined by

$$k_r = \frac{P_r}{1+P_r} F. \tag{2}$$

Thus, Troe calculated values of k_r, k_0, and k_∞ using an RRKM model, and developed simple formulas for expressing the "broadening factor," F, as a function of temperature and pressure. The value of the Troe approach lies in its retention of the simplicity of the Lindemann-Hinshelwood form and the ease with which it may be used to model unimolecular reactions of molecules important in combustion.

We shall show later that the Troe form allows the representation of rate constants to better than 25% accuracy. We can always look at a detailed RRKM calculation of a particular rate constant if a sensitivity analysis shows us that higher than 25% accuracy is required. Concomitantly, we might have suggested a Lindemann format or a format such as in Eq. (2) with F equal to some universal constant. (The latter is sufficient for stratospheric modeling.) Perhaps this last recourse would have limited us to ~60% accuracy; it is easy to argue that 60% may be sufficient. We point out that in order to establish k_∞ and k_0, we have essentially all the information needed for an RRKM calculation. Since we have facilities for easily performing such calculations, we have taken the effort to produce F as a three-parameter function of temperature. It is not our hope or suggestion that modelers perform their own RRKM calculations, rather we offer the beginning of the handbook for reaction rate constants mentioned earlier.

In this paper we have applied the Troe approach to the study of the temperature and pressure dependence of unimolecular reaction by fission of the central carbon-carbon bond in ethane, butane, hexane, and octane and of the carbon-hydrogen bond in methane and formaldehyde. We also compare ethyl radical decomposition (to ethylene and hydrogen atoms), which has a threshold energy less than half that of the other examples.

II METHOD OF CALCULATION

For the calculation of the reduced unimolecular rate constant as a function of temperature and pressure, we have used the RRKM quantum statistical model. Molecular vibrational eigenstate densities were calculated with use of the Whitten-Rabinovitch [2] approximation, and anharmonic corrections were made according to the procedure developed by Haarhof [3]. Vibrational eigenstate sums for the activated complex were calculated with use of an exact count routine. Overall rotational degrees of freedom were treated as adiabatic.

Frequency assignments for alkanes were based on the generalized normal-mode study of C_2 to C_{12} saturated hydrocarbons of Schachtschneider and Snyder [4] as adapted for use in RRKM calculations by Chua and Larson [5].

Frequency assignments for activated complexes were made so as to fit the high-pressure limit A-factors: $\log A_\infty = 17.0$ at 1500K for C-C bond rupture and $\log A_\infty = 15.5$ at 1500K for C-H bond rupture [6]. One 950 cm^{-1} C-C stretch frequency was deleted from the alkane assignment (reaction coordinate) and five frequencies in the alkane (four bending modes and one torsion which are associated with the breaking C-C bond and which become overall rota-

tions and relative translations in the products) were lowered, until the correct valve for A_∞ was obtained. Figure 1 shows how the calculated k_∞ for ethane compares with determinations reported in the literature [7–12]. (We discuss later the effect of using a fixed vibrational model for the transition state instead of one which tightens with increasing energy.)

Collision frequencies were calculated based on a Lennard-Jones model; collision diameters of 5–6 Å and a value for ϵ/k of 173K were used for the N_2–alkane mixtures.

Threshold energies for central C–C bond rupture of butane, hexane, and octane were fixed at 80.0 kcal mol^{-1} and for ethane at 87.7 kcal mol^{-1}; 105 kcal mol^{-1} and 90 kcal mol^{-1} were used for methane and formaldehyde, respectively, and 40 kcal mol^{-1} was used for the ethyl radical.

III RESULTS

Arrhenius plots of the RRKM calculated high- and low-pressure rate constants k_∞ and k_0 are shown in Fig. 2. The characteristic curvature in the low-pressure plots is especially pronounced for the larger molecules; the low-pressure rate constant for octane is nearly temperature independent at high temperature. In contrast, the high-pressure Arrhenius plots are only slightly curved upward; thus, high-pressure activation energies between 1000 and 2500K increase by only about 1 kcal mol^{-1}. The curvature in the high-pressure Arrhenius plot is the maximum possible due to the use of a fixed vibrational model for the transition state in these calculations.

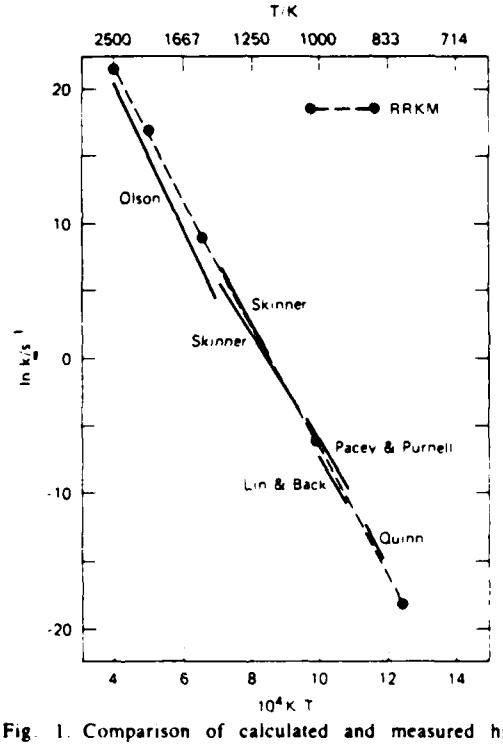

Fig. 1. Comparison of calculated and measured high pressure rate constants for ethane pyrolysis.

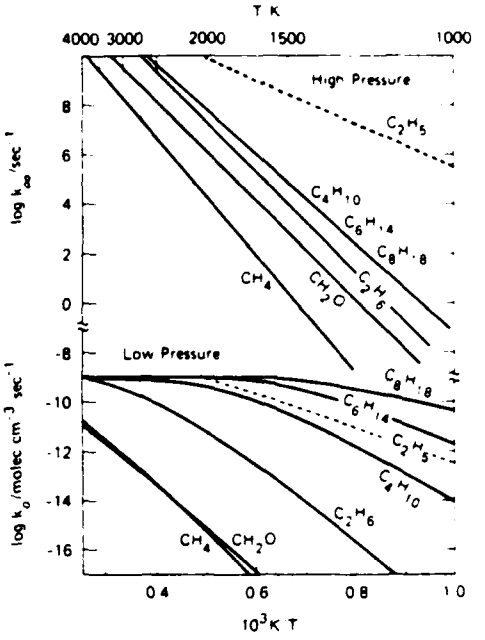

Fig. 2. Calculated Arrhenius behaviour of high- and low-pressure rate constants. Dotted lines apply to ethyl radical

Figure 3 shows a comparison between the Lindemann-Hinshelwood falloff curve and those calculated with the RRKM model for octane and butane at 1000K. The broadening factor at the center of the fall of curve, F_c, is defined at $P_r = 1$ as the ratio of the k_r calculated by RRKM to k_r calculated with the Lindemann model.

Figure 4 illustrates the pressure dependence of the falloff broadening parameter of octane at

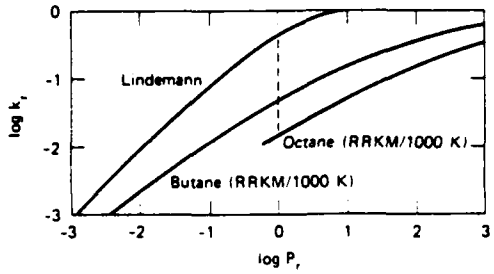

Fig. 3. Comparison of Lindemann falloff with RRKM falloff for butane and octane at 1000K.

1550 and 2500K. The asymmetric "Gaussian-like" shape is typical of all molecules, and the minimum value of F is found only slightly to the low-pressure side of the "falloff" center: $F_c \approx F_{minimum}$. Also, the pressure range over which the deviations from Lindemann falloff behavior are significant spans several orders of magnitude.

Figure 5 shows the temperature dependence of the central broadening parameter, $F_c(T)$, for the five alkanes, formaldehyde, and the ethyl radical. The figure shows, and the Troe approach predicts, that the central broadening factor approaches unity at the zero and infinite temperature limits. Also, $F_c(T)$ for the larger molecules passes through a minimum near 1000K; the minimum deepens and moves to lower temperatures as the molecular size increases.

IV DISCUSSION

The temperature dependences of high- and low

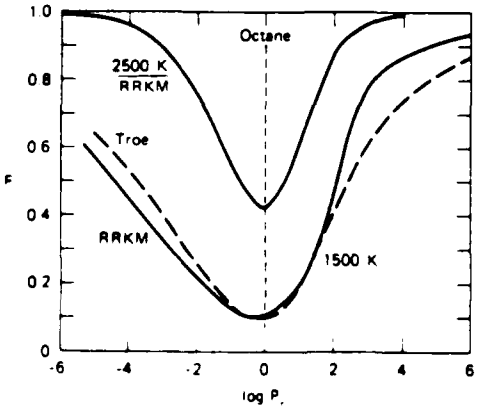

Fig 4 Broadening factor as a function of reduced pressure and comparison with Troe approximation.

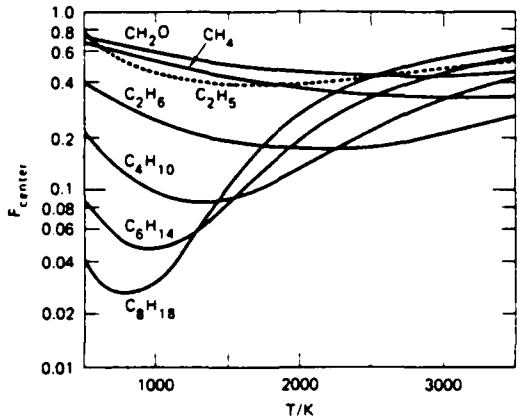

Fig. 5. Temperature dependence of central broadening factor. The dotted line applies to ethyl radical.

pressure-limiting rate constants $k_0(T)$ and $k_\infty(T)$, illustrated in Fig. 2, and the temperature/pressure dependences of the Troe broadening factor $F(T, M)$, illustrated in Fig. 4, provide *all* the information required to write parameterized analytical functions that make it possible to calculate with ease the strong collision unimolecualr rate constant, $k(T, P)$.

High- and Low-Pressure Limits

The limiting rate constants are easily written in the customary way as 3-parameter functions of temperature:

$$k_0(T) = AT^n \exp(-B/T) \tag{3}$$

and

$$k_\infty(T) = CT^m \exp(-D/T). \tag{4}$$

Figure 2 shows that C and D are often very close to the high-pressure Arrhenius A-factor and activation energy, respectively, and that $m \approx 0$.

The curvature in the Arrhenius plot for k_0, which is more pronounced for larger molecules, is representable to within 1% by the nonlinear, 3-parameter expression. Table 1 summarizes the results of parameter evaluation from least squares fits of these expressions to the k_0 and k_∞ calculated from RRKM theory. The nonlinear regression algorithm given by Bevington [13] was used in this evaluation.

TABLE 1
Values of Parameters for Representation of High- and Low-Pressure Rate Constants[a]

Molecule	log(A) (cm^3 $molecule^{-1}$ s^{-1})	n	10^3B (K)	log(C) (s^{-1})	m	$10^{-3}D$ (K)
Formaldehyde	5.14	−3.1	46.9	13.77	0.65	45.1
Methane	13.29	−5.0	56.9	13.70	0.61	53.8
Ethane	37.16	−11.2	52.2	16.66	0.28	46.6
Butane	57.16	−17.2	45.4	16.87	0.03	41.3
Hexane	42.43	−13.5	31.3	16.87	0.03	41.3
Octane	15.86	−6.5	15.6	16.87	0.03	41.3
Ethyl	19.23	−7.1	23.5	11.79	0.74	19.7

[a] $k_0(T)$ is in cm^3 $molecule^{-1}$ s^{-1}, and $k_\infty(T)$ in s^{-1}; 1000–3000K.

Broadening as a Function of Pressure

Troe presents three forms as successive levels of approximation to express the pressure dependence of F in terms of F_c:

1. symmetric broadening about $P_r = 1.0$:

$$\log F_1 = [1 + (\log P_r)^2]^{-1} \log F_c; \quad (5)$$

2. including width broadening:

$$\log F_2 = \left[1 + \left(\frac{\log P_r}{0.9 - \log F_c}\right)^2\right]^{-1} \log F_c; \quad (6)$$

3. including width plus asymmetric broadening:

for $P_r > 1$:

$$\log F_3 = \left[1 + \left(\frac{\log P_r - 0.12}{0.85 - 0.67 \log F_c}\right)^2\right]^{-1} \times \log F_c; \quad (7)$$

for $P_r < 1$:

$$\log F_3 = \left[1 + \left(\frac{\log P_r - 0.12}{0.65 - 1.87 \log F_c}\right)^2\right]^{-1} \times \log F_c. \quad (8)$$

Figure 6 shows how the broadening factor from Troe's highest level approximation, F_3(Troe), compares with the RRKM calculated

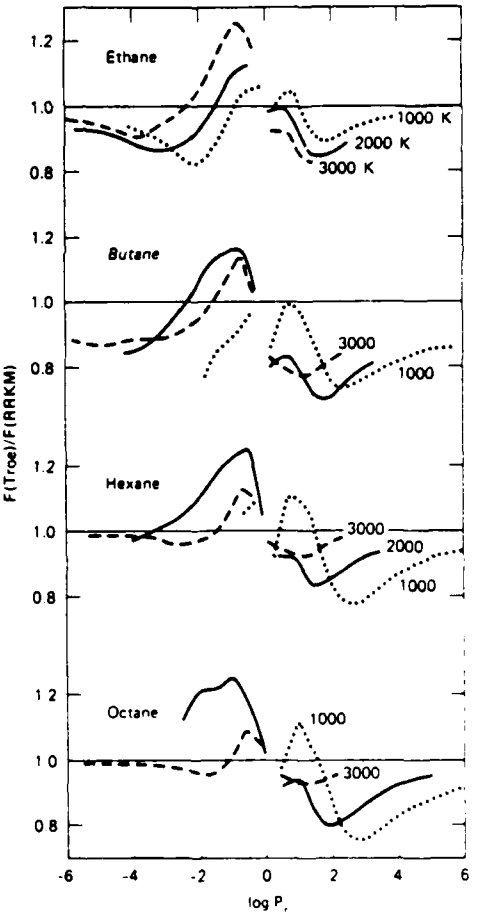

Fig. 6. Comparison of calculated and approximate fall off broadening.

broadening, F(RRKM), in which F_c is taken from this RRKM calculation. The figure shows that the Troe expression predicts $F(M)$ to within 30% over the pressure and temperature ranges studied. The simpler expressions [Eq. (6) or (7)] are less satisfactory, and, since they are not significantly easier to use, they are not recommended.

Center Broadening as a Function of Temperature

Troe has suggested a 4-parameter expression to describe the temperature dependence of F_c as follows:

$$F_c(T) = \exp(-T^{**}/T) + \exp(-T/T^{***}) + a(\exp(-T/T^{*}) - \exp(-T/T^{***})). \quad (9)$$

We have evaluated the performance of a similar 3-parameter, 2-term expression,

$$F_c(T) = a\ \exp(-b/T) + \exp(-T/c), \quad (10)$$

and find that a, b, c values listed in Table 2 reproduce the RRKM calculated $F_c(T)$ shown in Fig. 5 to within better than 15%. Thus, the 6 parameters of Eqs. (3) and (4) (A, n, B, C, m, D) contain the information required to construct Lindemann falloff curves, and the 3 parameters of Eq. (10) contain the information required to correct the Lindemann falloff to the more realistic falloff predicted by the RRKM model.

Effect of Transition State Model on Broadening

The RRKM model that has been described so far is one in which the transition state has been treated as a normal molecule with fixed vibrational frequencies. However, it is well known that this kind of treatment generally overpredicts the curvature in Arrhenius plots of high-pressure limiting rate constants for dissociation reactions, and also that it is unable to predict correctly the temperature dependence of rate constants for recombination reactions. Other models, which allow the structure of the transition state to tighten as its internal energy increases, such as the statistical adiabatic channel model (SACM) [14] or minimum density of states RRKM models [15, 16], have been more successful in this regard. Since these treatments essentially involve adjusting the energy dependence of the microscopic rate constant for decomposition, $k(E)$, their use would be expected to affect predictions concerning broadening parameters. Table 3 gives the strong collision-broadening parameters for CH_4 decompostion as a function of temperature for the fixed vibrational model and also for a minimum density of states model. Since $k(E)$ is a less steep function of E for a minimum density of states model (i.e., more Lindemann-like), the broadening parameters are closer to unity at each temperature than for a fixed vibrational model for this kind of transition state treatment. The fixed vibrational model thus indicates the *maximum* broadening that might be expected.

TABLE 2
Values of Parameters for Representation of $F_c(T)$, 1000-3000K

Molecule	a	b (K)	c (K)
Formaldehyde	0.507	629.2	939.4
Methane	0.366	564.2	885.1
Ethane	0.233	585.6	431.8
Butane	1.896	5222.3	335.8
Hexane	2.016	4525.8	209.4
Octane	2.226	4247.9	158.9
Ethyl	0.411	73.4	422.8

TABLE 3
Broadening Parameters for CH_4 Decomposition

T	F_c (fixed model)[a]	F_c (minimum density model)[b]
500	0.694	0.753
1000	0.518	0.640
1500	0.438	0.579
2000	0.384	0.506
2500	0.350	0.493
3000	0.334	0.488

[a] This work.
[b] According to Ref. [16]

Weak Collisional Energy Transfer

In the preceding sections, we have calculated low-pressure rate constants, k_0^{sc}, and center-broadening parameters, F_c^{sc}, based on a strong collision approximation. It is customary to characterize a weak collider in terms of its collision efficiency, β, defined by $\beta = k_0^{wc}/k_0^{sc}$, where k_0^{sc} is the low-pressure rate constant for the weak collider.

Weak collision processes affect unimolecular falloff in two distinct ways. First, the reduced pressure appropriate to weak collider falloff, P_r^{wc}, is simply scaled according to β:

$$P_r^{wc} = k_0^{wc}[M]/k_\infty = \beta P_r^{sc}.$$

Second, the center-broadening factor for a weak collider, F_c^{wc}, is smaller than F_c^{sc}, so that weak collider falloff occurs over a larger pressure range. However, the empirical approximation, $F_c^{wc} \sim \beta^{0.14} F_c^{sc}$, found by Troe to apply to a variety of molecules and weak collision models, shows that computed falloff behavior in weak collider systems is much more sensitive to the absolute value of β that is used as a scaling factor in p_c^{wc} than to the additional broadening brought about by weak collisions.

The temperature dependence of β is still subject to some controversy [17] and represents the largest uncertainty in the prediction of falloff behavior. Using an exponential model for energy transfer, Troe [18] has suggested the following approximate relationship:

$$\beta = \left(\frac{\alpha}{\alpha + F_E kT}\right)^2,$$

where α is the average energy transferred per collision in "down transitions" and F_E is the energy dependence of the density of states, a quantity that increases with temperature and the size of the molecule. α is generally taken to be temperature independent or only weakly dependent on temperature. This equation predicts a steady decline in β with increasing temperature, but it is only valid for $F_E \leq 3$; at high temperature, F_E rapidly increases beyond this limit, especially for large molecules. Under such conditions, a more exact treatment indicates that β will begin to increase with temperature again after a certain point. The more complex the molecule, the earlier the decrease of β will cease, since F_E will become a strongly increasing function of temperature.

These most recent calculations [18] for a large molecule and weak colliders, whose α values vary between ~1 and ~6 kcal mol^{-1}, show that minima in β occur near 1200K that are about half the values at 900 and 2100K. In contrast, the range in the absolute values of the calculated minima span one order of magnitude, viz., $\beta = 0.2$ to $\beta = 0.02$ as $\alpha = 6$ to $\alpha = 1$ kcal mol^{-1}. Thus, we infer that the uncertainties in an educated guess of the absolute value of β are greater than the variation in β over a large temperature range (900–2100K). For combustion calculations, the state of the art at this point suggests that β might best be treated as an adjustable parameter whose value and temperature dependence may be constrained by reasonable estimates to within a factor of two.

Applications to Combustion Modeling

In order to evaluate the conditions where unimolecular falloff has its greatest impact on combustion phenomena, we compute the relationship between an actual weak collider pressure *at the falloff center*, P_c^{wc}, and temperature. Figure 7 shows this relationship for each of the molecules studied. For this illustration, we have used $\beta = 0.1$, independent of temperature, to simulate a nitrogen bath gas. Thus, $P_c^{wc} = (k_\infty/\beta)k_0^{sc}$ defines the pressure axis.

We have defined a "combustion window" by the pressure range (0.01–10 atm) and the temperature range (500–3000K), which are relevant to most combustion processes. Thus, a molecule whose P_c versus T curve passes through the combustion window exhibits its *maximum* deviation from Lindemann behavior within this important pressure and temperature range. At pressures two to three orders of magnitude above or below their P_c versus T curve, the molecules are in their high- or low-pressure limits.

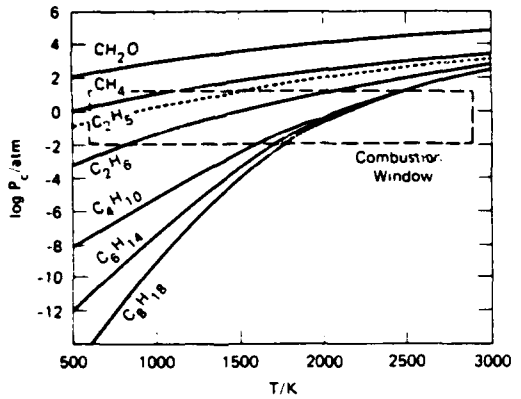

Fig. 7. The combustion window and relation between temperature and pressure at the center of the falloff. Dotted line emphasizes ethyl radical.

Larger molecules enter the window at higher temperatures, where their F_c values are larger. Thus, values of F_c within the "combustion window" are greater than ~0.1 for all molecules of the current study. For molecules larger than butane, falloff needs to be considered at temperatures greater than about 1700K. Below 1500K, the rate constants for dissociation of the larger molecules are in their high-pressure limit.

At atmospheric pressure, methane pyrolysis is second order at temperatures greater than ~600K, but for ethane, maximum broadening occurs at about 1500K, and falloff considerations are important at all combustion temperatures. For formaldehyde at 1500K, a weak collider pressure of ~1000-10,000 atm would be required to bring its decomposition to the center of the falloff; at atmospheric pressure, formaldehyde pyrolysis is in its second order limit at all temperatures.

At atmospheric pressures, ethyl radical decomposition, whose threshold energy (~40 kcal mol^{-1}) is less than half that of ethane, is second order at temperatures greater than ~1000K. Smaller radicals, with similar or lower thresholds to reaction, would also be second order above 1000K. Thus, under these conditions, falloff considerations for this large and important group of combustion intermediates have little or no impact.

Competitive Multiple Reaction Channels

Ethane and the higher alkanes contain multiple dissociation channels for C-C and C-H bond rupture which have not been considered in the present calculations. Generally, C-H rupture is 10-20 kcal mol^{-1} more endothermic than C-C rupture. Under conditions where C-H and C-C rupture are both in the high-pressure limit, C-H rupture (per C-H bond) may amount to as much as 0.5% of C-C rupture (per bond) at 1000K. At 3000K, the C-H rate approaches 20% of the C-C rate on a per-bond basis.

In the falloff and low-pressure limits, C-H rupture would tend to be less competitive with C-C rupture. However, it is important to note that at pressures lower than the high-pressure limit, different dissociative channels cannot be treated as if they were independent of one another.

SUMMARY

The initiation of combustion is governed by the reaction that produces an H-atom, i.e., the unimolecular decomposition of the fuel. These calculations indicate that ethane pyrolysis ($C_2H_6 \rightarrow CH_3 + CH_3$) is near its maximum pressure sensitivity at combustion tempertures. A simple format is presented to include the pressure and temperature dependence of these important reactions in terms of 9 parameters and the collision efficiency, β:

$$k_{diss} = k_\infty (1 + P_r^{-1})^{-1} F,$$

$$P_r = k_\infty / (\beta k_0^{sc} M), \qquad F = F(P_r, F_c(a, b, c)),$$

$$k_\infty = CT^m \exp(-D/T),$$

$$k_0 = AT^n \exp(-B/T).$$

The Lindemann model generates the maximum sensitivity of k_{diss} to pressure and requires 6 parameters and β. Application of the RRKM correction causes falloff to occur over a broader pressure range and thus desensitizes k_{diss} to pressure. If weak collider-broadening correc-

tions are also applied (by Troe's $\beta^{0.14}$ factor), k_{diss} is even less sensitive to pressure.

Finally, the falloff behavior of the reverse combination reaction may be coded with 3 additional parameters (s, l, H) to specify the equilibrium constant, $K_{eq} = ST^l e^{-H/T}$. These parameters are related to the quantities ΔS, ΔC_p, and ΔH for the reaction which are often known or may be estimated from group additivity [6].

REFERENCES

1. (a) Troe, J., *J. Phys. Chem.* 83:114 (1979); (b) Troe, J., *Ber. Bunsenges. Phys. Chem.* 87:161 (1983), extends the treatment to larger molecules: methyl- and propyl-cyclohexatriene, toluene, etc.
2. Whitten, G. Z., and Rabinovitch, B. S., *J. Chem. Phys.* 38:2466 (1963).
3. Haarhof, P. C., *Mol Phys.* 6:101 (1963).
4. Schachtschneider, J. H., and Snyder, R. G., *Spectrochim. Acta., Part A* 19:117 (1963), 21:169 (1965).
5. Larson, C. W., Chua, P. T., and Rabinovitch, B. S., *J. Phys. Chem.* 76:2507-2517 (1972).
6. Benson, S. W., *Thermochemical Kinetics*, 2nd Ed., Wiley, New York, 1976.
7. Skinner, G. B., and Ball, W. E., *J. Phys. Chem.* 64:1462 (1972).
8. Pacey, P. D., and Purnell, J. H., *J. Chem. Soc. Faraday I* 68:1462 (1972).
9. Olson, D. B., and Gardiner, W. C., *J. Phys. Chem.* 83:922 (1979).
10. Skinner, G. B., Ruehrwein, R. A., *J. Phys. Chem.* 63:1736 (1959).
11. Lin, M. C., and Back, M. A., *Can. J. Chem.* 44:2537 (1966).
12. Quinn, C. P., *Proc. Roy. Soc.* A275:190 (1963).
13. Bevington, P. R., *Data Reduction and Error Analysis*, McGraw-Hill, New York, 1969, p. 237.
14. Troe, J., *J. Chem. Phys.* 79:6017 (1983).
15. Bunker, D., and Pattengill, M., *J. Chem. Phys.* 48:772 (1968).
16. Patrick, R., Pilling, M. J., and Rogers, G. J., *Chem. Phys.* 53:279 (1980).
17. (a) Barker, J. R., *Chem. Phys.* 77:301 (1983); (b) Heymann, M., Hippler, H., and Troe, J., *J. Chem. Phys.* 80:1853 (1984); (c) Barker, J. R., and Golden, R. E., *J. Phys. Chem.* 88:1012 (1984).
18. Gilbert, R. E., Luther, K., and Troe, J., *Ber. Bunsenges Phys. Chem.* 87:169 (1983).

Received 20 April 1984; revised 12 July 1984

Spin-orbit splittings and rotational constants for vibrationally excited levels of NCO($X^2\Pi_i$)

RICHARD A. COPELAND AND DAVID R. CROSLEY
Molecular Physics Department, SRI International, Menlo Park, CA 94025 U.S.A.

Received June 18, 1984

Laser-induced fluorescence excitation spectra at 0.3-cm^{-1} resolution have been obtained for the $A^2\Sigma^+ - X^2\Pi_i$ system of NCO present in an atmospheric pressure CH_4-N_2O flame. This combination of selectively detected laser fluorescence and a flame environment has permitted the high-resolution investigation of levels inaccessible in conventional room temperature experiments. Spin-orbit splittings, and rotational and vibrational constants have been determined for eight vibrational levels having $K = v_2 + 1$, and for the 010 $^2\Sigma$ and the 020 $^2\Pi$ levels, primarily by fits to band-head positions using previously determined $A^2\Sigma^+$ constants. The results are in good agreement with theoretical predictions of Renner–Teller interactions. Fermi resonance with an interaction strength of 10 cm^{-1} describes variations in spin–orbit splittings and rotational constants for four levels with $v_1 = 1$ quite well.

Des spectres d'excitation de fluorescence induite par laser ont été obtenus avec une résolution de 0.3 cm^{-1} pour le système $A^2\Sigma^+ - X^2\Pi_i$ de NCO présent dans une flamme de CH_4-N_2O à pression atmosphérique. Cette combinaison de la fluorescence laser avec détection sélective et de l'environnement d'une flamme a permis l'investigation à haute résolution de niveaux inaccessibles dans des expériences conventionelles effectuées à température ambiante. Les subdivisions spin-orbite, et les constantes rotationnelles et vibrationnelles ont été déterminées pour huit niveaux de vibration avec $K = v_2 + 1$, et pour les niveaux 010 $^2\Sigma$ et 020 $^2\Pi$; cette détermination a été faite principalement par ajustement sur les positions des têtes de bande en utilisant les constantes relatives à $A^2\Sigma^+$ obtenues antérieurement. Les résultats sont en bon accord avec les prédictions théoriques concernant les interactions Renner–Teller. La résonance de Fermi avec une force d'interaction de 10 cm^{-1} décrit bien les variations des subdivisions spin-orbite et des constantes rotationnelles pour quatre niveaux avec $v_1 = 1$.

Can. J. Phys. 62, 1488 (1984)

1. Introduction

Nonzero electronic orbital angular momentum in a normally linear triatomic molecule strongly affects the vibrational level pattern, producing a phenomenon generally known as the Renner–Teller effect. Predicted theoretically (1) approximately 25 years before the first experimental observation, it received further theoretical attention, notably in the work of Pople (2) and Hougen (3); extensions of the theory and a comprehensive discussion have appeared in a series of recent papers by Jungen and Merer (4, 5). The first linear molecule for which observation of the Renner–Teller effect was reported (6) was $X^2\Pi_i$ NCO, the subject of this paper. Other $^2\Pi$ species exhibiting the Renner–Teller effect in experimentally observed spectra include NCS, N_3, CCN, CNC, C_3, and BO_2, citations for which may be found in ref. 4 save for some more recent studies on BO_2 (7).

The electronic spectroscopy of NCO itself has been extensively studied. The classic work by Dixon (6) consisted of absorption measurements in a flash photolysis system; it has been repeated and extended in a more recent experiment by Bolman *et al.* (8). In each case very high resolution was achieved, although the low temperature of the system restricted the number of accessible ground state vibrational and rotational levels. More recently, laser-induced fluorescence (LIF) studies have been performed. The first of these (9) consisted of measurements of the $A^2\Sigma^+ - X^2\Pi$ emission spectrum following laser excitation of NCO in an Ar matrix. The precision, estimated at ± 2 cm^{-1}, furnished vibrational spacing information in the matrix environment that agreed with conventional infrared absorption matrix studies (10). In a room temperature discharge flow system, measurements (B. J. Sullivan, D. R. Crosley, and G. P. Smith, manuscript in preparation) of the LIF emission spectrum (± 5 cm^{-1}) were made for excitation of both the $A-X$ and $B^2\Pi - X^2\Pi$ systems, yielding similar information for the gas phase. (Other LIF experiments in a flow system (11) have concentrated on lifetime measurements and spectroscopic data were not reported). Finally, it has been found that one of the fixed-frequency lines of an Ar laser overlaps the $Q_2(31)$ line of the (000)–100) band of the $A-X$ system (12) of NCO in a flame. Rotationally resolved (± 1.8 cm^{-1}) fluorescence spectra of the emission lines from the pumped $F_2(31)$ level to the (000), 100, and 001 levels of $X^2\Pi$ have been used to obtain spectral constants for these states (13).

We describe here a study of the spectroscopy of several higher-lying levels of the ground $X^2\Pi$ state of NCO, using wavelength-selective detection of fluorescence excited by a tunable laser in NCO present in an atmospheric pressure flame. The laser bandwidth of 0.3 cm^{-1} determines our spectral resolution. The high temperature of the flame produces significant popu-

lations in excited vibrational levels. The dual selectivity of LIF, through tuning both the laser and the wavelength of the detected fluorescence, permits a discrimination among overlapped bands not possible in conventional absorption spectroscopy. (Although conventional emission spectra of NCO have not been reported at a resolution comparable to the studies cited, it would likely be too congested to be useful).

Using some rotational analyses but primarily fits of band-head positions with previously measured (6, 8) constants for the $A^2\Sigma^+$ state, we have obtained spin-orbit splittings, and vibrational and rotational constants for several excited vibrational levels not previously studied. Values of α_e and variations in A for each type of vibration, and cross anharmonicities are measured. Differences in both spin-orbit splitting and the values of B for the separate spin-orbit components are explained in terms of Fermi-resonance interactions. Other values are compared with expectations based on the Renner–Teller theory.

Part of the initial motivation for our study was the establishment of the LIF signatures of NCO (and NH_2) in flames so as to permit their measurement in combustion research; those aspects have been separately reported (14). The LIF spectroscopy of atoms and diatomics in flames has undergone rapid recent development as a tool for the understanding of flame chemistry (15). In the present study, the flames serve as a tool for obtaining new spectral information. They were the initial source for knowledge on the existence of and spectral data for many free radicals, especially diatomics (16), but have recently not been utilized much for spectroscopic purposes. The rapid collisional rates in an atmospheric pressure flame affect the emission patterns of the laser-excited molecules and greatly reduce the overall quantum yield of fluorescence compared with that in a low-pressure system (17). This does not, however, cause complications for purely spectroscopic studies with LIF so long as some emission can be found. This combination, the resolution and selectivity of LIF with the abundant number of vibrationally excited transient species in atmospheric pressure flames, offers much promise for expanding our spectroscopic understanding of small free radicals.

2. Vibrational energy levels in a $^2\Pi$ triatomic

Here we briefly define the parameters needed to describe the vibrational energy level pattern when the Renner–Teller effect is present, as manifested for the bending vibration (v_2) of a $^2\Pi$ triatomic tending toward Hund's case (a) behavior. This is the situation appropriate to NCO. More general and comprehensive discussions can be found elsewhere (1–5).

Needed for the description are the Renner parameter

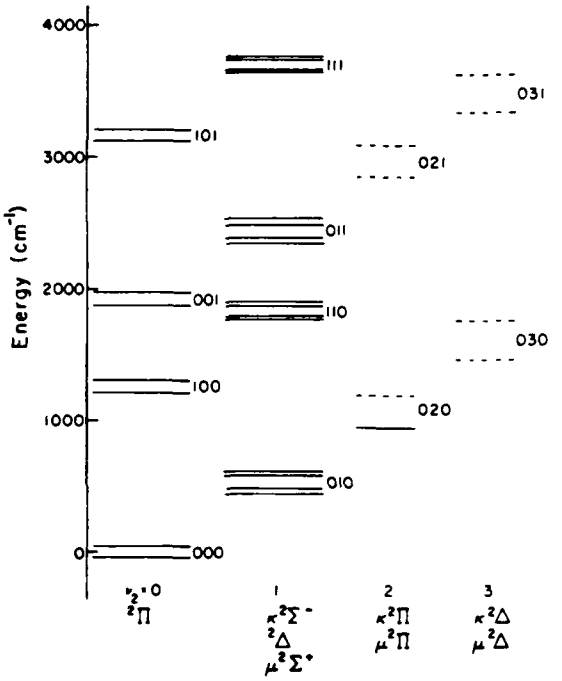

FIG. 1. Energy levels of NCO ($X^2\Pi_i$) observed in this study (solid lines) plus others involved in Fermi resonance (dashed lines). The levels are organized horizontally according to the value of v_2. Term symbols for each set are given below; the spin splitting of the κ and μ sets is not distinguished in the figure.

ϵ, the spin-orbit constant A, and the harmonic bending frequency ω_2. ϵ is a measure of the splitting between the two Born–Oppenheimer potential curves that touch at the linear configuration to form the $^2\Pi$ state. A represents the coupling between spin and orbital angular momentum. The effective value of the spin-orbit splitting in a given level depends on the value of v_2 and K. K, the total angular momentum along the internuclear axis is the sum of the projections of the orbital (Λ) and vibrational (l) angular momenta. Useful also is the angle β, which represents the relative degree of Renner–Teller and spin-orbit splittings:

$$[1] \quad \tan 2\beta = \epsilon\omega_2[(v_2 + 1)^2 - K^2]^{1/2}/A$$

β is needed for the expression of a given level (v_2K) in terms of the basis sets $|\Lambda, v_2, l\rangle$ and $|\Lambda - 2, v_2, l + 2\rangle$; for the pertinent states in NCO, β is in the range 60–80°.

The rotational levels within each vibrational level are described with rotational and centrifugal distortion constants B and D, a spin-rotation interaction constant γ, and, where appropriate ($K > 0$), doubling constants p and q.

There is finally a small but significant contribution

(5, 18) caused by the mixing of the Π electronic state with upper Σ and Δ states. This leads to an additional energy term $g_A|K|$ to be added to all levels. For NCO ($X^2\Pi_i$), g_A has been found (8) to be 3.64 cm^{-1}, falling within the range 3−5 cm^{-1} indicated for several triatomic nonhydrides (18). We will adopt this previously determined value in our analyses, as it is indistinguishable from anharmonicity effects in our range of data.

Expressions for the vibrational term values may be found in ref. 4, and those for the rotational energies in refs. 3 and 8. The vibrational pattern is illustrated in Fig. 1. When $K = v_2 + 1$, which includes the single pair of Π levels for $v_2 = 0$, there exists a pair of spin-orbit states spearated by

$$[2] \quad A_{\text{eff}} = A\left[1 - \frac{1}{8}\epsilon^2 K(K+1)\right]$$

In NCO, the states are inverted so that the one with $\Omega = K + \frac{1}{2}$ lies lower. For $K > 0$, there are four states forming two pairs of spin doublets. The pairs are separated by $2r$ where

$$[3] \quad r = \frac{1}{2}\{A^2 + \epsilon^2\omega_2^2[(v_2+1)^2 - K^2]\}^{1/2}$$

and each doublet exhibits a small, effective, spin-orbit splitting $\epsilon^2\omega_2 A K\Sigma/4r$, reflecting the quenching of Λ by l. The upper component (denoted by κ) is regular while the lower component (μ) is inverted. For $K = 0$, one finds a pair of states (also denoted κ and μ) separated by $2r$; the upper is labeled $^2\Sigma^-$ and the lower is labeled $^2\Sigma^+$.

Fermi-resonance interactions can also occur between levels (v_1, v_2, v_3) and $(v_1 - 1, v_2 + 2, v_3)$. Hougen (19) has treated the case of Fermi interactions in Π electronic states. The interactions occur only between states of the same K value, and there are two different possible matrix elements involved. The first, denoted by W_1, connects states having the same value of Λ and l, while the second, W_2, connects Λ and l with $\Lambda \pm 2, l \mp 2$. In most of the cases investigated (6, 7), W_1 is found to be in the order of tens of cm^{-1} while W_2 is close to zero. Now each spin-orbit component is an admixture of $\Lambda = 1, l$ and $\Lambda = -1, l + 2$ as described by the angle β (see [1]), and the overall Fermi interaction for a given pair of states must include this. Thus, for example, the $^2\Pi_{1/2}$ component of (1, 0, 0) will interact more strongly with the $\mu^2\Pi_{1/2}$ state (0, 2, 0) than with the $\kappa^2\Pi_{1/2}$ state, while the $^2\Pi_{1/2}$ state of (1, 0, 0) interacts more with $\kappa^2\Pi_{1/2}$ than with $\mu^2\Pi_{1/2}$ (see Fig. 1). The appropriate strengths W can be calculated using β and Hougen's equations (19) given a value for W_1.

The rotational constants are also affected by the Fermi resonance (20). The resulting B values are given in terms of those for the unperturbed states and the mixing coefficient ξ between the states,

$$[4] \quad \begin{aligned} B_1 &= \xi^2 B_1^0 + \sqrt{1-\xi^2}\, B_2^0 \\ B_2 &= \sqrt{1-\xi^2}\, B_1^0 + \xi^2 B_2^0 \end{aligned}$$

Because the α_e values for the stretch and bend are opposite in sign, this can be consequential.

A complete calculation of the interaction of each $^2\Pi$ component of the 100 level with both the corresponding κ and μ components involves a 3 × 3 matrix. Even so, the values of the energy separations and the W_i's pertinent to NCO make sufficient a sum of 2 × 2 treatments involving each level separately, which more transparently shows the effects discussed in the following.

3. Experimental

3.1 Method

The experimental method was quite straightforward and will be outlined here; further details, especially those pertinent to LIF flame diagnostics measurements, may be found in ref. 14. Rich flames of CH_4 and N_2O at atmospheric pressure were stabilized on a slot burner patterned after a type designed explicitly for laser probing (21). An excimer laser pumped a dye laser, operated with various dyes over the range 420−500 nm. The laser bandwidth, as determined by scans over isolated lines in the CN molecule where the Doppler contribution did not complicate matters, was 0.3 cm^{-1}. The beam was directed into the flame zone where the NCO concentration was highest. We did not directly measure the temperature in our flame, but it is expected (13) to be ~2400 K in this region. The Doppler width for NCO at this temperature is 0.12 cm^{-1}, so the laser line width limits the resolution.

The fluorescence at right angles to the beam was focussed onto the slit of a 0.35-m monochromator having a resolution of 22 Å/mm. The slit was oriented parallel to the laser beam, but we often used an aperture to limit the effective height to the center 5 mm. It was operated at a 2-mm width although the laser beam image was slightly smaller than this so that the resolution was ~3 nm. The fluorescence was detected with a photomultiplier whose output was amplified, processed with a gated integrator, and recorded on a strip chart as the laser was scanned. (A few scans were also taken using a photomultiplier and an interference filter having a peak transmission at 440 nm and a bandwidth of 8 nm.)

The spectrometer was set at 440.0 or 437.5 nm to view emission in the 000 → 000 band, or at 435.0 nm to view emission in the 010 → 010 band. In addition to the selective detection of certain excitation bands, as described later, this served to filter out strong fluorescence excitations of the CH, CN, and C_2 radicals, which were present in the wavelength regions covered

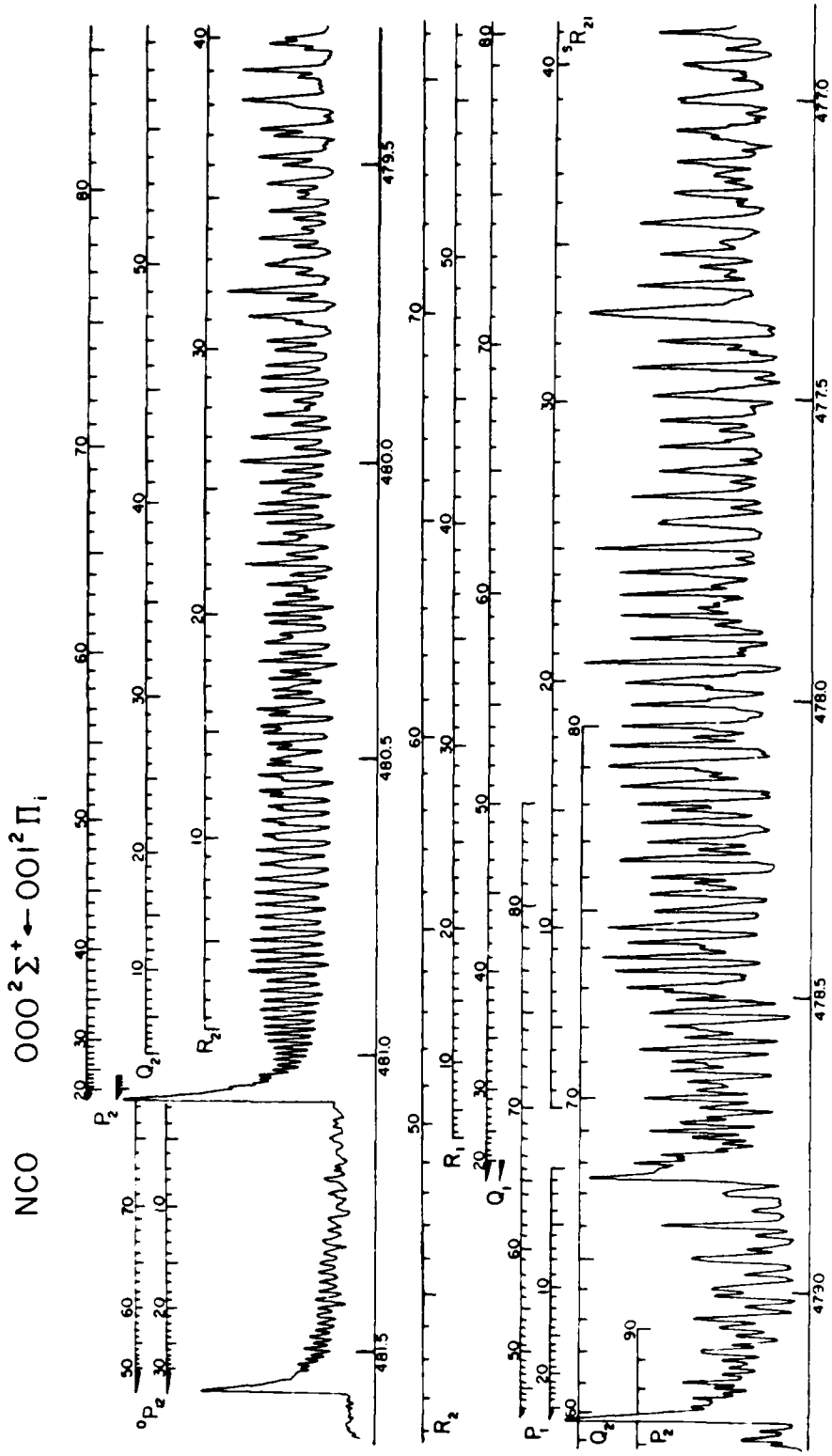

FIG. 2. Excitation scan in the region of the (00) (01) band. The monochromator is set at 440 nm to detect only emission from (00) of the $A^2\Sigma^+$ state. Rotational line assignments and wavelengths are from calculations using the constants determined from the band heads, as described in the text. The line labels shown are $J = 1/2$ for all branches.

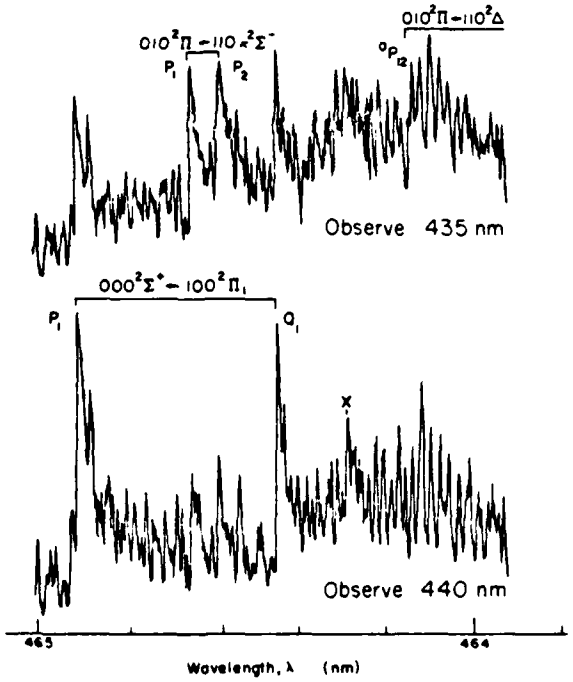

FIG. 3. (Lower panel) A portion of excitation scans showing the P_1 and Q_1 heads of the 000−100 band. The monochromator is tuned to 440 nm so that only this band is observed. (Upper panel) Excitation scan of the same region but with the monochromator set at 435 nm to detect emission from 010 of the $A^2\Sigma^+$ state. Here the 000−100 band is suppressed and the P_1 and P_2 heads of 010−110 $\kappa\ ^2\Sigma^-$ and the $^oP_{12}$ head of 010−110 $^2\Delta_{1/2}$ appear. This illustrates the ability to distinguish among congested spectra using selectively detected LIF. (The band head marked X, prominent in the lower scan, is thus far unassigned.)

However, the presence of these diatomics proved very useful for calibration of the laser wavelength. For these purposes, we tuned the spectrometer to 431 or 388 nm to detect the $\Delta v = 0$ bands of $A^2\Delta - X^2\Pi$ CH or $B^2\Sigma^+ - X^2\Sigma^+$ CN respectively. The 0−1 band of CH (22) was used for calibration in these studies. Further corroboration was obtained by comparison of measured line positions in the 000−000 and 010−010 bands with the tables of Dixon (6) and Bolman *et al.* (8). We estimate an overall absolute accuracy of ± 0.5 cm^{-1} for our measurements, while relative line positions in a given band (more pertinent to most of our results) are accurate to within the laser bandwidth, <0.2% of the scan ranges used.

3.2 Results

The overall spectral region covered includes the 000−000 band, the 000−010 band allowed by $\Sigma - \Pi$ mixing (23), and numerous other hot bands. The spectrum to the shorter wavelength side of the 000−000 band at 438−404 nm is very congested (see ref. 14 for a survey scan), and our concentration here has been primarily on hot bands to the red side, where the upper $A^2\Sigma^+$ vibrational level involved in the absorption is 000 or 010.

A scan of a small portion of the 000−001 region is shown in Fig. 2. This exhibits the full rotational resolution capability of the laser; it is from scans of this resolution that the data were taken for quantitative analysis.

For the scan in Fig. 2, the spectrometer was set at 440.0 nm to detect fluorescence originating from the 000 level populated by the 000−001 absorption. When the spectrometer setting is changed, other bands appear in the same excitation region. An example is shown in Fig. 3. The lower panel is a part of the spectrum of the 000−100 band (like that shown in Fig. 2 for the 000−001 region) and was detected at 440 nm. For the scan in the upper panel, the spectrometer was set at 435 nm (recall that bandpass is 3 nm), where the 010 level of the $A^2\Sigma^+$ state emits in the 010−010 band. Lines from the 000−100 band are now greatly suppressed (although not entirely eliminated), while features belonging to the 010−110 band, as marked in the figure, stand out.

Figure 4 shows two bands of different types. In the top panel is exhibited the 000 $^2\Sigma^+ - 010\ \mu\ ^2\Sigma^+$ band, and the lower trace shows the 010 $^2\Pi - 020\ \mu\ ^2\Pi$ transition. This selective detection of LIF using a spectrometer has been essential in picking out bands associated with excited bending levels of the ground state. Clearly, a conventional absorption spectrum or even broad-band-detected LIF would be too congested to permit identification of any but the most intense features.

For this approach to be successful, it is important that the bulk of the emission come from the pumped level itself. That is, the 010−110 band would be more noticeable in the lower scan in Fig. 3 if vibrational transfer in $A^2\Sigma^+$ from the 010 to the 000 level had occurred to a significant degree. Because the two $A^2\Sigma^+$ levels in question are separated by only 680 cm^{-1}, compared with $kT \sim 1600$ cm^{-1} in this region, upward vibrational transfer with a rate related to the downward one by detailed balancing (as observed in OH in flames (24)) could cause 000−100 contamination in the upper scan of Fig. 4. In the flame at atmospheric pressure, collision processes fully control the fate of the upper state level populations (17). The fact that the two scans in Fig. 4 are different then means that the collisional quenching rate is rapid compared with vibrational energy transfer between the 010 and 0 0 levels of $A^2\Sigma^+$. This condition is necessary for selective detection of the LIF to be successful. It is generally true

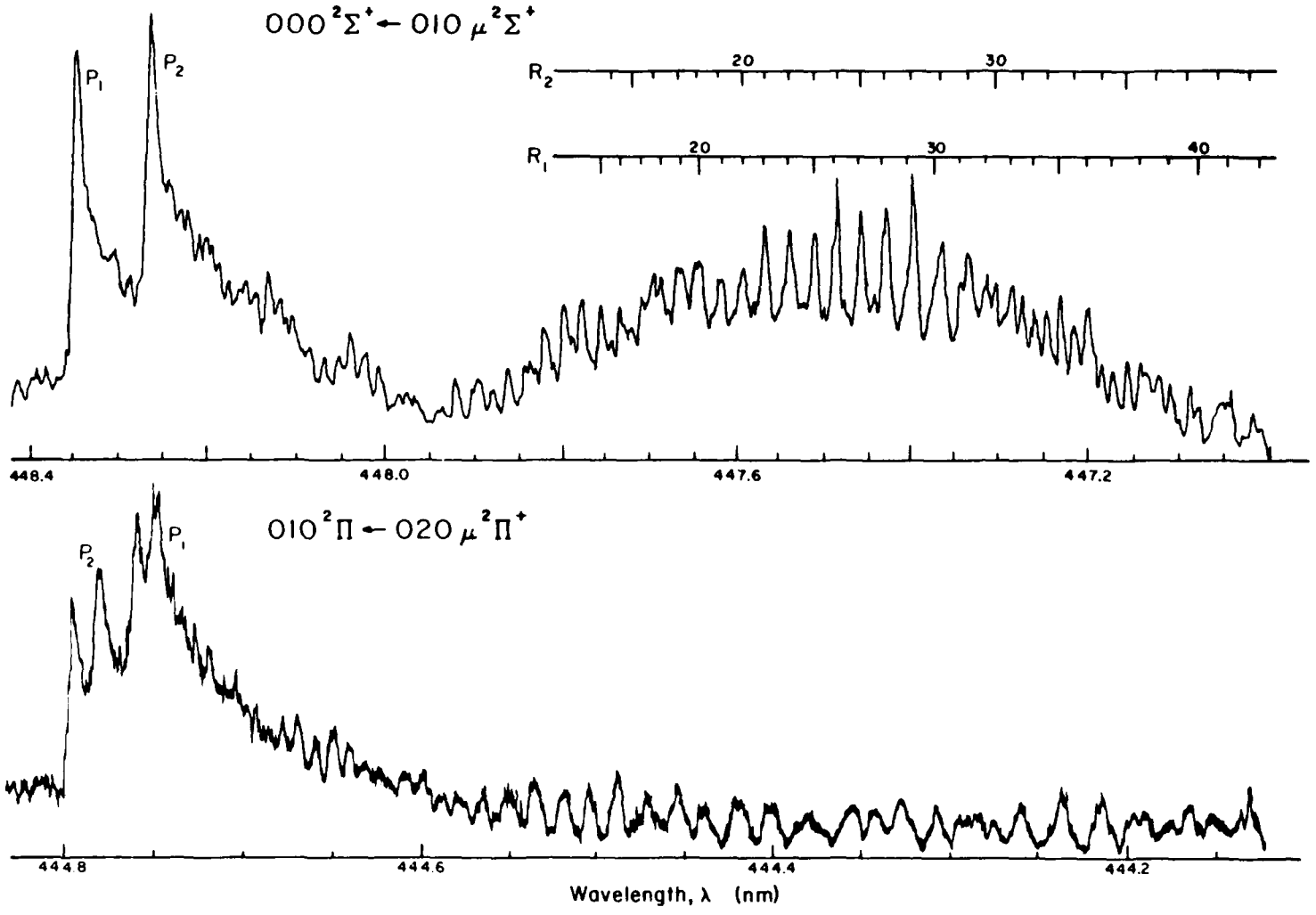

FIG. 4. "Forbidden" $\Delta K = 0$ bands. Each has only P- and R-branches, which are marked for the $\Sigma' - \Sigma'$ band in the upper panel. The P band heads of the $\Pi - \Pi$ band in the lower panel are marked. There are four heads altogether due to the K doubling in the upper and lower states. The R-branches (unmarked) lie to shorter wavelengths in the figure. The monochromator was set to 440 and 435 nm for the top and bottom scans respectively. Note that the horizontal scale is expanded in the lower scan compared with the upper one.

TABLE 1. $A^2\Sigma^+$ rotational constants fixed in fits (cm^{-1})

	Bolman *et al.* (8)[a]	Dixon (6)
	000 Level	
B	0.402163	0.40211
10^6D	0.190	0.177
$10^3\gamma$	0.52	≤1.5
	010 Level	
B	0.402725	0.402677
10^6D	0.161 (0.188)[b]	—
$10^3\gamma$	0.73 (0.36)[b]	—
10^3q	−0.651	0.661[c]

[a]Used in fit.
[b]Alternative values from other bands.
[c]Sign not determined.

in the few cases of diatomic radicals that have been studied (17), and for NH_2 (14). A direct study of collisional phenomena for NCO in flames forms part of our future plans.

4. Data analysis

4.1 Method

Most of the quantitative data were in the form of accurately determined band-head positions, whose spacings were suitable for determining vibronic term energies, rotational constants, and (where applicable) spin-orbit splitting constants. This was done using the appropriate equations for the vibrational and rotational term values of $X^2\Pi_i$.

The upper states were always the 000 level of $A^2\Sigma^+$ for excitation from $v_1 0 v_3$ of $X^2\Pi_i$, or the 010 level for excitation from $v_1 1 v_3$. The spectral constants for these electronically excited levels were held fixed throughout the analysis. The $A^2\Sigma^+$ energy expressions used are given in ref. 8. The upper state bending vibration term value has been reported as 680.83 and 680.77 cm^{-1} in refs. 6 and 8, respectively; we used the latter value. Values of the electronic energy are 22 754.07 and 22 753.98 cm^{-1} from refs. 8 and 6 respectively. $\epsilon\omega_2$ in the expression for r was taken as −76.9 cm^{-1}, as determined in ref. 8 for the $0v_20$ sequence. It was fixed at this value throughout irrespective of possible variation of ϵ with v_1 or v_3. The remainder of the constants were taken from ref. 8; these are listed in Table 1 together with those reported in ref. 6 for comparison.

Trial fits to the full set of rotational lines in our 000−000 and 000−001 band data showed that we could not obtain improved values of D for the $X^2\Pi_i$ state, or independently determined values of the Λ-doubling parameters p and q. These too were fixed in our band-head position fits at the values determined by Bolman *et al.* (8) for the 000 level: $D = 1.93 \times 10^{-7}$ cm^{-1}, $p = 2.70 \times 10^{-3}$ cm^{-1}, and $q = 6.2 \times 10^{-5}$ cm^{-1}. Although the values reported in ref. 6 are ~25% smaller, this difference has negligible effect on our fits. The value of $\gamma = -1.5 \times 10^{-3}$ cm^{-1} in the $B - \frac{1}{2}\gamma$ replacement term was taken from a microwave measurement (25); again the precise value does not affect our results.

For the $000 - v_1 0 v_3$ bands having $^2\Pi$ symmetry in the ground state, there are four prominent heads (see Fig. 2): $^0P_{12}$, P_2, P_1, and Q_1. These form our set of data, which are then fitted to the three constants E_v, A, and B. In spite of the fact that three constants are fitted to four data, the results are precise because of the lack of correlation between the fitted values. The $^0P_{12} - P_2$ and $P_1 - Q_1$ splittings are sensitive to the value of B, while the $P_1 - P_2$ separation yields A. Determination of the band origin (E_v) includes some contribution from both B and A, but comes primarily from the overall wavelength.

For transitions involving $^2\Delta$ levels of $010 - v_1 1 v_3$ transitions, the same four band heads are present and they are fitted in the same way. We found it more difficult to precisely pick out the $^0P_{12}$ head and the results have larger uncertainty (see Fig. 3).

For bands involving $^2\Sigma$ components of the $X^2\Pi$ states in $010 - v_1 1 v_3$ bands, there are only two well-defined heads (P_1 and P_2) for each of the $\mu^2\Sigma^+$ and $\kappa^2\Sigma^-$ components (see Fig. 3). The $000\ ^2\Sigma^+ - 010$ $\mu^2\Sigma^+$ and $010\ ^2\Pi - 020\ ^2\Pi$ bands exhibited in Fig. 4 are forbidden in a first approximation because $\Delta K = \Delta\Lambda$. A small amount of mixing of the $A^2\Sigma^+$ and $X^2\Pi$ states (23) furnishes the finite intensities. Each of these bands has only P- and R-branches; in the $\Pi - \Pi$ case, there is a pair of each type due to K doubling in the upper and lower states. In all of these cases, the A and B values were calculated using theoretical considerations, and were used to determine vibrational term values $E_{v,K}$.

For the 000−200 band, only the $^2\Pi_{3/2}$ heads ($^0P_2$ and P_2) could be identified with certainty. A B value could be determined, but independent spin-orbit splitting or term values could not be obtained.

4.2 Errors

Uncertainties in the fitted constants were estimated by forcing small variations in the fitted values and recalculating the band-head positions. Refitting after fixing one of the constants at a wrong value confirmed the small correlation among A, B, and E_v. For the best-determined bands, Π levels of $v_1 0 v_3$, we recurrently obtained sharp minima in χ^2 values with σ much smaller than the laser line width. From the results of these trials, we conservatively estimate for the Π levels that the B values carry an uncertainty of 0.0002 cm^{-1}

TABLE 2. Vibrational term values (cm $^{-1}$)

Reference	Bondybey and English (9)	Milligan and Jacox (10)	Sullivan *et al.*[a]		Wong *et al.* (13)	This work
Method	matrix fluorescence spectra	matrix infrared spectra	gas-phase fluorescence spectra: experiment	gas-phase fluorescence spectra: calculated	gas-phase fluorescence spectra	excitation spectra
Error	±2	±2	±10	±8	—	±0.5
010[b]	531	—	—	—	—	533.7
100	1272	1275	1270	1276	1270±2.7	1270.4
110	1823	—	—	—	—	1821.5
001[c]	1923	1922	1912	1914	1921.06±0.89	1921.8
011	2438	—	—	—	—	2441.5
101	3167	—	3157	3162	—	3168.0
111	3706	—	—	—	—	3704.1

[a] B. J. Sullivan, D. R. Crosley, and G. P. Smith, manuscript in preparation.
[b] Also 533.6 cm $^{-1}$ from absorption spectra (refs. 6 and 8).
[c] Also 1921.0 from laser magnetic ersonance, ref. 27.

TABLE 3. Spin-orbit coupling constant, A (cm $^{-1}$)

Level	Dixon (6)	Bolman *et al.* (8)	Wong *et al.* (13)	This work (±0.4)
0, 0, 0 $^2\Pi$	−95.59±0.02	−95.585±0.003	−95.35±0.44	−95.59
0, 1, 0 $^2\Delta$	−94.14±0.02[a]	−94.191±0.005	—	−94.02
1, 0, 0 $^2\Pi$	—	—	−90.17±0.40	−89.81
1, 1, 0 $^2\Delta$	—	—	—	−81.16
0, 0, 1 $^2\Pi$	—	—	−97.16±0.13	−97.07
0, 1, 1 $^2\Delta$	—	—	—	−95.20
1, 0, 1 $^2\Pi$	—	—	—	−92.13
1, 1, 1 $^2\Delta$	—	—	—	−85.35

[a] Refitted by Bolman *et al.* (8).

and the A values an uncertainty of 0.3 cm^{-1}. From the aforementioned fits, E_v is determined to ±0.2 cm^{-1}, but the additional error due to absolute wavelength calibration raises the overall uncertainty to between 0.5 and 0.8 cm^{-1}, depending on the band. For the Δ levels, similar uncertainties are estimated.

The $X^2\Pi_i$ constants are, of course, strongly correlated with the values chosen for $A^2\Sigma^+$, which have been fixed. There is, therefore, the possibility of further error in the absolute values, particularly for B. However, because common 000 or 010 upper states are involved in all the bands, the significance of differences in B among levels of $X^2\Pi_i$ is best gauged by the fit uncertainty estimates.

For each band, a full set of rotational lines was calculated using the constants fitted from band-head positions, and this was used for assignment purposes. For the 000−000 and 000−001 bands, quantitative comparison between our measured and calculated positions was made. There is some deviation for J values of 60−70 (this may indicate a need to revise the D, p, or q values, but we have not explored this aspect). Comparison of the 000−000 lines published by Bolman *et al.* (8) with our calculations was also performed. Good agreement was obtained with deviations less than the laser line width. These tests gave us additional confidence in the values calculated from band-head positions.

4.3 Results for levels with $K = v_2 + 1$

The fitted results for E_v, A, and B for the $v_1 0 v_3$ and $v_1 1 v_3$ levels are presented in Tables 2−5 for bands with $K = v_2 + 1$. Results for other bands are collected in Table 6. Where comparisons exist, we have also listed values obtained by other investigators. In all such cases satisfactory agreement is seen, except for the matrix LIF value (9) for $E_v(200)$. This may be an erroneous assignment; our assignment and measurement of Fig. 1*b* of ref. 9 suggests 2510 cm^{-1} as the result.

A comment is warranted concerning the B values for

TABLE 4. Rotational constant, B (cm^{-1})

Level	Dixon (6)	Bolman *et al.* (8)	Wong *et al.* (13)	This work (±0.0002)
0,0,0 $^2\Pi$	0.38940±0.00004	0.3895161[a]	0.3913±0.0030	0.38936
0,1,0 $^2\Delta$	0.39046±0.00002	0.3905470	—	0.39058
1,0,0 $^2\Pi$	—	—	0.3892±0.0027	0.38856[b]
1,1,0 $^2\Delta$	—	—	—	0.38990[b]
0,0,1 $^2\Pi$	—	—	0.3865±0.0009	0.38613
0,1,1 $^2\Delta$	—	—	—	0.38732
1,0,1 $^2\Pi$	—	—	—	0.38547[b]
1,1,1 $^2\Delta$	—	—	—	0.38747[b]

[a]From the microwave data of Amano and Hirota (27).
[b]Average, single-B, fitted value; see Table 5 and text for spin-component dependent B's.

TABLE 5. Spin-state specific rotational constants (cm^{-1})

	$^2\Pi$ (v_2 = 0)		$^2\Delta$ (v_2 = 1)	
v_1, v_3	1/2	3/2	3/2	5/2
0,0	0.38937	0.38932	0.39065	0.39046
1,0	0.38837	0.38907	0.38973	0.39047
0,1	0.38613	0.38616	0.38736	0.38732
1,1	0.38524	0.38603	0.38733	0.38782

000. In their rotational analysis, Bolman *et al.* (8) actually fixed the value at that determined by microwave data (25), 0.389516 cm^{-1}. They then used this to determine a B value for the 000 level of $A^2\Sigma^+$. We in turn fixed $B(A^2\Sigma^+, 000)$ at the Bolman *et al.* (8) value, but recovered a slightly different B (000) in $X^2\Pi$, 0.38936 cm^{-1}. While the difference is less than our quoted error in B, we obtain a noticeably poorer fit if we force B to be 0.38952. Our result, in fact, agrees well with Dixon's (6), although we have fixed D' and D'' at the values given in ref. 8 whereas in ref. 6 they are both noticeably smaller, which may make this agreement fortuitous. We do not understand this discrepancy with the microwave data, even though it is minor.

The levels with $K = v_2 + 1$ have been fitted allowing separate values for different spin components. (Note this is not the same as the $B_{effective}$ value obtained (3) by expansion of the square root, as is often done.) The results, given in Table 5, show the same B value except when $v_1 = 1$. A plot of B (lower) − B (upper) is exhibited in Fig. 5. The lines drawn both have a slope of unity. The lower line has an intercept at the origin, and the upper line has an intercept reflecting the difference of 7×10^{-4} cm^{-1}. These differences, ΔB = B (upper spin component) − B (lower spin component), will be examined later in terms of Fermi interactions. Attempts to fit data using a single B value for both components in these levels resulted in a significantly poorer result, even though the differences expressed in Table 5 are not much larger than twice the estimated uncertainty of 0.0002 in each B-value determination. That is, ΔB is better determined than twice the error of the individual B's.

4.4 Results for other bands

Several bands involving the Σ levels belonging to vibrational levels with v_2 = 1 were identified. These were analyzed only to determine the corresponding band origins, by assuming that the appropriate A and B values may be taken from the $^2\Delta$ levels with the same value of v_2. This procedure is subject to some uncertainty, in view of Bolman *et al.*'s (8) finding that their fitted B's for the $\mu^2\Sigma^+$ and $\kappa^2\Sigma^-$ levels differed by 7×10^{-4} cm^{-1}, while that for the $^2\Delta$ (010) level from the microwave data (25) was in between. Also, A_2 may be calculated from $A_\Pi(000)$ or $A_\Delta(010)$; the values obtained differ by 0.4 cm^{-1}. Nonetheless, we proceeded, using the appropriate equations to determine the band origins. The estimated errors due to the assumptions on A and B are incorporated into the quoted uncertainties. This analysis was applied to the κ and μ levels of 010 and 110 and the $\kappa^2\Sigma^-$ level of 110. Neither the $\mu^2\Sigma^+$ level of 110 nor the Σ levels for 111 were identified with certainty.

In each case, the $P_1 - P_2$ spacings for each $^2\Sigma$ subband agreed well with calculated values, but the spacing between the $\mu^2\Sigma^+$ and $\kappa^2\Sigma^-$ bands differed from experiment by 0.9 cm^{-1} for 010 and 2.4 cm^{-1} in the case of 011. This suggests r is not calculated correctly and corresponds to differences in A of 2−4 cm^{-1} or in ϵ of 0.001−0.002 cm^{-1} compared with the nominal values.

The positions of the heads of the $000^2\Sigma^+ - 010^2\Sigma^+$ transition, fitted with the Bolman *et al.* (8) constants, yielded a band origin agreeing with that of ref. 8 within the 0.3-cm^{-1} laser line width. Individual line assignments and calculated energies also agreed well up to $\sim J = 40$, but there was a small (1−2 cm^{-1}) systematic difference between calculated and our measured posi-

TABLE 6. Band origins for other levels (cm^{-1})

$v_1 v_2 v_3$	Components	Origin	Ref. 9	Others
010	$\mu^2\Sigma^+$, $\kappa^2\Sigma^-$	531.9±0.8	529	531.8 (ref. 8)
110	$\kappa^2\Sigma^-$	1812±5	1805	—
011	$\mu^2\Sigma^+$, $\kappa^2\Sigma^-$	2440.3±0.8	2436	—
020	$\mu^2\Pi$	948±10	933	—
200	$^2\Pi_{1/2}$	2532.1±1.0	2366	2522, 2520[a]

[a]Experimental and calculated values, respectively, from B. J. Sullivan, D. R. Crosley, and G. P. Smith, manuscript in preparation.

tions for high J (60−70) R-branches. The $000^2\Sigma^+ - 010\kappa^2\Sigma^-$ band was absent (<10% of the $\mu^2\Sigma^+$ subband) in accordance with symmetry considerations.

The $010^2\Pi - 020\mu^2\Pi$ band, shown in Fig. 4, was fitted to obtain a term value for the $\mu^2\Pi$ level. The $010^2\Pi - 020\kappa^2\Pi$ band was sought but could not be found (intensity <10% of the $\mu^2\Pi$ level.) We see no obvious reason for its absence, but it agrees with the gas-phase, room-temperature, LIF experiments, (B. J. Sullivan, D. R. Crosley, and G. P. Smith, manuscript in preparation), where fluorescence from the pumped $010^2\Pi$ level to the $\mu^2\Pi$ level is observed, but that to the $\kappa^2\Pi$ level is not.

The $^2\Pi_{1/2}$ level of the 200 state was observed. The $^0P_{12}$ and P_2 branches were well formed. No clear P_1 or Q_1 band heads, however, stand out in the region 80−90 cm^{-1} to the red side, in contrast to the case for all the other bands with $K = v_2 + 1$. It is possible that Fermi resonance mixes the 200, 120, and 040 states so thoroughly as to dilute the intensity to the normal 200 $^2\Pi_{3/2}$ component.

The B value of the $^2\Pi_{1/2}$ component of the 200 state was found to be 0.38685 cm^{-1} from the $^0P_{12} - P_2$ separation. The term-value results, together with those from other investigations, are collected in Table 6.

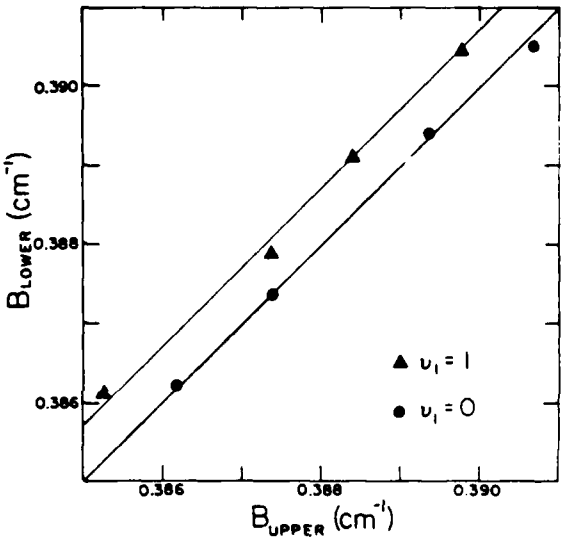

FIG. 5. Rotational constant B for the lower spin component vs. that of the upper spin component. Circles, levels not in Fermi resonance ($v_1 = 0$); triangles, levels in Fermi resonance ($v_1 = 1$). Each line has a slope of unity. The lower line has an intercept at the origin and the intercept of the upper one is offset by 7×10^{-4} cm^{-1}, reflecting the average difference ΔB for these levels.

5. Discussion: spectral constants and interactions

The spectral constants determined in this study and listed in Tables 2−6 represent a fairly comprehensive collection of vibrationally dependent parameters for a non-$^1\Sigma$ triatomic. The high precision furnished by the measured band-head positions and full rotational analysis is determined by trial fits as well as complete rotational line comparisons for 000−000 and 000−001 bands. Gratifyingly, agreement is seen to be within common experimental error wherever comparison measurements exist, although the precision varies for each quantity in a given experiment. For example, the Wong *et al.* study (13) used fluorescence lines from a common J'; their B values were determined with less precision than ours, but their $A(001)$ values, in particular, were determined with greater precision. Altogether, these results reflect the utility of selectivity detected LIF performed in a flame where large populations of vibrationally and rotationally excited free radicals exist.

In this section we further examine the trends in the spectral constants with vibrational level. They can be used to determine the gas-phase values of ω_1 and ω_3 for the first time, and to extract vibration−rotation interaction constants. For levels with $K = v_2 + 1$ and $v_1 = 1$, variations in the A values and the difference between B values for different spin components can be satisfactorily explained in terms of Fermi-resonant interactions. A small dependence of A on v_3 is observed for levels having $v_1 = 0$. In the next three subsections we consider the levels having $K = v_2 + 1$, and conclude this section with comments on the other levels studied.

5.1 *Vibrational constants*

From differences among the vibrational term values

TABLE 7. Vibrational constants (cm^{-1})

	Present results	Sullivan *et al.*[a]	Bondybey and English (9)	Dixon (6)	Bolman *et al.* (8)
x_{12}	17.0	—	4.5	—	—
x_{23}	−14.6	—	−8	—	—
x_{13}	−24.8	−27.8	−14	—	—
x_{11}	—	−10.3	−64	—	—
x_{22}	—	—	−2.7	0.7	—
x_{33}	—	−11.6	−17	—	—
$\omega_1 + 2x_{11}$[b]	1266.1	1273	1144	—	—
$\omega_2 + 3x_{22}$	536.4	—	521.4	541.5	537.5
$\omega_3 + 2x_{33}$	1949.1	1943	1889	—	—
ω_1[b]	1286.7	1293	1272	—	—
ω_2	534.3	—	529.5	539.4	535.4
ω_3	1972.5	1966	1923	—	—

[a]B. J. Sullivan, D. R. Crosley, and G. P. Smith, manuscript in preparation.
[b]Ignoring Fermi resonant contributions of ~4 cm^{-1}.

TABLE 8. Energies of levels involved in Fermi resonance (cm^{-1})

Level pair	$\|h\rangle$[a]	$\|b\rangle$[b]	$\|\kappa\rangle$[c]	$\|\mu\rangle$[d]
100−020	1315	1225	1193	954
110−030	1862	1781	1760	1474
101−021	3214	3122	3085	2847
111−031	3747	3661	3638	3352

[a]Upper component of (1, v_2, v_3), observed.
[b]Lower component of (1, v_2, v_3), observed.
[c]$^2\Pi_{1/2}$ or $^2\Delta_{3/2}$ component of κ (0, v_2 + 2, v_3), calculated.
[d]Average of μ (0, v_2 + 2, v_3), calculated.

listed in Table 2, we can obtain several vibrational constants. Given in the table are the energy level positions following removal of the spin-orbit, Renner–Teller, and rotational contributions discussed in Sect. 2. The term values for levels with $v_2 = 1$ are obtained from the Δ components. Because the energies still contain the $g_A|K|$ term (18), an amount $g_A = 3.6\ cm^{-1}$ must be subtracted from all differences between levels having $\Delta v_2 = 1$, in order to consider pure vibrational energy.

From the term value differences, we can obtain directly the three cross-anharmonic terms x_{12}, x_{23}, and x_{13}, and the sums $\omega_1 + 2x_{11}$, $\omega_2 + 3x_{22}$, and $\omega_3 + 2x_{33}$. The values for the two independent determinations of any single quantity have ±0.6 cm^{-1} uncertainty, although the full set is not overdetermined and all results (and errors) are correlated. The term $x_{11}l^2$ cannot be distinguished from x_{22} and $g_A|K|$ in these studies and is ignored. The results are listed in Table 7, where they are compared with medium-resolution determinations using fluorescence spectra following laser excitation of the $A\,^2\Sigma^+$ state in a matrix (9) and the $B\,^2\Pi_i$ state in the gas phase. The value of $\omega_2 + 3x_{22} = 536.4\ cm^{-1}$ may also be compared to 537.5 cm^{-1} using the Bolman *et al.* (8) value for ω_2 and Dixon's determination (6) of x_{22}, +0.7 cm^{-1}. Using this value for x_{22} and the gas-phase results (B. J. Sullivan, D. R. Crosley, and G. P. Smith, manuscript in preparation) for x_{11} and x_{33}, the harmonic constants ω_1, ω_2, and ω_3 can be obtained and are also listed together with comparisons.

Levels with $v_1 = 1$ can be in Fermi resonance with lower-lying levels having two more quanta in v_2, which would push the $v_1 = 1$ levels higher than their unperturbed vibrational energy. This has been ignored in the present vibrational analysis although the results of Sect. 5.3 show that it is present. The results from that treatment indicate an upward shift of ~2 cm^{-1} for 100 and 101, and ~6 cm^{-1} for 110 and 111 compared with the values obtained here. For the analysis method used, this means that our result for ω_1 would be ~4 cm^{-1} too high.

5.2 *Spin-orbit splittings*

An inspection of the set of A values in Table 3 reveals three distinct trends. We initially consider the four levels that cannot be involved in Fermi resonance. First, an increase in the magnitude of A occurs with stretching vibrations; from the pairs 001−000 and 011−010, this amounts to an increase of 1.3 cm^{-1} when v_3 is augmented by one quantum, perhaps reflecting a tendency toward a O—CN limit. Second, the ratios of A_{eff} for corresponding $^2\Delta$ and $^2\Pi$ levels may be compared. Equation 2 predicts a decrease of 1.0% in $|A_{eff}|$ in going from $^2\Pi$ to $^2\Delta$. The 010−000 pair shows a decrease of 1.6%, while that of the 011−001 set is 1.9%. Thus, these trends are reasonable agreement with expectations.

The other four levels show larger and less apparently regular differences. For each of these, $v_2 = 1$ so there exists the possibility for Fermi resonance. The distinction between these same two sets of levels is also

TABLE 9. Shifts due to Fermi resonance (cm^{-1})

	$\lvert\Delta A\rvert$		$10^4\,\Delta B$	
Level	calculated	measured	calculated	measured
$100\,^2\Pi$	6.3	5.8	6.4	7.0
$110\,^2\Delta$	11.5	12.9	13.7	7.4
$101\,^2\Pi$	5.6	4.9	5.4	7.9
$111\,^2\Delta$	9.7	9.9	8.6	4.9

evident in the ΔB values of Table 5. The spin-orbit splittings and ΔB values can be satisfactorily explained by this interaction.

The only levels that interact with ($v_1 = 1$, v_2, v_3) are the κ and μ pair of (0, $v_2 + 2$, v_3) lying at lower energies. A calculation was performed for the unperturbed energies of these latter states using the vibrational constants in Table 2, calculated pair splittings, and effective spin-orbit splittings. The results are listed in Table 8 along with the observed energies of the ($v_1 = 1$, v_2, v_3) levels. Because the lower spin component $|b\rangle$ of ($v_1 = 1$, v_2, v_3) always lies closer to its κ counterpart, and because it interacts more with the κ level than does the upper spin component $|h\rangle$, it will be affected more by the Fermi interaction. Thus, the energies of both components of the levels with $v_1 = 1$ are increased, the lower one more so, thus decreasing the apparent spin-orbit splitting.

The 110 and 111 levels lie closer to the perturbing levels, and would thus be expected to exhibit a larger change in A than 100 and 101. This is in accord with the results: the first pair has an $|A|$ that is 10–13 cm^{-1} lower than the corresponding non-Fermi interacting pair (010 and 011 respectively), while the decrease of $|A|$ in the latter is 5–6 cm^{-1} (compared with 000 and 001).

Needed for a quantitative calculation of the energies of the interacting pair are the energies in Table 8 and an estimate of the interaction strengths W. These are given for the four possible interactions $b-\kappa$, $b-\mu$, $h-\kappa$, and $h-\mu$ using [1] to describe the levels and the matrix elements for Fermi resonance given by Hougen (20). Of the two Fermi interaction terms W_1 and W_2 for a $^2\Pi$ triatomic, W_1 might be expected to be 10–40 cm^{-1} and W_2 to be near zero. Our data do not permit determination of both with confidence, and we set $W_2 = 0$ in Hougen's equations.

A straightforward fit of W_1 shows that an excellent description of the $|A|$ values is obtained for an interaction constant of $W_1 = 10.1$ cm^{-1}. (This corresponds to $W_{b\kappa} = 15.7$, $W_{h\kappa} = 9.7$, $W_{b\mu} = -13.1$, and $W_{h\mu} = -18.0$ cm^{-1}.) The results for the calculated vs. measured shifts of the spin-orbit splitting are given in Table 9. The calculations predict that the $|h\rangle$ component in each case is shifted upwards by 1.8 cm^{-1} owing to interaction with the μ and κ states, and that the $|b\rangle$ component is shifted upwards 0.8 cm^{-1} by interaction with μ. The remainder arises from the $b-\kappa$ interaction, leading to the net shifts $|\Delta A|$ listed.

The agreement seen in Table 9, involving calculated level positions and only W_1 as an adjustable parameter, is quite good, and constitutes a satisfactory description of the variation in spin-orbit splitting due to Fermi interaction.

TABLE 10. Rotation–vibration interaction constants (10^{-4} cm^{-1})

	Band combinations	α
α_1	100–000	1.00
	101–001	0.89
	110–010	0.92
	average	0.94
	ref. 13	2.1
α_2	010–000	−1.22
	110–100	−1.36
	011–001	−1.19
	average	−1.26
	ref. 6	−1.06
	ref. 8	−1.03
α_3	001–000	3.23
	011–010	3.26
	101–100	3.13
	average	3.21
	ref. 13	4.8

5.3 Rotational constants

We first consider differences in B values, as listed in Table 4, to obtain results for α_1. For levels with $v_1 = 0$, the average B is used. When $v_1 = 1$, the β value of the lower spin component $|b\rangle$ is affected by Fermi resonance, but the upper component $|h\rangle$ is not significantly perturbed. We therefore take the B value of the $|h\rangle$ component to represent that of the unperturbed state. B-value differences involving the 111 level do not fit the patterns well. We do not know the reason why, but it is ignored in the analysis.

The results for the α's listed in Table 10 show consistent results. Results from other investigations exist only for a single pair of levels in each case (see Table 4). Our results for α_1 and α_3 are one-half and two-thirds, respectively of those found by Wong *et al.* (13), although not outside their error bars. Our results agree well with those of Dixon (6) and Bolman *et al.* (8) for α_2.

For levels involved in Fermi resonance, that is, the lower spin components $|h\rangle$ of those levels having $v_1 = 1$, the rotational constants are affected (see [4]). Be-

cause $\alpha_2 > 0$ and $\alpha_1 < 0$, the $(v_1 = 1, v_2, v_3)$ levels have a smaller B than the perturbing $(v_1 = 0, v_2 + 2, v_3)$ levels in each case; thus the B of the $|b\rangle$ component should be greater than that of the $|h\rangle$ component. This is in agreement with the experimental results (Table 5 and Fig. 5). The levels not in Fermi resonance have $\Delta B = (-6 \pm 9) \times 10^{-5}$ cm^{-1} while those with $v_1 = 1$ have $\Delta B = (68 \pm 13) \times 10^{-5}$ cm^{-1}.

The predicted ΔB due to Fermi interaction was calculated according to [4], considering only the κ level as perturbing. The B for the unperturbed $v_1 = 1$ level was set equal to that of the upper spin component, which is little mixed by the interaction. The B for each $(v_1 = 0, v_2 + 2, v_3)$ level was calculated using the α constants of Table 9. We assume for the present purpose that the rotational constant within these bending levels does not depend on K or the κ, μ ordering, despite the fact that Bolman *et al.* (8) found a difference of 0.0009 cm^{-1} in the B values for $\kappa\,^2\Sigma$ and $\mu\,^2\Sigma^+$ of the 010 level. W_1 as determined from the $|\Delta A|$ splittings in the preceding section was used to compute the mixing coefficients ξ.

The results are given in Table 9. As with the $|\Delta A|$ values, the predicted and experimental results are sensibly ordered and of the correct overall size. Thus, the Fermi interaction with $W_1 = 10.1$ cm^{-1} satisfactorily describes both the spin-orbit splitting and rotational constant differences for all four vibrational levels.

5.4 Results for other levels

The vibrational term values of the $^2\Sigma$ and $^2\Delta$ pairs of levels of a $(v_1, v_2 = 1, v_3)$ level should differ by an amount (8) $2gK - 1/2\epsilon^2\omega_2$ or 1.8 cm^{-1}. This prediction is well borne out by the values in Tables 2 and 6. The difference is 1.8 cm^{-1} for the 010 set and 1.2 cm^{-1} for the 011 set. In the case of 110, the difference is 10 ± 5 cm^{-1}, perhaps reflecting the additional upward shift due to the Fermi resonance with 030.

The term value for 200, 2532 cm^{-1}, was obtained from the measured term value for the $^2\Pi_{1/2}$ component, 2580 cm^{-1}, assuming that this component is $0.5A_{200}$ higher than the vibrational energy. This may be compared with a value of 2521 cm^{-1} calculated using the constants from this work and the low-pressure results (B. J. Sullivan, D. R. Crosley, and G. P. Smith, manuscript in preparation) given in Table 7. The difference may be partly due to an overall upward shift due to Fermi interaction with both 120 and 040.

The B value for the $^2\Pi_{1/2}$ 200 level does not conform to $\alpha_1 = 0.94 \times 10^{-4}$ as given in Table 10: $B(200) - B(100) = 1.52 \times 10^{-3}$ cm^{-1}. The reason for this difference, however, cannot be found in Fermi resonance because the $^2\Pi_{1/2}$ level is little affected and the difference would be smaller, not larger.

The value given for the vibrational term value of 200 from the matrix fluorescence spectra (9) is much lower than that obtained here. Our inspection of Fig. 1*b* of ref. 9 suggests a 200 assignment with a term value of 2510 cm^{-1}. This may also be the reason for the large magnitude of x_{11} from the matrix work (see Table 7).

Recall that while the $^rP_{1/2}$ and P_2 heads belonging to the $^2\Pi_{1/2}$ component of 200 were well defined, the P_1 and Q_1 heads associated with $^2\Pi_{3/2}$ did not stand out. There are possible heads ~74 and ~105 cm^{-1} to the red side. It is possible that here the Fermi resonances cause significant mixing and dilute the oscillator strength over two or three $^2\Pi_{3/2}$ components. A future experiment to address this question would involve scanning the monochromator so as to obtain a fluorescence spectrum from each excitation, so as to ascertain the principal identity of each of the head features.

6. Summary

This study has demonstrated the promise for spectroscopic determinations using selectively detected LIF in a flame environment where a copious number of vibrationally and rotationally excited radical species exist. Vibrational, rotational, and spin-orbit constants have been obtained for several levels of NCO ($X^2\Pi_i$) inaccessible using conventional spectroscopic methods. A description in terms of Renner–Teller interactions, with a previously known parameter $\epsilon = 0.144$ cm^{-1}, and Fermi resonances, with a newly determined $W_1 = 10.1$ cm^{-1}, provides excellent agreement with measured quantities.

Acknowledgments

We thank Bill Anderson for sending us a copy of ref. 13 in advance of its publication. This research was supported by the U.S. Army Research Office.

1. R. Renner, Z. Phys. **92**, 172 (1934). G. Herzberg. Electronic spectra of polyatomic molecules. D. Van Nostrand Company, Inc., New York, NY. 1966. pp. 26–38.
2. J. A. Pople. Mol. Phys. **3**, 16 (1960).
3. J. T. Hougen. J. Chem. Phys. **36**, 519 (1962).
4. Ch. Jungen and A. J. Merer. Molecular spectroscopy, modern research. *Edited by* K. N. Rao and C. W. Mathews. Academic Press Inc., New York, NY. 1976. Chapt. 3.
5. Ch. Jungen and A. J. Merer. Mol. Phys. **40**, 1 (1960).
6. R. N. Dixon. Philos. Trans. R. Soc. London Ser. A. **252**, 165 (1980).
7. D. K. Russell, M. Kroll, and R. A. Beaudet. J. Chem. Phys. **66**, 1999 (1977). R. N. Dixon, D. Field, and M. Noble. Chem. Phys. Lett. **50**, 1 (1977). A. Fried and C. W. Mathews. Chem. Phys. Lett. **52**, 363 (1977). K. G. Weyer, R. A. Beaudet, R. Straubinger, and H. Walther. Chem. Phys. **47**, 171 (1980).
8. P. S. H. Bolman, J. M. Brown, A. Carrington, I.

KOPP, and D. A. RAMSAY. Proc. R. Soc. London Ser. A. **343**, 17 (1975).
9. V. E. BONDYBEY and J. H. ENGLISH. J. Chem. Phys. **67**, 2868 (1977).
10. D. E. MILLIGAN and M. E. JACOX. J. Chem. Phys. **47**, 5157 (1967).
11. H. REISLER, M. MANGIR, and C. WITTIG. Chem. Phys. Lett. **47**, 49 (1980); G. HANCOCK and G. W. KETLEY. J. Chem. Soc. Faraday Trans. II, **78**, 1283 (1982); T. R. CHARLTON, T. OKAMURA, and B. A. THRUSH. Chem. Phys. Lett. **89**, 98 1982; B. J. SULLIVAN, G. P. SMITH, and D. R. CROSLEY. Chem. Phys. Lett. **96**, 307 (1983).
12. W. R. ANDERSON, J. A. VANDERKOFF, A. J. KOTLAR, M. A. DEWILDE, and R. A. BEYER. J. Chem. Phys. **77**, 1677 (1982).
13. K. N. WONG, W. R. ANDERSON, A. J. KOTLAR, and J. A. VANDERHOFF. J. Chem. Phys. **81**, 2970 (1984).
14. R. A. COPELAND, D. R. CROSLEY, and G. P. SMITH. Symposium (International) on Combustion, 20th. The Combustion Institute, Pittsburgh, PA. 1984. In press.
15. D. R. CROSLEY (*Editor*). Laser probes of combustion chemistry. Am. Chem. Soc. Symposium Series. Vol. 134, 1980; D. R. CROSLEY and G. P. SMITH. Opt. Eng. **22**, 545 (1983).
16. G. HERZBERG. Spectra of diatomic molecules. 2nd ed. D. Van Nostrand Company Inc., New York, NY. 1950.
17. D. R. CROSLEY. Opt. Eng. **20**, 511 (1981).
18. J. M. BROWN. J. Mol. Spect. **68**, 412 (1977).
19. J. T. HOUGEN. J. Chem. Phys. **37**, 403 (1962).
20. G. HERZBERG. Infrared and raman spectra. D. Van Nostrand Company Inc., New York, NY. 1945. p. 378.
21. R. A. BEYER and M. A. DEWILDE. Rev. Sci. Instrum. **53**, 103 (1982).
22. C. E. MOORE and H. P. BROIDA. J. Res. Nat. Bur. Stand. Sect. A, **63**, 1 (1959).
23. P. S. H. BOLMAN and J. M. BROWN. Chem. Phys. Lett. **21**, 213 (1973).
24. G. P. SMITH and D. R. CROSLEY. Appl. Opt. **22**, 1428 (1983).
25. S. SAITO and T. AMANO. J. Mol. Spectrosc. **34**, 383 (1970).
26. C. E. BARNES, J. M. BROWN, A. D. FACKERELL, and T. J. SEARS. J. Mol. Spectrosc. **92**, 485 (1982).
27. T. AMANO and E. HIROTA. J. Chem. Phys. **57**, 5608 (1972).

J. Quant. Spectrosc. Radiat. Transfer Vol. 33, No. 6, pp. 591–595, 1985
Printed in Great Britain

0022-4073/85 $3.00 + .00

RELATIVE TRANSITION PROBABILITY MEASUREMENTS IN THE A–X AND B–X SYSTEMS OF CH

NANCY L. GARLAND and DAVID R. CROSLEY
Molecular Physics Department, SRI International, Menlo Park, CA 94025, U.S.A.

(*Received* 26 *October* 1984)

Abstract—Relative Einstein emission coefficients have been measured for transitions from the $v' = 0$ and 1 levels in the $A^2\Delta$–$X^2\Pi$ and $B^2\Sigma^-$–$X^2\Pi$ systems of the CH radical. The measurements were made in an atmospheric pressure methane–air flame, and the results are compared with theoretical calculations.

INTRODUCTION

Emission from the CH radical is responsible for the familiar violet coloration of hydrocarbon flames. This emission has been used in studies of the combustion of practical systems, such as pulse combustors and gas turbine engines, to locate the position of the reaction zone of the flame. CH has also been observed in absorption in flames and is readily detectable using laser-induced fluorescence (LIF). Its emission and absorption are found in systems of astrophysical interest, in the spectra of comets and stars.

Quantitative measurements of CH concentrations and experiments investigations of energy transfer in the radical[1] require knowledge of relative and absolute transition probabilities for different vibrational bands. We report here measurements of relative transition probability ratios for several bands in the $A^2\Delta$–$X^2\Pi$ and $B^2\Sigma^-$–$X^2\Pi$ systems of CH in the blue and near ultraviolet. The experiments were performed in an atmospheric pressure flame, and the results are compared with theoretical calculations involving electronic transition moments which vary with internuclear distance. Although the precision of the experimental results ranges from 10 to 20%, they are adequate to establish the form of the transition moment and for use in applications of emission and LIF monitoring of CH.

EXPERIMENTAL METHOD AND RESULTS

A methane–air flame was burned at atmospheric pressure on a small torch burner. CH was present in copious quantity in the reaction zone, where the temperature, determined from excitation scans furnishing the ground state rotational population distribution, was 2040 K. An excimer laser was used to pump a dye laser whose beam was directed into the flame, exciting specific levels of the A or B state. The resulting fluorescence was collected at right angles and focused onto the slit of a 0.35-m focal length monochromator; the slit was aligned parallel to the laser beam. Following amplification, the signal was processed with a boxcar integrator and stored either on a strip-chart recorder or on a laboratory computer. The laser power was monitored during the runs to normalize the signals. The wavelength-dependent response of the spectrometer and photomultiplier detector was calibrated against a standard tungsten lamp.

With the laser wavelength fixed so as to excite a particular vibrational level v' in one of the electronic states, the spectrometer was scanned to measure the fluorescence intensity of each band emitted by that level. The observed bands and their wavelengths (Q-branch origins) are listed in Table 1. The resolution employed depended on the signal level and possible interference with other bands; it varied from 2 to 40 Å. Although the (1, 1) and (0, 0) bands of the A–X system are severely overlapped, the lack of significant vibrational transfer[1] in the flame permitted distinction between them when $v' = 1$ was pumped.

The experimental results for ratios of Einstein coefficients $A_{v'v''}$ for the $v' = 0$ and 1 levels in both the B and A states are given in Table 2. Listed in Table 3 are ratios of the vibrational transition probabilities

$$p_{v'v''} \propto A_{v'v''}\lambda_{v'v''}^{-3}. \tag{1}$$

Table 1. Observed bands.

System	Band v',v"	Wavelength nm	Franck-Condon factor[a]	Einstein emission coefficient sec^{-1}	Absorption oscillator strength
$A^2\Delta-X^2\Pi$	0,0	431.5	0.992	1.8×10^6	5.1×10^{-3}
	0,1	489.0	0.0072	2.7×10^4	9.9×10^{-5}
	1,0	385.9	0.0074	2.0×10^4	4.4×10^{-5}
	1,1	431.4	0.986	1.8×10^6	5.1×10^{-3}
	1,2	485.9	0.0056	3.9×10^4	1.4×10^{-4}
$B^2\Sigma^- - X^2\Pi$	0,0	388.6	0.865	2.8×10^6	3.2×10^{-3}
	0,1	435.3	0.114	1.7×10^5	2.4×10^{-4}
	1,0	363.3	0.118	8.8×10^5	8.8×10^{-4}
	1,1	403.4	0.569	1.8×10^6	2.2×10^{-3}
	1,2	450.4	0.171	2.9×10^5	4.4×10^{-4}

[a] Obtained from Morse potentials for A–X; from Ref. 7 for B–X.

The errors quoted arise from an estimate of the accuracy in each measurement, together with scatter in replicate measurements of the same ratio.

DISCUSSION

The transition probability for the (v', v'') band may be written in terms of an integral of the electronic transition moment $R_e(r)$ over the vibrational wave functions as

$$p_{v'v''} = \left| \int \phi_{v'}(r) R_e(r) \phi_{v''}(r)\, dr \right|^2, \tag{2}$$

where r is the internuclear distance.

$$R_e(r) = \int \Psi'_e(r, r_{el}) M(r, r_{el}) \Psi''_e(r, r_{el})\, d\tau_{el} \tag{3}$$

Table 2. Experimental results. Einstein emission coefficient ratios.

System	Ratio	Value
$A^2\Delta-X^2\Pi$	A_{01}/A_{00}	0.015 ± 0.005
	A_{12}/A_{11}	0.022 ± 0.002
	A_{10}/A_{12}	0.50 ± 0.12
$B^2\Sigma^- - X^2\Pi$	A_{01}/A_{00}	0.06 ± 0.02
	A_{10}/A_{11}	0.5 ± 0.2
	A_{12}/A_{10}	0.3 ± 0.1

Table 3. Vibrational band intensity ratios.

	This Study			
Ratio	Experiment	Calculated	Ref. 5	Ref. 6
$A^2\Delta$-$X^2\Pi$				
P_{01}/P_{00}	0.022 ± 0.007	0.022	0.031	7×10^{-5}
P_{10}/P_{11}	0.008 ± 0.002	4×10^{-4}	0.001	0.029
P_{12}/P_{11}	0.031 ± 0.003	0.031	0.064	0.005
$B^2\Sigma$-$X^2\Pi$				
P_{01}/P_{00}	0.08 ± 0.03	0.076	0.047	-
P_{10}/P_{11}	0.37 ± 0.15	0.30	0.72	-
P_{12}/P_{11}	0.17 ± 0.08	0.14	0.24	-

describes the probability of the electronic transition as a function of r; M is the transition dipole moment function.

The A–X transition of CH is highly diagonal, i.e. the potential curves for the two electronic states are nearly identical, and the wave functions are close to orthogonal. This fact is reflected in the small Franck–Condon factors

$$q_{v'v''} = \left| \int \phi_{v'} \phi_{v''} \, dr \right|^2 \tag{4}$$

for the off-diagonal ($\Delta v \neq 0$) bands (see Table 1). The relative values of $p_{v'v''}$ for these bands, while small, are larger than the relative $q_{v'v''}$ because regions of small and large r are weighted differently by the r-dependent transition moment, Eq. (3), reducing the degree of cancellation in the integral in Eq. (2). A proper theoretical description of the relative transition probabilities must thus take into account the variation of R_e with r, as is necessary in the A–X systems of the diatomic hydrides OH (Ref. 2) and NH (Ref. 3).

Functional forms of $R_e(r)$ have been calculated from *ab initio* wave functions for the A–X system of CH in three studies. Huo[4] found a nearly linear form when r was near the equilibrium value for the two states; however, the range covered in Ref. 4 is too restricted for the present purpose. Hinze *et al* (HLL)[5] have performed calculations over a larger range of r and used the resulting $R_e(r)$, together with ϕ_v from their theoretically obtained potentials, to determine $A_{v'v''}$. Larsson and Siegbahn (LS)[6] have used a slightly different basis set to calculate values of ϕ_v and $R_e(r)$. We have converted their reported band oscillator strengths to relative $p_{v'v''}$ for comparison with the experimental results. The results of HLL and LS, in the form of ratios of vibrational transition probabilities, are given in Table 2.

We have used Morse oscillator wave functions and a linear form of the electronic transition moment

$$R_e(r) = c(1 - \rho r), \tag{5}$$

with a slope determined by fitting the observed transition-probability ratios p_{01}/p_{00} and p_{12}/p_{11}. The Morse wave functions should be valid for the low v', v'' encountered here and should form a better representation of the A and X states of CH than the ϕ_v determined from the *ab initio* potentials. A reasonable description of the two ratios p_{01}/p_{00} and p_{12}/p_{11} can be obtained with a slope $\rho = 0.43$ Å^{-1}, but the calculated p_{10}/p_{11}

ratio is much too small compared with the experimental value. This is also the case for the HHL values. The results are listed in Table 3.

The r-centroid

$$\bar{r}_{v'v''} = \int \phi_{v'} r \phi_{v''} \, dr \Big/ \int \phi_{v'} \phi_{v''} \, dr \tag{6}$$

represents the average value of the internuclear distance sampled during the electronic transition for the (v', v'') band. Because it is larger for (1, 0) than for (1, 1) and $p_{10}/p_{11} \geq q_{10}/q_{11}$, no form of $R_e(r)$ as in Eq. (5) will correctly describe this ratio. An examination of the *ab initio* transition moments[5,6] shows at large r an upward deviation from the linear decrease, producing a larger transition probability ratio p_{10}/p_{11} than would be expected from the linear form. We conclude that a linear moment is clearly inappropriate, although neither *ab initio* calculation produces agreement with experiment.

For the B–X system, the single *ab initio* calculation by HLL can be well represented in linear form with a slope of 0.59 Å^{-1}. In this case we are, however, faced with a different theoretical problem. The form of the vibrational wave functions is highly uncertain. The $B^2\Sigma^-$ state has a very shallow potential, with only two bound vibrational levels for CH and three for the CD isotopic form. Consequently, Morse wave functions are not expected to form a valid representation of the $\phi_{v'}$. Available are $q_{v'v''}$ and $\bar{r}_{v'v''}$ values from RKR curves.[7] These incorporate a larger value of the anharmonicity in the B-state (374 cm^{-1}) than that currently accepted (230 cm^{-1}) from isotopic scaling from the CD value. Nonetheless, we used them to fit the experimental values for the vibrational transition probability ratios to a linear form for $R_e(r)$; we find a best-fit slope of $\rho = 0.443$ Å^{-1}. The calculated values are listed in Table 3 along with the experimental results and ratios from HLL.

Several radiative lifetime measurements have been made on the A-state and one on the B-state. The most reliable values appear to be 540 nsec for $v' = 0$ of $A^2\Delta$, from both a high-frequency deflection method[8] and an LIF measurement.[9] Only one measurement has been made for $B^2\Sigma^-$, also by high-frequency deflection; the result[8] for $v' = 0$ is 340 nsec. We combine these lifetimes with our experimental transition probability ratios, recalling that

$$A_{v'} = \sum_{v''} A_{v'v''}, \tag{7}$$

in order to calculate Einstein emission coefficients and absorption oscillator strengths for the bands studied here. The absorption oscillator strength for the B–X transition is half that of the emission oscillator strength, due to the difference in degeneracy between the two states. The results are listed in Table 1. Finally, we can compare the ratios of the oscillator strengths for the (0, 0) bands of the B–X and A–X systems with experimental results of Linevsky[10] using absorption in a graphite furnace containing H_2. Our value of $f_{0,0}(B)/f_{0,0}(A) = 0.62$ may be compared with Linevsky's experimental result of 0.61 ± 0.10.

In a hydride, with its large centrifugal distortion, the effective r-centroid within a vibrational band can increase with rotational quantum number J, causing a J-dependent transition probability and radiative lifetime.[11] Because of rapid rotational energy transfer in the flame, such a dependence was not observable in our experiments. However, measurements of the lifetime in both the A and B states[8] have been made as a function of J. For $B^2\Sigma^-$, an increase is found as J increases, consistent with a decrease in R_e with increasing internuclear distance. For $A^2\Delta$, the experimental results are not definitive.

The experimental uncertainties lead to errors of 5% in the results listed in Table 1 for the Einstein emission coefficients and absorption oscillator strengths for the (0, 0) bands of both systems and the (1, 1) band of A–X. Errors of 10–40% are present in the remainder of the results listed, as a direct consequence of the uncertainties listed in the first column of Table 1. This level of precision is adequate to demonstrate experimentally that the electronic transition moment for both systems decreases with r, and to furnish

transition probability information useful for the purposes noted in the Introduction. A more definitive test of the deviation from linearity of $R_e(r)$ of the A–X system will require more precise measurements and, if possible, extension to a larger range of v' and v''.

Acknowledgements—This study was supported, in part, by the U.S. Army Research Office, and in part, by the Basic Research Department of the Gas Research Institute.

REFERENCES

1. N. L. Garland and D. R. Crosley, Paper 84-61, Western States Meeting of the Combustion Institute, Stanford, California, October 1984; Comb. Flame (to be published).
2. D. R. Crosley and R. K. Lengel, *JQSRT* **15**, 579 (1975).
3. P. W. Fairchild, G. P. Smith, D. R. Crosley and J. B. Jeffries, *Chem Phys Lett.* **107**, 181 (1984).
4. W. M. Huo, *J Chem Phys* **49**, 1482 (1968).
5. J. Hinze, G. C. Lie and B. Liu, *Astrophys J.* **196**, 621 (1975).
6. M. Larsson and P. E. M. Siegbahn, *J Chem Phys.* **79**, 2270 (1983).
7. J. C. McCallum, W. R. Jarmain and R. W. Nicholls, Spectroscopic Report No. 1, Centre for Research in Experimental Space Science, York University, Toronto, Ontario (1970).
8. J. Brzozowski, P. Bunker, N. Elander and P. Erman, *Astrophys J* **207**, 414 (1976).
9. K. H. Becker, H. H. Brenig and T. Tatarczyk, *Chem Phys Lett* **71**, 242 (1980).
10. M. J. Linevsky, *J Chem Phys* **47**, 3485 (1967).
11. D. R. Crosley and R. K. Lengel, *JQSRT* **17**, 59 (1977).

Twentieth Symposium (International) on Combustion/The Combustion Institute, 1984/pp. 595–603

RATE CONSTANTS FOR USE IN MODELING*

D. M. GOLDEN AND C. W. LARSON
Department of Chemical Kinetics
SRI International, Menlo Park, CA 94025

The current status of quantitative understanding of reaction rate constant data for use in combustion modeling is discussed. It is pointed out that simple bimolecular and unimolecular reactions can be tabulated as functions of various physically meaningful parameters over wide ranges of temperature and pressure. Also discussed are the more complicated problems of complex surfaces and their manifestations. Major emphasis is placed on the underlying framework for critical evaluation of rate data.

We point out that currently used values for $2CH_3 \xrightarrow{\Delta} + C_2H_5 + H$ are incompatible with the reverse reaction and that the temperature dependence of the branching ratio $H + N_2O \begin{cases} \nearrow NH + NO \\ \searrow OH + N_2 \end{cases}$ can be understood in terms of an energy-dependent transition state for the NH channel.

Introduction

Computer-based modeling of chemical reaction systems is becoming very common.[1] The computational frontiers are constantly being pushed ahead and greater numbers of scientists have taken advantage of standard codes that have been developed.

Many modelers and compilers of combustion kinetic data have developed the habit of abstracting the literature for the necessary model inputs without critical analysis. Unfortunately, given the great difficulty of performing and understanding experiments, values that are both suspect on physical grounds and internally inconsistent often find their way into the data base.

As these chemical models are adapted for larger systems the need increases for an internally consistent method for critical evaluation of the rate constants that make up a given model, as well as for intercomparison of models. Rate constants must be correct not only in absolute magnitude at a given temperature but also with respect to their temperature, pressure, and environmental (i.e., nature of the colliding partners) variations. Furthermore, since complex chemical mechanisms invariably contain competing steps and the branching ratios evolving from these competitions may carry the mechanism in distinctly different directions, it is crucial to have a consistent treatment of competing pathways.

This paper reviews the guidelines already well established[2] for a framework in which to evaluate rate data. Also discussed will be those areas where this framework needs further substantiation. In addition, some development of the treatment of that increasingly ubiquitous class of reactions that appear to proceed via a bound intermediate will be presented.

It is intended to enable modelers to have the courage, based on knowledge, to extend individual rate parameters for elementary chemical reactions and chemical mechanisms beyond the range of current measurement. Indeed, this is a modeling requirement since most of the kinetic laboratory studies are performed at temperatures less than 1000 K and most of the flame temperatures of interest are between 1200 and 2000 K.

Ground Rules

Framework

The model for elementary reactions based on the transition state theory (TST) is discussed in most text books (see, for example, Ref. 2a). The entirety of chemical reactions is limited to two basic classes: 1) Simple bimolecular reactions, such as described by the potential surface in Fig. 1a, and 2) simple unimolecular reactions, such as described by the potential surface in Fig. 1b.

The barrier could be as small as zero, and often is. Reactions that follow pathways such as depicted in Fig. 1b are pressure and temperature depen-

*This work was supported by the U. S. Army Research Office (Contr. & No. DAAG29-80-K-0049).

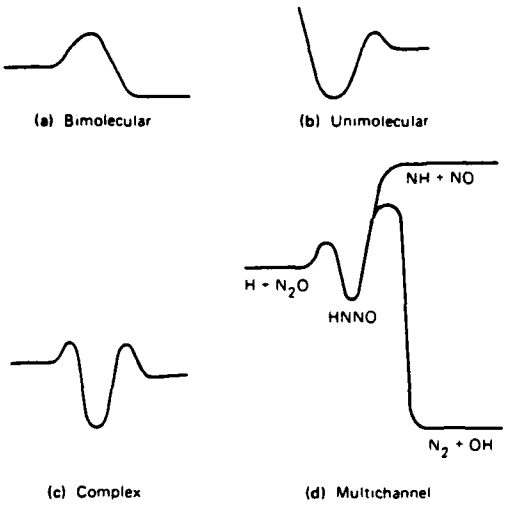

FIG. 1. Schematic potential energy surfaces for:
(a) simple bimolecular processes
(b) simple unimolecular processes
(c) complex elementary processes
(d) The two pathways for $H + N_2O$.

dent, and depend on the nature of the colliding partners, whereas those that follow potentials of the type in Fig. 1(a) are only temperature dependent. According to the principle of detailed balancing, bimolecular processes that are the reverse of a unimolecular decomposition are subject to *exactly* the same pressure and partner dependence. The complex surfaces (Figs. 1(c) and 1(d)) are combinations of the simple surfaces and are discussed later in this paper.

Simple Bimolecular Reactions

In TST the thermal (canonical) rate constant is expressed in terms of a single parameter, $\Delta G_T^{\ddagger}$, the free energy difference between transition state and reactants at the temperature T. (k_B is the Boltzmann constant and h is Planck's constant.)

$$k = \frac{k_B T}{h} \exp(-\Delta G_T^{\ddagger}/RT) \qquad (1)$$

Choice of units for k implies choice of standard state for $\Delta G_T^{\ddagger}$. $\Delta G_T^{\ddagger}$ is a function of temperature. This, along with the explicit first power of T in the transition state formula, implies that over any reasonable temperature range the rate constant should be described by at least three parameters.

$$k = AT^B \exp(-C/T). \qquad (2)$$

It is clear that these parameters may be understood in terms of molecular models for reactant and transition state and the nature of breaking and forming bonds, thus, the parameters are subject to evaluative criteria beyond the bounds of any particular experiment. Furthermore, physically reasonable parameters should enable rate constants to be extrapolated beyond the measured temperature range.

The parameters most easily subject to evaluative criteria are A and B which are related to $\Delta S^{\ddagger}$ (the entropy of activation) and $\Delta C_p^{\ddagger}$ (the heat capacity of activation) and thus to reactant and transition state structure. The parameter C, related to $\Delta H^{\ddagger}$ (the enthalpy of activation), requires potential surface information, but can often be judged based on comparison of similar reactions.

As has been stated many times previously, the ab initio evaluation of $\Delta S^{\ddagger}$ requires potential surface information, but limiting ranges can be deduced by chemical common sense, and comparison of homologous series forces a certain order.

As an example, consider the reaction:

$$O(^3P) + CH_4 \rightarrow OH + CH_3 \qquad (3)$$

This process has been well studied[4] up to ~2000 K from ~300 K. (Caution should be exercised concerning results from the low temperature experiments, since very small amounts of higher hydrocarbon impurities would consume significant quantities of O-atoms.) This process has also been the subject of analysis by transition state theory[2f,3] and the agreement on rate constant parameters is universal:

$$[k/(\mathrm{dm^3\ mole^{-1}\ s^{-1}})] = 10^{4.07} T^{2.06} \exp(-3540/T) \qquad (4)$$

On an Arrhenius plot ($\ln k$ vs T^{-1}), this expression produces a strongly curved line that yields values of k at 2000 K that are a factor of ten higher than would have been predicted by extrapolation of a straight line, two-parameter, Arrhenius fit to the data in the 300 to 800 K range.

It would be inconsistent then, when considering the reaction $O(^3P) + C_2H_6 \rightarrow C_2H_5 + OH$, to use a two-parameter expression determined in the low temperature range. Consistency demands that a model transition state be described based to some extent on $O + CH_4$, which, when its parameters are fit to the low temperature data, will automatically produce a curved Arrhenius plot that should be described with at least three parameters.

Of course, in a particular model study, the computed property of interest may not be sensitive to the curvature in the Arrhenius plot of any particular rate constant. Nevertheless, if the model is to be extrapolated to a different problem, the tem-

TABLE 1
Arrhenius parameters for H-atom abstraction from ethane*

Reaction	Set I*			Set II*		
	A	B	C	A	B	C
(a) $O + C_2H_6 \rightarrow OH + C_2H_5$	1.82E10	0	3070	1.5E10	0	3201
(b) $HO + C_2H_6 \rightarrow H_2O + C_2H_5$	6.31E10	0	1812	8.7E6	1.05	911
(c) $CH_3 + C_2H_6 \rightarrow CH_4 + C_2H_5$	5.5 E11	0	10820	5.5E-4	4.0	4167

*Units of k are dm^3 $mole^{-1}$ s^{-1}.

perature dependences of the rate constants should be consistent with what is understood from TST.

Two sets of bimolecular rate constant parameters for the reactions of O-atom, hydroxyl radical and methyl radical with ethane have recently been tabulated as follows: (There are others in the literature as well.)

The rate constants one calculates from each of these parameter sets agree to within a factor of two between 1000 and 2000 K. However, the direction of decrease of A-factors in parameter set I is inverted from the TST prediction. A-factors should decrease in this series of reactions in going from the atom to the diatom to the polyatomic species because the loss of rotational entropy accompanying formation of the series of transition states increases in this order. There are many examples in the modeling literature where relations among rate constant parameters of bimolecular reactions are inconsistent with simple TST constraints. In most cases where these constraints have been tested, they have been remarkably useful.[5]

Simple Unimolecular Reactions

Reactions that follow potential energy surfaces such as depicted in 1(b) may be described by the Lindemann mechanism[6]

$$A + M \underset{-1}{\overset{1}{\rightleftarrows}} A^* + M \qquad 5$$

$$A^* \xrightarrow{2} \text{Products}$$

These reactions are always the result of energy transfer by collision of the reactant A with bath gas M, step 1 and −1, and the spontaneous decomposition of the energized molecules A^*.

In the so-called "high pressure limit" the unimolecular rate constant may be described by TST in the same manner as were bimolecular reactions. Values of the A-factors and activation energy may be evaluated by consideration of the changes that occur upon formation of the transition state from the reactants. In general, the temperature dependence of the rate constant may also be represented by three parameters, but often two will suffice; see Fig. 2). Reverse bimolecular association processes may always be computed from the overall equilibrium constant. Adequate representation of the temperature dependence of the equilibrium constant will usually require at least three parameters as ΔC_p for the reactions is not usually zero.

The unimolecular reactions of interest may not be at their "high pressure limits," because spontaneous reaction of energized reactant (process 2) might be much faster than the collisional energizing process, thus, at lower pressures an equilibrium population would not be maintained. Under this condition canonical TST does not apply and the rate constant for unimolecular dissociation (and the re-

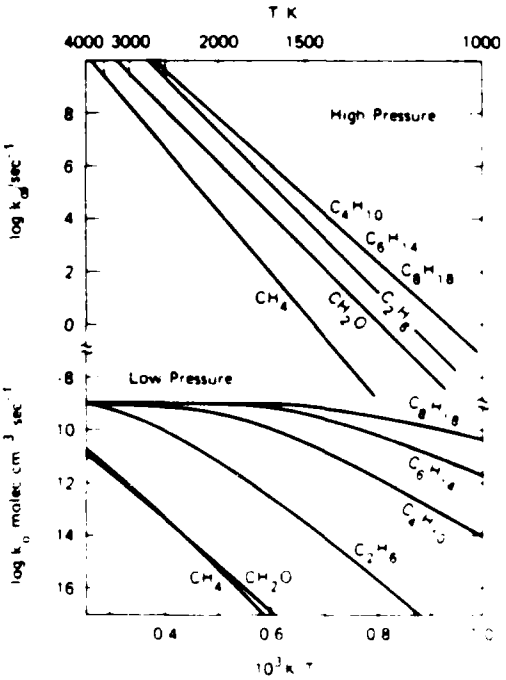

FIG. 2. Temperature dependence of k_∞ and k_0 for several fuel pyrolysis reactions. k_∞ in dm^3 mole^{-1} s^{-1} may be obtained by multiplying by 6×10^7

verse bimolecular association) becomes pressure dependent (fall-off).

According to standard unimolecular rate theory,[6] the observable rate constant $k_{uni}(T,M)$, may be evaluated by averaging the microcanonical specific rate of spontaneous decomposition of energized reactant, $k(E)$, over the appropriate non-equilibrium distribution function:

$$k_{uni}(T,M) = \int_o^\infty k(E) \frac{\omega}{\omega + k(E)} B(E)\, dE \qquad (6)$$

The effective rate of strong collisions of reactant with bath gas is denoted by ω, and $B(E)$ is the normalized Boltzmann distribution of reactant. The microcanonical rate constant, $k(E)$, may be evaluated quantum statistically (RRKM theory) but simpler approximations of the pressure dependence will usually suffice for modeling purposes (see below).

In Figure 3, RRKM calculated "fall-off" curves for butane and octane at 1000 K are compared with the Lindemann fall-off curve. The Lindemann fall-off curve, obtained by solution of the three differential rate equations of the Lindemann mechanism, has a particularly simple form explicit in pressure, viz.,

$$k_{uni}^{Lindemann}/k_\infty = (1 + k_\infty/k_o M)^{-1} \qquad (7)$$

The constants, k_o and k_∞, are functions only of temperature. $k_o M$ and k_∞ are the actual values of the unimolecular rate constant in the low-pressure ($M \to 0$) and high-pressure ($M \to \infty$) limit. The temperature dependence of k_o and k_∞, shown in Fig. 2 for a variety of hydrocarbon fuel pyrolysis reactions, may be represented adequately by three-parameter expressions of the same form as has been used for simple bimolecular reactions, equation (2). The k_o values plotted in Fig. 2 are strong collision values. Weak collisions can be adequately represented by a multiplicative factor (β_c) which effectively changes the A-factor.)

Troe[7] has demonstrated that accurate empirical relationships between the Lindemann and actual fall-off curves exist, viz.,

$$k_{uni}^{actual}(T,M) = k_{uni}^{Lindemann}(T,M)\, F(T,M) \qquad (8)$$

Troe shows that the "broadening factor," $F(T,M)$, may be written in a variety of universal forms of varying accuracy, the most simple of which is:

$$\log F(T,M) = [1 - (\log k_o M/k_\infty)^2]^{-1} \log F_c(T). \qquad (9)$$

In all of Troe's forms, the temperature dependence of $F(T,M)$, is carried entirely by $F_c(T)$, the broadening factor at the center of the fall-off (Figure 3).

Figure 4 shows $F_c(T)$ for a variety of fuel pyrolysis reactions. $F_c(T)$ may be adequately described by a three parameter function, viz.,

$$F_c(T) = a \exp(-b/T) + \exp(-T/c). \qquad (10)$$

This is slightly different from that suggested by Troe. In the limits of zero or infinite temperature or pressure, all unimolecular reactions approach Lindemann behavior and $F_c(T)$ and $F(T,M)$ approach unity.

Values of the broadening factor in regimes of pressure and temperature relevant to combustion processes (e.g., 1-atm ($\sim 10^5$ pa) and 1000 K to 2000 K) are unity for all small molecule fuels with energy thresholds around 420 kJ mol^{-1} (e.g., CH_4, NH_3, CH_2O) because unimolecular pyrolysis for these small molecules (a process important to initiation of combustion) is in its low pressure limit, $k_{uni} = k_o M$, Figure 5. Pyrolysis of larger molecule

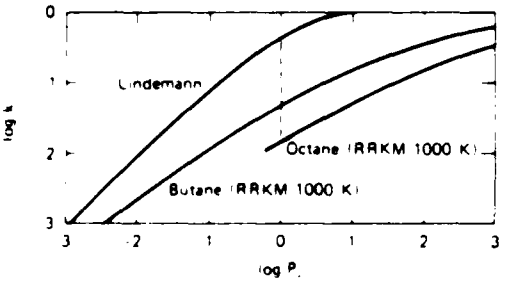

FIG. 3 Comparison between RRKM calculated fall-off and Lindemann fall-off on a reduced basis: reduced pressure = $P = k_o M/k_\infty$, and reduced rate constant = $k = k_{uni}/k_\infty$. At the center of the fall-off $P = 1$, $k^{Lindemann} = 0.5$, and $F = 0.5/k^{RRKM}$.

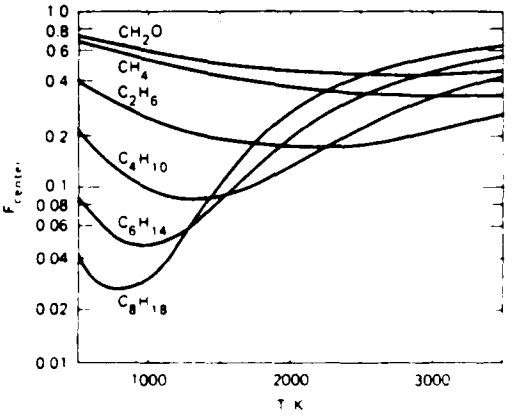

FIG. 4 Temperature dependence of the center broadening factor for several fuel pyrolysis reactions.

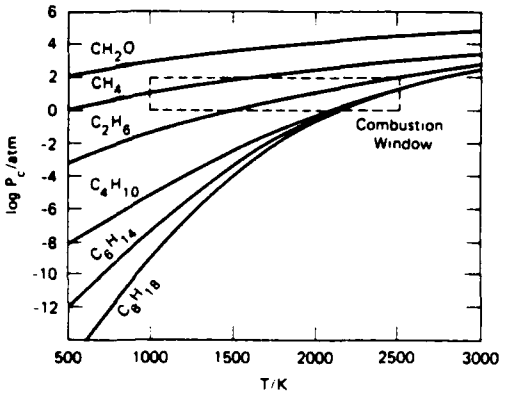

FIG. 5. The pressure at the fall-off center, P_c, as a function of temperature for several fuel pyrolysis reactions and the "combustion window," 1–100 atm and 1000–2500 K. Around atmospheric pressure, butane and larger molecular pyrolyze near their high pressure limit and methane and smaller molecules pyrolyze in their low pressure limit (1 atm ~ 10^5 pa).

fuels (with thresholds around 320 kJ/mol^{-1}, e.g., butane and larger molecules) also have unity broadening factors because $k_{uni} = k_\infty$. At atmospheric pressure and 1500 K, ethane pyrolysis is at the center of the fall-off, and its center broadening factor, also the maximum broadening factor, is around 0.2.

Thus, it seems proper to take into account our understanding of these processes by tabulating data for modeling purposes to be consistent with Troe's expressions. It is suggested in complete analogy to the tabulation of pressure-dependent association reactions by the NASA Stratospheric Rate Constant Evaluation Panel, that for a given reaction, values of the two sets of three parameters that will describe k_∞ and k_0, as well as the three parameters that are defined in equation (10), be tabulated. These nine parameters used with equations (8) and (9) describe $k(M,T)$ for the process well enough for the modeling exercise. It must be reiterated that these formulae allow considerable extrapolation far from the reported conditions.

Complex Elementary Processes

In its simplified form a chemical mechanism consists of a number of sequential and consecutive elementary reactions. It is usual to treat these independently in a model, describing each with $k(T)$ or $k(M,T)$ as appropriate (see previous discussion). There are, however, some oft-occurring instances in which elementary reactions cannot be separated in the usual way. Consider the reaction proceeding along the surface depicted in Fig. 1(c). (The barriers may be as low as zero.) Such a surface describes three processes: the unimolecular decomposition of substance Y via two pathways, the bimolecular reaction of A and B to form C and D (and possibly Y), or the reverse bimolecular reaction. In each case different non-thermal energy distributions (Chemical Activation) may obtain and simple canonical TST may be not applicable. However, if the pressure is sufficiently high so that substance Y is present in thermal equilibrium, the competing unimolecular processes

$$Y \xrightarrow{1} A + B \tag{11}$$

$$Y \xrightarrow{2} C + D \tag{12}$$

may be separately described by their respective k_∞ values, or the bimolecular process,

$$A + B \xrightarrow{k_{bi}} C + D, \tag{13}$$

can be written as the sum of the two reactions

$$A + B \xrightarrow{k_{-1}} Y \tag{14}$$

$$Y \xrightarrow{k_2} C + D \tag{15}$$

It is important to recognize that these simplifications do not apply for nonthermal distributions where the lifetime of Y is pressure dependent.[12d] In these cases the rate constants k_1, k_{-1}, and k_2 must be specified at the microcanonical level and the overall rate constant and branching ratios are pressure as well as temperature dependent. However, if $k_2 << k_1$, k_{bi} will be pressure independent.

For example, for the overall bimolecular reaction between methyl radicals

$$CH_3 + CH_3 \xrightarrow{k_{bi}} C_2H_5 + H, \tag{16}$$

We may depict this process by the scheme

$$\begin{array}{ccc} CH_3 + CH_3 & \underset{k_1}{\overset{k_{-1}}{\rightleftarrows}} & C_2H_6^* \\ & k_{-3}[M] \Big\uparrow \Big\downarrow k_3[M] & \\ & C_2H_6 \xrightarrow{k_2} C_2H_5 + H & \end{array} \tag{17}$$

The rate constant for H-atom formation may be written[6]

$$k_{bi} = K_{eq} \int_{E^0}^{\infty} \frac{k_1(E)k_2(E)[1 + (1 - p^2)\beta\omega/k_1(E)]\, B(E)dE}{k_1(E) + k_2(E) + \beta\omega} \tag{18}$$

K is the equilibrium constant for $2CH_3 \rightleftarrows C_2H_6$

and p is the probability that the thermal dissociation of C_2H_6 will produce H-atoms.

Under conditions where $k_2(E) << k_1(E)$, which apply here since the overall process is 40 kJ mol^{-1} endothermic, $p = 0$ and at all pressures $k_{bi} = K_{eq} k_2^*$. Thus, we have a simple means of evaluating experimental determinations of k_{bi}, since all the appropriate values of molecular parameters required to calculate k_2^* and K_{eq} are known or can be easily estimated.

Production of H-atoms by the methyl-methyl reaction has been advocated as an important contributor to the dominant pathways in methane combustion. The temperature dependence of the rate constant used in current modeling[1,4] ($10^{11.9}$ exp $-$ 26.5/RT dm^3 mol^{-1} sec^{-1}) is in substantial disagreement with the value $K_{eq}k_2^* = 10^{8.3}$ exp $-$ 10.0/RT, which agrees with new experimental evidence.[5] Thus, although the absolute value of the rate of the methyl-methyl reaction currently in use is correct at 1000 K, it is a factor of 16 too large at 1500 K and 64 too large at 2000 K. The consequences of this observation may impact strongly on the methane combustion model, especially at higher temperatures, where initiation and H-atom propagation reactions dominate the properties of the youngest parts of a flame.

When complex surfaces, such as depicted in Figure 1(c) give rise to situations in which $k_2(E) \approx k_1(E)$, the overall reaction may exhibit pressure as well as temperature dependence. The temperature dependence can easily give rise to a negative activation energy if the ratio $k_1(E)/k_2(E)$ increases with temperature.[2d]

Multi-Channel Bimolecular Processes-Branching

The potential energy surface shown in Fig. 1(d) is the result of recent state-of-the-art theoretical calculation for the H + N_2O system[9] and exemplifies a class of multi-channel bimolecular processes with branching that are common in combustion chemistry.

The kinetics of the overall bimolecular reactions, viz.,

$$H + N_2O \xrightarrow{k_{bi2}} OH + N_2 \qquad (19)$$

$$H + N_2O \xrightarrow{k_{bi3}} NH + NO \qquad (20)$$

may be deduced through analysis of the unimolecular reactions of intermediate HNNO.

Measures of the branching ratio, $R = k_{bi3}/k_{bi2}$, have been inferred at ~2000 K by direct observation of laser induced fluorescence from HN and OH in a H_2/N_2O flame and at 873 K in a static system.[10] The weak temperature dependence of $R_1R_{2000K} \sim 0.04$ and $R_{873K} \sim 0.004$) yields an apparent activation energy difference of only about 30 kJ/mol^{-1}, less than half the difference between the critical energy thresholds of the branches, 71 kJ/mol^{-1}, Figure 1(d).

The modeling of the observation of the very weak temperature dependence of branching may be carried out with a hindered Gorin model transition state[2,11] for reaction channel 3. Properties of the hindered Gorin model have been studied in the past[11] in connection with radical-radical recombinations and their reverse unimolecular bond scission.

It has been customary to evaluate the effect of momentum conservation constraints by use of the quasi-diatomic model.[6] Thus, an "effective" potential energy surface may be defined at any given temperature which conserves the overall rotational quantum number. On this surface, the dissociation energy of HNNO is less than its value at the absolute zero. In addition to this temperature dependent centrifugal energy effect, a temperature dependent hindrance parameter, η, causes the entropy of the transition modes in the hindered Gorin model to decrease with temperature.[11] In this case, the transition modes are the two overall rotations in the separated diatomics which become hindered internal rotors in the activated complex.

The empirical Gorin model hindrance parameter, is defined in terms of a ratio of A-factors, $A_H/A = (100 - \eta))/100$, where A_H and A are A factors for the hypothetical high pressure unimolecular reaction for the hindered and unhindered model, respectively.

In the case of the Channel 3 reaction, a hindrance parameter that varies between 84 and 99% (1000 K–2000 K) has been required to fit the observed branching ratio, k_{bi3}/k_{bi2}. The radical-radical interactions modeled in the past have also required values between 85 and 99.5% (220 K–1200 K). Thus, the ideas embraced by the hindered Gorin model, with $A_H/A \sim 0.2$ to 0.005, are appropriate for description of reactions involving simple bond fission. The consequence of using of the hindered Gorin model to predict the pressure and temperature dependence of k_{bi3} is to produce a nearly pressure independent Arrhenius plot and an activation energy and A-factor that decrease with increasing temperature. The consequences of this for the reverse reaction (−20) is the prediction of a negative activation energy.

Conclusions

This work describes the current status of the overview that is applicable to the critical evaluation of chemical rate data for combustion modeling. Specifically:

1. Simple bimolecular reactions should all be tabulated as a function of temperature alone.

Three parameters are required, and the parameters should be evaluated keeping in mind the relative values of appropriate physical quantities, such as $\Delta S^{\ddagger}$, $\Delta H^{\ddagger}$, and $\Delta C_p^{\ddagger}$.

2. Simple unimolecular reactions should be tabulated as a function of temperature and pressure. It is convenient to characterize the temperature dependence of both high and low pressure-limiting rate constants by three parameters. The fall-off curve can then be reproduced by a parameterization that requires three additional parameters.
3. Complex surfaces must be recognized and apparent bimolecular processes must be distinguished from simple bimolecular processes. The possibilities for both pressure dependence and negative activation energies for the former must be accounted for correctly.
4. Discussion of the important problem of energy transfer has been bypassed. Collisional rate constants and their temperature dependences must be expressed terms of the average energy transferred per collision.[12] In general, only empirical relationships currently exist.

REFERENCES

1. Westbrook, C. W. and Dryer, F. L., *Prog. Energy Comb. Sci. 10*, 1 (1984).
2. (a) Benson, S. W., *Thermochemical Kinetics*, 2nd Ed., John Wiley and Sons, Inc., 1976.
   (b) Golden, D. M., Fourteenth Symposium (International) on Combustion, p. 121, The Combustion Institute, 1973.
   (c) Golden, D. M., *Dynamics and Modeling of Reactive Systems*, (W. F. Stewart, W. H. Ray, C. C. Conley, Eds.), p. 315, Academic Press, 1980.
   (d) Golden, D. M., J. Phys. Chem. 83, 108 (1979).
3. Michael, J. V., Keil, D. G., and Klemm, R. B., Int. J. Chem. Kinetics *15*, 705 (1983), and references therein.
4. Levy, J. M. and Sarofim, A. F., Combustion and Flame *53*, 1 (1983).
5. (a) Cohen, N., Int. J. Chem. Kinetics *14*, 1339 (1982).
   (b) Cohen, N., Nineteenth Symposium (International) on Combustion, p. 31, The Combustion Institute, 1983.
6. (a) Forst, W., *Theory of Unimolecular Reactions*, Academic Press, 1973.
   (b) Robinson, P. J., and Holbrook, K. A., *Unimolecular Reactions*, John Wiley and Sons, Inc., NY, 1972.
7. (a) Troe, J., J. Phys. Chem. 83, 114 (1979), and references therein.
   (b) Troe, J., Ber. Bunsenges. Phys., Chem. 87, 167 (1983).
8. Keifer, J. H. and Budach, K. A., Int. J. Chem. Kinetics *16*, 679 (1984).
9. Melius, C. F. and Binkley, J. S., Private communication (1983).
10. (a) Cattolica, R., Snooke, M., Dean, A., *A Hydrogen-Nitrous Oxide Flame Study*, Paper presented at the 1982 Fall Meeting of the Combustion Institute, Sandia National Laboratories, Livermore, CA, 11–12 October 1983, Paper WSS/CI 82-95
    (b) Baldwin, R. R., Gethin, A., Plaistowe, J., Walker, R. W., Trans. Faraday Soc. I, 6, 1265 (1975).
11. (a) Smith, G. P. and Golden, D. M., Int. J. Chem. Kinetics *10*, 489 (1978).
    (b) Baldwin, A. C., Lewis, K. E., and Golden, D. M., Int. J. Chem. Kinetics *11*, 529 (1979).
12. Barker, J. R., J. Phys. Chem. 88, 11 (1984).

COMMENTS

J. E. Dove, University of Toronto, Canada. Dr. Golden has quite rightly stressed that one must consider possible non-Arrhenius effects when choosing values of rate constants for modeling. Indeed, since equilibrium constants in general do not rigorously obey an Arrhenius type of temperature dependence, the existence of the rate quotient law $k_r/k_f = K_{eq}$ already demonstrates that at least half of all rate constants must deviate somewhat from the Arrhenius law, and one hopes this will soon be accepted without argument.

However it should be emphasized that fitting rate constants to the modified Arrhenius form $AT^b \exp(-E/RT)$ does not necessarily solve the problem of extrapolation outside the temperature range of measurement. Unfortunately the exponent b is itself in principle temperature dependent. Using the statistical mechanical form of activated complex theory (ACT) of bimolecular reactions, and neglecting quantum tunneling and re-crossing effects, one can show from rather simple considerations about numbers of degrees of freedom that b tends to the value $(\Delta r - 1)/2$ at low temperatures where vibrations are only weakly excited and to $(3 - \Delta r)/2$ at high

temperatures where the vibrations approach classical behavior. Here, Δr is the change in total number of rotations (internal and external) in going from reactants to complex. For example, where the activated complex and both of the reactant species are nonlinear, $\Delta r = -3$, and b varies from -2 to $+3$ with increasing temperature. The thermodynamic form of ACT which Dr. Golden uses will give essentially the same result, but I feel that the physical meaning of b is easier to understand in the statistical mechanical formulation. (I cannot agree with the statement of another speaker that b has no physical significance.)

I would also like to support Dr. Golden's remarks about taking into account all reasonable possible elementary reactions when considering mechanism. The temptation to use only the minimum set of reactions which is needed to explain experimental results is strong, partly because it is usual in science to use minimum explanations, but also because it reduces the chances of one being accused of having enough non-fixed parameters to fit the proverbial elephant! However there is a very real danger of creating a false sense of security about the correctness or uniqueness of the resulting interpretation, if reactions which may be significant are omitted.

Authors' Reply. Professor Dove is, of course, correct in stating that "b" is temperature dependent. However, for most situations, the range he cites is much too great.

First of all, let me define some terms and at the same time point out that I don't consider that there is a difference between the "statistical mechanical" and "thermodynamic" forms of TST given the direct relationship of thermodynamic quantities to partition functions. Since thermodynamic quantities are usually tabulated for standard states of 1 atm at constant pressure, we note that, if for a simple bimolecular reaction

$$k/\text{con}^{-1}\,\text{time}^{-1} = AT^{b}\exp(-E/RT),$$

then

$$A = [R^2/(N_0 hT_0(\Delta C_p^{\ddagger}/R))]\exp[((\Delta S_{T_0}^{\ddagger}) - (\Delta C_p^{\ddagger})T_0/R]$$

$$b = ((\Delta C_p^{\ddagger}) + 2R)/R \quad (\Delta C_p^{\ddagger}) = (\Delta C_{p\,T} - \Delta C_{p\,T_0}^{\ddagger})/1$$

All standard states are 1 atm

$$E = \Delta H_{T_0}^{\ddagger} - (\Delta C_p^{\ddagger})T_0$$

For the reaction $A + B \rightarrow X^{\ddagger}$ we can define $\Delta r_{ex}^{\ddagger}$ = the change in external rotations going to the transition state $= n_{ex}^{\ddagger} = n_{ex}^{\ddagger} - n_{ex}^{R}$, where n_{ex}^{i} = # of external rotations for species i. $\Delta r_{in}^{\ddagger}$ = the analogous quantity for internal rotations.

Then,

$$\Delta C_p^{\ddagger}, \text{ trans} = -\frac{5}{2}R$$

$$\Delta C^{\ddagger}, \text{ ext rot} = \Delta r_{ex}^{\ddagger} * R$$

$$\Delta C^{\ddagger}, \text{ int rot} = \Delta r_{in}^{\ddagger} * \frac{R}{2} \quad \text{at high temperature}$$

$$= 0 \quad \text{at low temperature}$$

$$\Delta C_{vib}^{\ddagger} = (5 - \Delta r_{in}^{\ddagger}) * R \quad \text{at high temperature}$$

$$= 0 \quad \text{at low temperature}$$

Thus,

$$\Delta C_p^{\ddagger}(\text{high temp}) = \frac{R}{2}(5 + \Delta r_{ex}^{\ddagger} - \Delta r_{in}^{\ddagger})$$

$$b(\text{high temp}) = \frac{1}{2}(9 + \Delta r_{ex}^{\ddagger} - \Delta r_{in}^{\ddagger})$$

$$\Delta C_p^{\ddagger}(\text{low temp}) = \frac{R}{2}(\Delta r_{ex}^{\ddagger} - 5)$$

$$b(\text{low temp}) = \frac{1}{2}(\Delta r_{ex}^{\ddagger} - 1)$$

Thus, while I agree with Professor Dove's low-temperature value of b, I don't agree with his assessment of the high-temperature value. If $\Delta r_{in}^{\ddagger} = 0$ and $\Delta r_{ex}^{\ddagger} = -3$, we would get the same limiting values.

$$\Delta C_p^{\ddagger}(\text{high temp}) = R,\ b(\text{high temp}) = 3$$

$$= 2\ \text{e.u.}$$

$$\Delta C_p^{\ddagger}(\text{low temp}) = -4R,\ b(\text{low temp}) = -2$$

$$= -8\ \text{e.u.}$$

This may be compared with calculations for the reaction $O + CH_4 \rightarrow [OH \cdots CH_3]^{\ddagger} \rightarrow OH + CH_3$, where $\Delta C_p^{\ddagger}$, 300 ≈ 0 and $\Delta C_p^{\ddagger}$, 1750 ≈ 0.6 e.u.

Obviously, in general, over reasonable temperature ranges, b is constant.

●

F. Kaufman, University of Pittsburgh, USA

(1) This question concerns the predictive value of theory. Even for the simplest atom-transfer, tight-transition-state cases there is the difficulty of incorporating tunneling effects for H-atom transfer, which Cohen does empirically by fitting experimental values near 300 K and using the theory only as in extrapolating device.

(2) For pressure effects in recombination/dissociation reactions Troe's falloff formulas require the knowledge of both the low and high pressure limit rate constants, which are usually unavailable.

(3) For reactions going through bound interme-

diates the situation is usually much worse yet, because few of the required parameters are known or can be estimated from first principles.

(4) It comes down to the fact that we are able to rationalize a posteriori but not predict a priori. Perhaps this should please me as an experimentalist, since it means that, when all is said and done, we need to measure most elementary steps in the absence of reliable theoretical predictions.

Authors' Reply. This comment is best addressed by breaking it into four parts, as indicated:

(1) In the case of H-atom metathesis reactions, Cohen,[1] Benson,[2] Golden,[3] and others,[4] have shown that extant data are well decribed by making a model of a fixed transition state that fits the data at 300 K and using the fore-ordained statistical thermodynamic machinery to generate rate constants up to 2000 K. Perhaps this is a fortunate cancellation of errors due to tunneling, recrossing, and variational effects, and the key questions would address the consistency with which one may expect thermochemical kinetics methods to apply.

It seems safe to use the simple thermochemical kinetics methods to extrapolate metathesis rate data to combustion temperatures. It would also appear to be quite useful to employ these same methods for the prediction of A-factors and activation energies of these reactions.

(2) It is true that the values of k_0 and k_∞ are required to use Troe's formalism, but the word "unavailable" is too strong. The ever-interacting interplay of theory and experiment very often allows the estimation and or calculation of these quantities within bounds fully justified by the sensitivity of the pressure- and temperature-dependent rate constant in a given calculation or model.

(3) Professor Kaufman is correct in stating that more problems exist with respect to reactions that proceed through bound intermediates. However, the situation is not as bleak as he pictures it. These processes may be envisaged from the point of view of many pathway unimolecular reactions. As in (2) above, we may estimate many of the transition states from the current state of knowledge.

(4) This statement may be too strong. We can certainly estimate many rate constants to within useful limits, over a range of pressure and temperature. It is true that some processes for which neither good numbers nor good analogues exist, may fall outside of these limits.

It is too difficult to decide whether errors in individual rate constants yield sufficiently accurate *predictive* combustion models. Often they will, but at least they will direct experimentalists towards meaningful measurements in the future.

REFERENCES

1. N. COHEN, Int. J. Chem. Kinetics, 1982, *14*, 1339.
2. S. W. BENSON, *Thermochemical Kinetics*, 2nd ed., John Wiley and Sons, Inc., New York, 1976.
3. D. M. GOLDEN, J. Phys. Chem., 1979, *83*, 108.
4. K.-M. JEONG AND F. KAUFMAN, 1982, *86*, 1816.

●

A. Fontijn, Rensselaer Polytechnic Institute, USA. As you discussed, many combustion reactions, observed over wide temperature ranges show a mild concave upward curvature in their Arrhenius plots, best described by $k(T) = AT^B \exp(-C/T)$. You also mentioned some exceptions due to more complex surfaces. One category of combustion reactions, i.e., oxidation reactions of metal atoms and metal monoxide radicals seems to consistently have other dependences. We have studied a number of those reactions over wide temperature ranges and have not yet observed any to have a clear $k(T) = AT^B \exp(-C/T)$ dependence. The latest example obtained in the AlO + CO_2 reaction, the rate coefficient of which has no measurable T-dependence from 450–1300 K, apparently due to formation of an intermediate complex, which dissociates preferentially to reactants.

●

D. Gal, Central Chemical Research Laboratory, Hungary. You mentioned at the end of your lecture that modeling should start with the generation of the possible mechanism. We have shown—see the poster—how to generate it by combinatorial methods. However, we suggest that followingly it is advisable to reduce it—before putting in the relevant rate constants—by objective methods (thermochemistry, complexity factors or chemical evidence). As a next step the main thing is to collect as many experimental data as possible and definitely not only concentrate *vs* time values but eventually rates obtained for network pathways.

I feel that sensitivity analysis cannot be avoided and the main aim should be to obtain a main contributory mechanisms yielding a key which rate constants should be computed with the utmost care.

●

A. Fontijn, Rensselaer Polytechnic Institute, USA. Did you (mean to) imply that the temperature dependence of the branching ratio of the H + N_2O reaction is well known? I did not think it was. Could you comment on this?

Authors' Reply. The branching ratio of the H + N_2O reaction is not well known, but there are measurements at 2000 K by laser induced fluorescence and at 873 K in a static system. These are references 10a and 10b in the paper.

Twentieth Symposium (International) on Combustion/The Combustion Institute, 1984/pp. 1195–1203

LASER-INDUCED FLUORESCENCE SPECTROSCOPY OF NCO AND NH_2 IN ATMOSPHERIC PRESSURE FLAMES

RICHARD A. COPELAND, DAVID R. CROSLEY AND GREGORY P. SMITH
Chemical Physics Laboratory
SRI International
Menlo Park, California 94025

Laser-induced fluorescence (LIF) is a powerful method for the sensitive detection of trace species in flames, and is permitting new insight into the detailed mechanism of combustion chemistry. However, LIF has been applied almost exclusively to diatomic radicals whereas the chemical networks contain many larger species whose presence can signal definite mechanistic paths. We describe here a comprehensive survey of the LIF spectroscopy of the NCO molecule in a CH_4/N_2O flame and the NH_2 molecule in NH_3/N_2O and NH_3/O_2 flames, all burning rich at atmospheric pressure. NCO was excited in the B-X and A-X systems in the ultraviolet and blue, respectively, the latter is much more intense and can be more easily made free of strong interfering transitions due to diatomics. NH_2 was excited in the $\tilde{A} - \tilde{X}$ transition. Excitation and fluorescence wavelengths furthest to the red minimize background interference due to underlying, unidentified absoption features and flame emission. Prescriptions for detecting these two species are presented, including a table of excitation and detection wavelengths, as well as some general observations on experimental technique which should be useful in extending flame LIF detection to other triatomic and larger radicals.

Introduction

Laser-induced fluorescence (LIF)[1] is the member of the family of laser spectroscopic probes[2,3] best suited for the detection of trace radical species in combustion systems. It possesses high sensitivity and selectivity coupled with spatial and temporal resolution and a non-intrusive nature. Such information is valuable for obtaining qualitative insight into the mechanisms of the combustion chemistry, and provides sensitive data for comparison with quantitative predictions from detailed computer models of that chemistry in simple laboratory flames.

Consider as the atomic constituents of naturally occurring fuels H, C, N, O and S. All of these atoms and the 15 diatomic molecules formed from them have been observed by LIF in low pressure discharge flows or static cells, and two of the atoms plus ten of the diatomics have been detected in flames by LIF (for the atoms, and H_2, N_2 and CO one must use two-photon excitation because their first absorption bands lie in the vacuum ultraviolet). However, only a few of these diatomics have yet been meaningfully fit into chemical kinetic schemes, and the flame chemistry involves many larger radicals as well.

Therefore it is important to extend LIF flame detection capability to larger species. Of the 35 triatomics which can be formed from these atoms (not counting the chemically and spectroscopically distinct isomers such as CCN and CNC), 14 have been observed in LIF cells or flows and another 13 are definite or possible candidates on spectroscopic grounds. However, only four have been detected by LIF in flames. SO_2[4] and NO_2[5] have been detected over wide wavelength regions but in each case the complexity of the absorption spectrum and the laser wavelengths and bandwidth used resulted in near-continuum-like excitation precluding definitive spectroscopic assignment. NCO[6] has been cleanly excited and studied, via the coincidental overlap of one of its absorption lines with one of the fixed-wavelength lines of an Ar^+ laser. NH_2, with a well-known LIF signature under low pressure conditions, has escaped LIF detection in atmospheric pressure flames in previous experiments in this laboratory as well as elsewhere,[7] although a recent report indicates it can be excited weakly with the frequency-doubled line of a Nd:YAG laser.[8] However, while it can be very convenient, such fixed-frequency excitation does not permit optimization of detection under a variety of conditions including potential interfering absorptions, and cannot be relied on as general for other molecules. NH_2 has also been detected in atmospheric pressure flames by absorption of laser radiation directly[9] and optoacoustically[10] but these methods do not have the pointwise spatial resolution attribute of LIF.

We have performed a survey of the LIF spectroscopy of the NCO and NH_2 molecules in at-

mospheric pressure flames, using lasers and detection systems tunable over a wide range of wavelengths. The burners and gas mixtures were chosen to optimize conditions for the spectroscopic studies, but the detection strategies developed can be later used on burners better suited for obtaining profiles for comparison with theoretical models.

NCO and NH_2 were chosen for study for two reasons. One is the existence of considerable spectroscopic information from previous studies, both in conventional spectroscopy and LIF experiments. This has not only facilitated initial detection but also permitted more general conclusions and extensive comparison. (In this connection, it is noteworthy that *all* the species, regardless of size, which have been detected by LIF were first studied spectroscopically in flame or plasma discharge emission or in flash photolysis absorption.) On the other hand, the use of LIF in flames has provided new spectroscopic information for NCO not previously attainable, as described below.

The other reason is the intrinsic potential importance of these radicals in certain combustion chemical networks. NCO has been postulated as an intermediate in the formation of NO_x from fuel-nitrogen[11] and was found to be present in copious quantity in CH_4/N_2O flames,[6] pertinent to nitramine combustion. NH_2 has been suggested as an intermediate in the production of prompt-NO[12] and in the ammonia de-NO_x process.[13]

We present here a description of our experiments. Because of the large amount of data on excitation and fluorescence spectra involved, we can include only a condensed version of the results. We hope that this will serve as an adequate guide to LIF detection of these two species in combustion experiments in other laboratories. In addition, we plan to assemble later in report form[14] a LIF spectroscopic atlas of the wavelength regions covered in these flames, including excitation of several diatomics whose fluorescence must be filtered out. We include some general observations about the experimental technique which we hope will prove useful in extension of LIF detection in flames to other triatomics and larger molecules.

Experimental Set-Up

Several burners were tried: a McKenna products porous plug burner, a small flat flame burner with 1 mm holes in the surface, a glassblowing torch, and a knife-edge slot burner patterned after a design explicit for laser probing.[15] This last burner, which presents a saddle-point-shaped flame and easy laser beam access underneath the reaction zone, proved the easiest to use and provided the largest signals for these spectroscopic experiments. The flames were run rich, so as to yield larger quantities of the oxygen-poor or oxygen-free radicals of interest. The relative flow rates used in most of the experiments were: $CH_4:N_2O:N_2 = 1.0:3.5:2.7$, $NH_3:N_2O = 5:3$; $NH_3:O_2 = 2:1$.

The first step in each case was measurement of the emission spectrum of each flame. In addition to the spectroscopic overview provided, this served two specific purposes. The first was the selection of gas mixtures yielding strong radical emission (the ground and excited state radical concentrations are not necessarily proportional but this was a useful guide). The second was the choice of detection wavelengths minimizing interference and noise from flame emission. In the case of CH_4/N_2O, no NCO emission could be seen but there were clearly favorable regions between different vibrational sequences of the CH, CN and C_2 emission. The NH_3/N_2O spectrum, apparently not previously described, was similar to that of the NH_3/O_2 flame, and consisted of OH, NH and NH_2 bands, with the NH_2 about half as strong, compared to the diatomics, for the N_2O-based flame as in the O_2-based flame. Here, the potential interference is NH_2 itself (and perhaps unassignable NO_2 underneath), the spectra suggest it is minimized as one operates furthest to the red.

The LIF arrangement was standard, with the laser beam passing through the movable burner and the fluorescence focussed at right angles onto a spectrometer, sometimes filtered with colored glass. An XeCl-pumped dye laser with typical pulse energy $E_l \approx 3$ mJ, bandwidth $\Delta\tilde{\nu}_l \approx 0.3$ cm^{-1} and repetition rate $r_l \sim 100$ Hz was used for the blue (A-X) NCO excitation, and a Nd:YAG-pumped dye laser ($r_l = 10$ Hz) was used in the fundamental ($E_l = 30$ mJ, $\Delta\tilde{\nu}_l = 0.15$ cm^{-1}) for NH_2 and frequency-doubled ($E_l = 1$ mJ, $\Delta\tilde{\nu}_l = 0.25$ cm^{-1}) for NCO B-X. The pulse length of each laser was 10 nsec, and the signals followed the laser in time. A 0.35 m spectrometer with dispersion 22 A/mm and cooled EMI 9558 Q photomultiplier were used for NCO A-X, the slit was aligned parallel to the laser beam. A 0.75 m spectrometer (11 A/mm) and uncooled 9558 or red-sensitive RCA 31034A photomultiplier were used for NCO B-X and NH_2, here the beam and slit were perpendicular.

The photomultiplier signal was amplified a factor of 100 using a Pacific video 2A50 preamp (50 Ω in and out) and fed to a gated boxcar integrator with a 20 nsec gate. This mode of fast pulse operation was always preferable and often essential to maximize the LIF to background emission ratio, in comparison with higher input impedance (e.g., 1MΩ) and a longer gate (1 μsec). Even so, care had to be taken to keep the photomultiplier operating voltage low enough that the tube did not saturate under the continuous flame emission current. An oscilloscope proved useful for signal searching and monitoring. The boxcar output was then fed to a

scanning stripchart recorder. The laser beam energy was continually monitored in a second boxcar channel.

During some of the NH_2 runs, where absorption due to unidentified bands and/or other species appeared present, a half-inch microphone was mounted near the burner to optoacoustically[10] monitor the total absorption.

NCO Radical

The NCO LIF spectrum over the range of one laser dye is illustrated in Figure 1. The top two scans are noise-free at this sensitivity, and concomitant excitation of CH, CN and C_2 in this region is not seen due to the choice of fluorescence wavelength. The top scan shows the overall pattern, increasingly sharply in intensity as one scans to shorter wavelengths through the electronic origin (000-000) near 440 cm. The transition from 000 to the first allowed excited vibrational level (100) of $A^2\Sigma^+$ occurs at 416 nm; the observed fluorescence for $\lambda <$ 437 nm thus is hot bands, originating from vibrationally excited levels in the ground state. Because the laser power is beginning to drop for $\lambda <$ 430 nm, the bands in this region appear much less intense in Fig. 1 than they actually are.

A 4 nm portion showing the four heads of the 000-000 band (marked by arrows) as well as other bands, is presented in the middle panel. In turn, a 0.45 nm section of this, exhibiting individual rotational lines of the $^oP_{12}$ satellite branch, is given in the bottom scan. Interestingly, the $^oP_{12}$ head, which occurs for J near 70, is barely discernable in room temperature flow system LIF spectra[16] (see Ref. 1 for a comparable scan) but is very marked in the flame.

The overall excitation spectrum throughout this region is clearly congested and complex, due largely to the significant fractional populations in vibrationally excited levels of the ground state at flame temperatures. In order to make quantitative measurements of NCO concentrations (even relative) it is necessary to have individual, assigned rotational lines at the level of resolution of those in the bottom panel of Fig. 1, due to the variation with temperature of population in a given v, J level. We have mapped a portion of the region $\lambda \leq 440$ nm but have concentrated our attention for hot flames on bands to the red, involving vibrationally excited levels whose excitation spectra are much less congested.

The vibrational level structure in the X, A and B states of NCO is illustrated in Fig. 2. A brief structural and spectroscopic description of NCO follows. (Details may be found elsewhere[14,16,19].) It is a linear molecule with two stretching (v_1 and v_3) and one degenerate bending vibration (v_2). The electronic orbital angular momentum of the ground

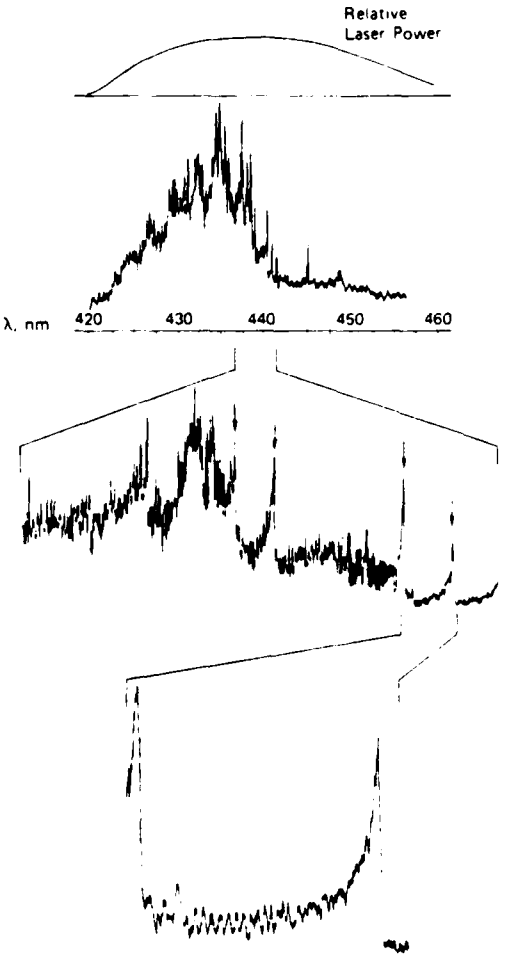

FIG. 1. LIF scans for the A-X system of NCO in a CH_4/N_2O flame. Fluorescence is collected at 465 nm with a 4 nm bandpass. Top scan, total excitation spectrum over the full range of one laser dye (Coumarin 440), not normalized to laser power. Middle: 4 nm portion covering the 000-000 band, with Q_1, P_1, P_2 and $^oP_{12}$ heads (left to right) marked by arrows, and hot bands at shorter wavelengths. Bottom, region from P_2 to $^oP_{12}$ head (0.45 nm) showing rotationally resolved $^oP_{12}$ branch.

Π state couples with the vibrational angular momentum ℓ of the bend ($\ell = v_2, v_2-2, v_2-4, \ldots 0$ or 1 as v_2 is even or odd), yielding a total angular momentum K exclusive of spin. The states of different ℓ split according to the so-called Renner-Teller interaction. This yields states of Π symmetry for $v_2 = 0$, Π and Φ for $v_2 = 2$, and Σ and Δ for $v_2 = 1$. The spin angular momentum of this doublet molecule then interacts to produce spin-orbit-split components. In state where $v_2 = 0$, this yields

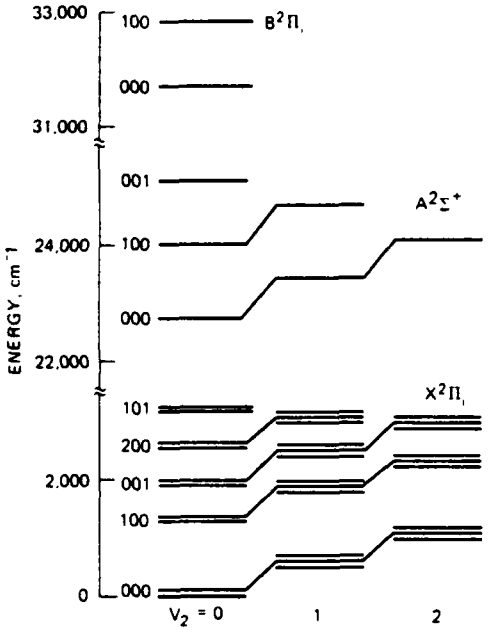

FIG. 2. Pertinent vibrational levels of the B, A and X states of NCO. Note the break in the energy scale. Levels are arranged for clarity according to the value of v_2. Those with $v_2 = 0$ have $^2\Pi$ symmetry ($^2\Pi_{1/2}$ and $^2\Pi_{3/2}$) in the X and B states and $^2\Sigma^-$ in the A state. For $v_2 = 1$ in X, there are 4 levels: $^2\Sigma^-$, $^2\Delta_{3/2}$ and $^2\Delta_{5/2}$ (not separated in the figure), and $^2\Sigma^-$ in order of decreasing energy. For $v_2 = 2$ in X, there are also 4 levels: $^2\Pi^-$, $^2\Phi_{5/2}$ and $^2\Phi_{7/2}$, and $^2\Pi^+$. In the A state, $v_2 = 1$ has $^2\Pi$ symmetry and $v_2 = 2$ has $^2\Sigma^-$, $^2\Sigma^+$ and $^2\Delta$, all close together.

$^2\Pi_{3/2}$ and $^2\Pi_{1/2}$ components like those in OH. In the transition to the upper $A^2\Sigma^+$ state the $^2\Pi_{1/2}$ spin-orbit component yields four discernible rotational branches. $^oP_{12}$, $P_2 + {}^PQ_{12}$, $Q_2 + {}^QR_{12}$ and R_2 with two heads, the $^2\Pi_{3/2}$ component has the P_1, $Q_2 + {}^QP_{21}$, $R_1 + {}^RQ_{21}$ and ${}^SR_{21}$ branches with two heads (see Figs. 1 and 3). Transitions originating from the Σ levels where $v_2 = 1$ have only P and R branches, two heads arising from excitation out of the higher Σ level (labelled $\kappa^2\Sigma^-$) are seen in Fig. 3. Transitions from higher Σ, Π and Δ levels have also been observed but will not be described here.

Figure 3 exhibits an excitation scan of the 000 ← 100 band which appears the most convenient for flame diagnostic measurements. Individual lines of this and of other bands were readily assigned from the 000-000 absorption spectra of Dixon.[17] The R_2 and Q_2 branches at 466 nm are the best individually resolved for quantitative measurements whereas the intense P_2 head is the best for signal searching.

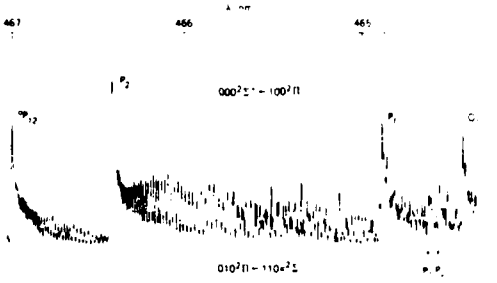

FIG. 3. Excitation scan for NCO, detecting at 440 nm with 4 nm bandpass, through the red end of the 000-100 band. The two heads of the 010 ← 110 $\kappa^2\Sigma^-$ transition are also marked.

Line strengths[14] may be calculated from standard diatomic-like $^2\Sigma^-$-$^2\Pi$ formulae. Radiative lifetimes and Franck-Condon factors, needed for vibrational band intensities, have been separately measured.[16]

The excitation scan of Fig. 3 was made with a monochromator bandpass of 4 nm centered on the 000 → 000 emission at 440 nm. This relatively narrow bandpass is needed to filter out flame emission and strong fluorescence from laser-excited C_2 in this same region. The need for careful setting of the monochromator, and the dual selectivity of LIF with variable excitation and detection wavelengths, is shown in Fig. 4. The bottom scan shows the P_1 and Q_1 heads, plus R_1 and $^1R_{21}$ lines of the 000 ← 001 band observed via 000 → 000 emission. When the monochromator is tuned to the 010 → 010 emission band only 5 nm away, the 001 excitation greatly

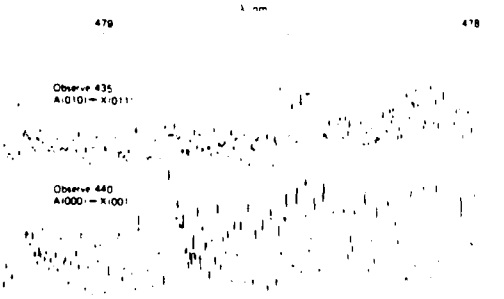

FIG. 4. Excitation scans for NCO with detection wavelengths as marked and 4 nm bandpass, showing the difference depending on observation region. Bottom: 000 ← 001 band seen observing 000 → 000 emission. P_1 and Q_1 heads plus R_1 and $^1R_{21}$ branches as the laser wavelength is decreased. Top: tuning to 010 → 010 emission to pick out 010 ← 011 transitions originating from $\kappa^2\Sigma^-$ near 478.5 nm and from $^2\Delta_{3/2}$ near 478.2 nm. The P_1 head decreases less than the Q_1 compared to the bottom scan because it occurs at higher J levels which emit more to the blue

decreases whereas the P_1 and P_2 heads of the 010 ← 011 $\kappa^2\Sigma^-$ transition near 478.5 nm, and the 010 ← 011 $^2\Delta_{5/2}$ component near 478.2 nm stand out (top scan). (Here, the P_1 head of 000 → 001 is still rather apparent, it involves high-J levels emitting Q and R branches at shorter wavelengths.)

Table I lists the excitation bands which have been observed for the A-X system and the emission bands furnishing the strongest signals free of interference from any diatomic LIF with excitation lines in the same region.

Previous conventional room temperature absorption spectra[17-19] originating from the lowest levels (000 and 010) have been of key importance enabling the present LIF search. However, the combination of the laser excitation and flame environment has also furnished new high-resolution spectroscopic information in excited vibrational levels of $X^2\Pi_i$. The band-head separations P_2-Q_1 depend largely on the spin-orbit splitting constant A whereas the $^0P_{12}$-P_2 separation furnishes a measure of the rotational constant B. The actual wavelengths were calibrated by changing the observation wavelength so as to excite previously measured or readily calculated bands of CH, CN or C_2 in the same wavelength region of the laser. We find by fitting the band heads that the magnitude of A (in cm^{-1}, with typical 0.3 cm^{-1} error) decreases with v_1 and increases with v_3: $A_{000} = -95.6$, $A_{100} = -89.8$, $A_{001} = -97.1$, $A_{101} = -92.1$. The Renner-Teller splitting also varies with stretching vibrations. To our knowledge, this represents the largest range of vibrationally-dependent A-values for a triatomic. A full fit and the results will be separately published;[20] we note these values to illustrate the spectroscopic potential for LIF in flames.

The B-X system[15] of NCO appears attractive for diagnostic purposes due to the shorter lifetime of the $B^2\Pi_i$ state[21] even though its fluorescence is spread over many bands[16] in contrast to that from the $A^2\Sigma^+$ state which is concentrated in a few. Scans through the 000-000 band near 315 nm showed it to actually be decidedly inferior to A-X. The B-X fluorescence was very weak by comparison and only the R_1 and R_2 heads, with indefinite J-values, could be discerned. Within the 1.5 nm region around these heads are also strongly interfering excitations in the 0,0 and 1,1 bands of OH A-X, the 1,0 and 2,1 bands of NH A-X and a band of CN B-X. We recommend the A-X system for flame diagnostic purposes.

NH_2 Radical

The ground $\tilde{X}^2B_1$ state of NH_2 is a bent, asymmetric top with an angle of 103° while the $\tilde{A}^2A_1$ state may be described as linear, corresponding to a Π electronic level. This large difference in equi-

TABLE I
Excitation and fluorescence wavelengths (nm)

NCO Band	λ (P_2 Head)	λ (Observe)	NH_2 Band	λ (Q-Head)	λ (Observe)
000 ← 000	440.35	465.0	0,10,0 ← 000	571.0	620, 687, 697
000 ← 100	466.42	440.0	090 ← 000	597.9	656[c], 726, 740[c]
000 ← 001	481.09	440.0	0,11,0 ← 010	591.0	543[c]
000 ← 200	495.60	437.5	0,12,0 ← 020	607.2	516[c]
000 ← 101	511.71	437.5	080 ← 000	630.2	695,774[c], 790[c]
010 ← 010 $\mu^2\Sigma^+$	435.06	462.5	170 ← 100	651.2	538
010 ← 010 $^2\Delta$	437.56	462.5	0,11,0 ← 100	655.7	543[c]
010 ← 010 $\kappa^2\Sigma$	438.48	462.5	070 ← 000	662.1	735, 824
010 ← 020 $^2\Pi$	444.80[a]	435.0			
000 ← 010 $\mu^2\Sigma^+$	448.35	440.0			
010 ← 110 $\mu^2\Sigma^+$	460.61	435.0			
010 ← 110 $^2\Delta$	462.22	435.0			
010 ← 110 $\kappa^2\Sigma$	464.56	435.0			
010 ← 011 $\mu^2\Sigma^+$	474.36[a]	435.0			
010 ← 011 $^2\Delta$	477.37	435.0			
010 ← 011 $\kappa^2\Sigma$	478.16[a]	435.0			

[a] Preliminary identification, final confirmation awaits a detailed analysis.
[b] Bands listed are emission to 010, 020, and 100 respectively except where noted.
[c] Emission at 575 also usable: 0,10,0 → 000.
[d] Emission at 603 also usable: 090 → 000.
[e] Calculated wavelength, but not studied in this work.
[f] 0,1,0 → 000 fluorescence wavelength.

librium geometries leads to large changes in the bending quantum v_2 for intense bands. v_3 must change by two units due to symmetry considerations, leading to bands which would fluoresce too far to the red to be seen here. In the ground state, the rotational levels (ignoring spin) are described by the total angular momentum N and its projections, K_a along the axis parallel to the H—N—H linear axis and K_c perpendicular to the molecular plane. In the excited state, K_a is (as in $X^2\Pi$ NCO) the sum of one unit of electronic orbital angular momentum plus the vibrational angular momentum, it thus takes on even values (0, 2, ...) for odd v_2' and odd values for even v_2'. The selection rules are $\Delta K_a = \pm 1$, and ΔK_c = even with zero the strongest. The most intense features are the $^PQ_{1N}$ heads of the so-called Σ bands (odd v_2') and the $^RQ_{0N}$ heads of the Π bands (even v_2'). These produce 3 and 4 emission branches respectively. Because of electronic spin, each branch is double, and nuclear spin statistics produce a 1:3 population ratio in alternate ground state levels.

Figure 5 exhibits the vibrational levels pertinent to flame diagnostic LIF. The basic spectroscopic source for NH_2 is the absorption study of Dressler and Ramsay,[22] and there are several useful recent conventional spectroscopic[23] and flow system LIF[24, 25] studies. The emission and LIF spectrum extends throughout the entire visible region, with a maximum intensity near 590 nm.

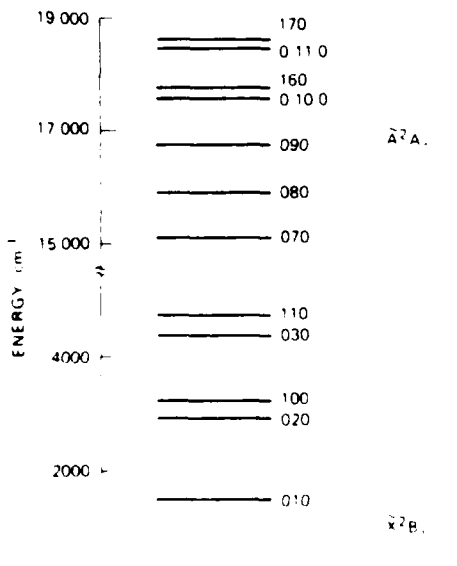

FIG. 5 Vibrational structure in NH_2, the 6 lowest levels having $v_3 = 0$ in $X\tilde{B}_1$ and the 7 levels in $A\tilde{A}_1$ for which LIF was observed in this study. Note the break in energy scale.

In the flames studied, the absolute NH_2 signal level has been adequate but major noise sources are posed by background flame emission and a complex, thus far unidentified, LIF excitation spectrum (perhaps NO_2 and/or hot bands of NH_2, also observed optoacoustically) underlying the assigned features. Most of our effort has been devoted to optimizing the desired signal in the midst of this background. Of course in other flames such as hydrocarbon-air, different interference problems may be present. Figure 6 shows a typical excitation spectrum and a scan of flame emission in the same band. Interference from flame emission can be minimized by using narrow temporal, spatial, and wavelength resolved detection of LIF in the bands further to the red. Altogether we have investigated 5 excitation bands between 570 and 660 nm. The most intense fluorescence, about 2/3 of the total, occurs in the $v_1v_2'0 \rightarrow 000$ band in each case, the remainder is typically spread over the terminal $\tilde{X}^2B_1$ 010, 100, and 020 states with a smaller amount in 030. When the $v_1v_20 \leftarrow 000$ band is excited, observation in the same band requires narrower spec-

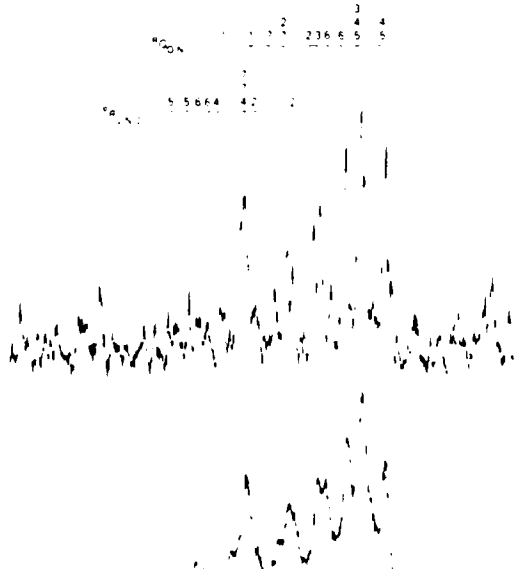

FIG. 6 Top: LIF excitation scan through the most intense portion of the 080-000 band of NH_2 with several lines marked. Each is present as a doublet due to the spin-doubling; note that the upper state perturbations render the doublet splitting irregular with N. Bottom: flame emission spectrum in the same region, using 25 μm slits in the 3/4-m spectrometer.

trometer slits to discriminate against the laser scatter, so that only one of the fluorescing rotational branches may be detected at one time. The NH_2 appears not to undergo significant energy transfer while in the upper state, but emits primarily from the pumped level (see below). Thus the coarse rotational structure of the transition means that R or P branch fluorescence following Q-excitation will occur at different wavelengths for different N'', which would require an impractical scanning of the spectrometer together with the laser for an excitation scan. This phenomenon was observed for 090 excitation.

The underlying background LIF, and total absorption measured optoacoustically, makes it undesirable to obtain flame profiles for NH_2 by simply parking on one excitation, rather a scan through the head as in Fig. 6 should be made at each position. Generally, observation of the bands at wavelengths to the red of that of the laser is preferable, so as to reduce flame emission interference. This also permits wider slits centered on a Q-head, and eliminates the double-scanning problem noted above. Excitation of $v_1'v_2'0$ from 010 or 100 and observation of $v_1'v_2'0 \rightarrow 000$ yields comparable intensities to the opposite scheme but flame emission is worse when observing the bands at shorter wavelength. In general it appears best to both excite and observe as far to the red as possible to avoid the background problems, even though the band intensities become weaker for lower v_2'. We recommend excitation of 090 or 070 for flame diagnostic purposes.

Figure 7 exhibits a scan of the $070 \rightarrow 010$ fluorescence following $070 \leftarrow 000$ excitation. Here the laser pumps overlapped lines of one of each doublet component of the 3_{03} and 3_{13} upper state levels. It can be seen from the resolved $^{P}P_{1}(N'=1)$ branch that only the pumped levels emit. The lack of transfer to the 4_{04} level is a symmetry-forbidden collisional propensity[24-26] but transfer to the allowed 1_{01} level is not seen either. A similar scan

FIG. 7. Fluorescence scan of the 070-010 of NH band following excitation near 660 nm in the 070-000 band. The laser is overlapping one doublet component of the $3_{03} \leftarrow 3_{13}$ transition and the other component of $3_{13} \leftarrow 3_{13}$ in that band. The fluorescence seen here consists of branches from each level. Note the absence of significant rotational energy transfer as evidenced by the presence of only two lines in the $^{P}P_{1}$ branch.

of the 090 band, however, does show evidence of limited rotational energy transfer from the 3_{03} upper state level. More detailed examination of several levels is in progress.

In the flames studied the concentration of NH is likely high[4] between 10^{13} – 10^{14} cm^{-3} and comparable to OH in these rich flames. The NH peaks at the flame front whereas the OH persists into the burnt gases. As a rough guide to expected signal levels we have compared optoacoustic cell absorption and LIF intensities for exciting the 0-0 band of OH P_1 7 and the 0-0 band of NH $^{R}Q_{1}$ 8 head. The appropriate oscillator strength for the NH_2 is about 1/3 of that for OH[27]. LIF is observed in the 0-0 Q-head region of OH $\sim$ 30% of total emission and 0-0 0 0 $\rightarrow$ 0 2 0 $\sim 10^{-4}$ for NH_2. Normalized to unit laser pulse energy the OH optoacoustic signal absorption is about 40 times that of NH_2 and the OH LIF is about 250 times larger. This suggests similar fluorescence quantum yields in these flames. NH_2 is known to undergo fast quenching even by He[28], while OH has quenching rates for NH_3, N_2O, and H_2O as efficient partners[29].

Acknowledgment

This research was supported by the U.S. Army Research Office under contract DAAG29-80-K-0044.

REFERENCES

1. CROSLEY, D. R., AND SMITH, G. P., Opt. Eng. 22, 545 (1983).
2. CROSLEY, D. R., Ed., *Laser Probes for Combustion Chemistry*, Amer. Chem. Soc. Symposium Series Vol. 134, 1980.
3. BECHTEL, J. H., DASCH, C. J., ..., DYER, R. E., "Combustion Research with Lasers," to appear in *Laser Applications*, R. K. Erf, and J. F. Ready, Eds., Academic Press, New York, 1985.
4. MUELLER, C. H., III, SCHOFIELD, K., STEINBERG, M., in ref. 2, p. 103.
5. BARNES, R. H., AND KAUFMAN, F., *Appl. Opt.* 17, 1089, 1978.
6. ANDERSON, W. R., VEIRS, D. K., ..., DEWILDE, M. A., ..., BAUER, S. H., *J. Chem. Phys.* 77, 1677, 1982.
7. MOSLEY, C., *Combust. Flame* 47, ..., 1982.
8. C. J. DASCH AND R. J. ..., General Motors Research Laboratories Report GMR-4..., December 1983.
9. CHOU, M. S., DIAS, A. M., ..., *J. Chem. Phys.* 76, 5354, 1982.
10. SMITH, G. P., DYER, M. J., ..., R. *Appl. Opt.* 22, 1965, 1983.
11. HAYNES, B. S., ..., *Fifteenth Symposium (International) on ...*

bustion p 1103 The Combustion Institute 1975
12 Fenimore C P *Seventeenth Symposium International on Combustion* p 661 The Combustion Institute 1979
13 Dean A M Hardy J E and Lyon R K *Nineteenth Symposium International on Combustion* p 97 The Combustion Institute 1982
14 Copeland R A Crosley D R and Smith G P to be published
15 Beyer R A and DeWilde M A Rev Sci Instr 53 103 1982
16 Sullivan B J Crosley D R and Smith G P to be published
17 Dixon R N Phil Trans Roy Soc London A252 165 1960
18 Dixon R N Can J Phys 38 10 1960
19 Bergman P S H Brown J M Carrington A Kopp I and Ramsay D A Proc Roy Soc London A340 17 1975
20 Copeland R A and Crosley D R Can J Phys in press
21 Sullivan B J Smith G P and Crosley D R Chem Phys Lett 96 307 1983
22 Dressler K and Ramsay D A Phil Trans Roy Soc London A251 553 1959
23 Johns J W C Ramsay D A and Ross S C Can J Phys 54 1804 1976
24 Hagers J B Hancock G Lenzi M and Welge K H J Chem Phys 63 4888 1975
25 Kinsey M J Chem Phys 63 3134 1975
26 Dixon R N and Field D Proc Roy Soc London A366 247 1979
27 Merienne-Lafore M F and Van de Sande M Mol Phys 44 1229 1981
28 Smith G P and Crosley D R *Eighteenth Symposium International on Combustion* p 1511 The Combustion Institute 1981
29 Fairchild P W Smith G P and Crosley D R J Chem Phys 79 1795 1983

COMMENTS

measurements in low pressure cells found the collision free radiative lifetime to vary from 5 μs to 50 μs [7] for different vibrational levels. Hanle effect measurements yielded values near 0.5 μsec. Rapid collisional quenching has been measured for several colliders [7]. Some rotational energy transfer is seen in these low pressure systems exhibiting propensity rules such as discussed here in connection with Figure 7.

In high pressure flames [8] that the temperature of the NH $^3\Sigma^-$ state is determined by collisional processes, the lifetime of flame temperature (~2000 K) gas the rate is expected to be rapid ~5 × 10^{-10} cm^3/sec making the measurement difficult. The rapid quenching will dominate the overall collisional behavior so that transfer among excited state levels will not occur to a large degree.

REFERENCES

1. J. B. Halpern, G. Hancock, M. Lenzi, and K. H. Welge, J. Chem. Phys. 63, 4808 (1975).
2. V. M. Donnelly, A. P. Baronavski, and J. R. McDonald, Chem. Phys. 43, 283 (1979).
3. M. Kneba, J. Chem. Phys. 62, 1805 (1975).

STATE-SPECIFIC COLLISION DYNAMICS OF OH RADICALS AND N ATOMS

Richard A. Copeland, David R. Crosley, and Jay B. Jeffries
Molecular Physics Department, SRI International,
Menlo Park, CA 94025

ABSTRACT

Open shell species, with a variety of spectroscopically accessible quantum states, offer opportunities for laser generation of nonequilibrium spatial distributions in both the laboratory (m_J) and molecular (Λ-doublet) frames. In addition, laser excitation can also select the relative orientation of the spin and orbital angular momentum in these systems. The quantum state distributions can be interrogated by a delayed second laser pulse or by resolving the polarization and/or wavelength of the resulting fluorescence. In experiments on the OH radical, we have observed propensities for retention of electronic parity and spatial orientation during rotationally inelastic collisions of, respectively, the $X^2\Pi_i$ and $A^2\Sigma^+$ electronic states. In nitrogen atoms, we have qualitatively determined the magnitude of fine structure, m_J and electronic state changing collisions in the $2s^22p^23p\ ^4D^o$ electronic state.

INTRODUCTION

Combining initial quantum state selection and final quantum state resolution in an experimental technique permits a detailed examination of the state specific processes which occur during the collision of two species. Often these interactions are extremely state specific and show surprising mechanistic selectivity for complex molecular and atomic collision events. Here, we describe three different experiments recently performed in our laboratory which examine the collision dynamics in the ground ($X^2\Pi_i$) and first excited ($A^2\Sigma^+$) state of OH and the $^4D^o$ state ($2s^22p^23p$) of N atoms.

Λ-DOUBLET PROPENSITIES IN OH($X^2\Pi_i$) COLLISIONS WITH H_2O

Doublet pi states of diatomic radicals possess nearly degenerate but spatially distinct Λ-doublet electronic states having opposite parity, in addition to the angular momenta resulting from electron orbital motion, spin and nuclear rotation. By observing changes in the electronic parity (e/f states) following rotationally elastic and inelastic collisions, we gain insight into the potential surfaces involved in the interaction.

0094-243X/86/146067-48$1.00

Using a two-laser infrared pump/time-delayed ultraviolet probe technique, we examined collisions of ground state OH(v=2) with water vapor.[1] Although the e/f pair differs in energy by less than 0.25 cm^{-1}, the excitation laser bandwidth and the characteristics of the A-X electronic transition permits selection of the initial e/f state and interrogation of the final e/f state. These experiments were performed at 0.14 Torr of H_2O in a room temperature discharge flow cell. For the lowest rotational level in the $^2\Pi_{3/2}$ state, elastic f→e transfer is one third to one half of the total collision removal rate. For inelastic collisions to the next higher rotational level f→f is favored over f→e by a factor of 2.7.

The results for A-doublet propensities in rotationally inelastic collisions are perhaps the most interesting and surprising in that the OH-H_2O system will most likely form a hydrogen bonded collision complex. Some indirect experimental evidence for the complex is the rapid electronic quenching of the $A^2\Sigma^+$ state of OH by H_2O.[2] Hence, one might expect little or no memory of the initial state in this strongly interacting collision system. This experiment clearly shows that even in systems where long range dipole-dipole forces dominate, collision processes can be controlled by the orientation of the electronic orbitals.

POLARIZED FLUORESCENCE FROM OH IN ATMOSPHERIC PRESSURE FLAMES

Observation of alignment effects in molecular collisions is not restricted to the well controlled environment of a low pressure cell or a molecular or atomic beam. When polarized lasers are used to examine systems at atmospheric pressure, nonequilibrium spatial distributions can be manifested in fluorescence which is significantly polarized. In this experiment we measured the polarization and relative magnitude of laser-induced fluorescence signals generated by a polarized laser which excites molecules to the $A^2\Sigma^+$ state of OH in the burnt gases of an atmospheric pressure methane oxygen flame.[3] The extent of the polarization can have a significant effect on the quantitative measurement of OH in systems where collision processes dominate (i.e. flames and the atmosphere).

In systems at atmospheric pressure collisions occur at a rate of ~10 ns^{-1}, suggesting that the elastic depolarizing collisions (J conserving, m_J changing) might totally destroy any polarization effects generated by the nonequilibrium m_J distribution created by the laser. However the important quantity is not the depolarizing rate D but the relative probability that a given collision will lead to depolarization. The total removal rate R, which includes electronic quenching plus vibrational and rotational energy transfer, is very rapid for collisions with the primary combustion products H_2O and CO_2. If R≫D polarized emission will be observed, however, if D≫R the emission will be unpolarized. For the initially prepared rotational level significant polarization is seen

by wavelength resolved fluorescence scans in the different relative laser and detection polarizations.

While quantitative results are difficult to obtain for this combustion system several important and new qualitative features emerged from this investigation. The first is the similarity in the magnitude of the rates R and D for $OH(A^2\Sigma^+, v=1)$ resulting in polarized fluorescence from the initially excited rotational level. A surprising result was the polarization of the fluorescence from neighboring rotational levels with the same spin component ($F_1 \leftrightarrow F_1$, $F_2 \leftrightarrow F_2$). This shows that rotationally inelastic collisions at these relative velocities (~1500K) prefer a retention of the m_J component. Collisions which reorient the spin ($F_1 \leftrightarrow F_2$) and rotational angular momentum, however, generate no observable polarization.

These experimental observations clearly show polarization of the fluorescence must be considered when making absolute concentration measurements in atmospheric pressure systems, and even in the complex environment of the flame the state specific nature of the collision dynamics is important.

COLLISION DYNAMICS OF NITROGEN ATOMS

In atomic systems the angular momentum J is the vector sum of the orbital angular momentum and the electron spin. Nitrogen in the $^4D^o$ state has four distinct fine structure components corresponding to total angular momentum J=1/2, 3/2, 5/2 and 7/2. Using the two photon transition at ~210 nm we excited nitrogen atoms from the ^4S ground state to a particular J component of the $^4D^o$ excited state.[4] Using the wavelength, polarization and time dependence of the fluorescence we can unravel the rates and pathways of collisional processes in this highly excited atomic species.[5]

From the time dependence of the fluorescence we obtained the radiative lifetime of the excited state and collisional quenching rates. He and N_2 were the collisior partners examined. From the pressure dependence of the observed fluorescence decay we obtain a radiative lifetime for the $^4D^o$ state of N of 45±5 ns, and a collisional quenching rate for N_2 of $5\pm1\times10^{-10}$ cm^3s^{-1} independent of the fine structure component. He does not significantly remove the excited state over the pressure range of 1 to 10 Torr.

The two-photon excitation process creates non-equilibrium distributions in the magnetic sublevels of the excited state, thus generating spatially anisotropic polarized fluorescence. The emission from the initially excited state was polarized. Hence m_J changing collisions are competitive with quenching in the case of N_2 and with fine structure changing collisions for He. To remove the ambiguities in the fine structure changing results due to non-equilibrium m_J distributions, a magnetic field was applied to randomize the magnetic sublevels and destroy the initial laboratory frame orientation produced by the laser.

Figure 1 shows resolved fluorescence scans after excitation of each of the four fine structure components of the $^4D^o$ state at a fixed pressure of N_2 and He. The peaks correspond to transitions between different fine structure components of the $^4D^o$ and ^4P states; the solid line is the best fit for the four $^4D^o$ populations contributing to the fluorescence. Similar data at different pressures of N_2 and He plus values of the radiative lifetime and quenching rates yield state-to-state fine structure changing collision rates. This phase of the investigation is currently underway; however, several qualitative features are already apparent. Most importantly, $\Delta J \neq 1$ transitions occur significantly faster than those with $\Delta J = 2$ and $\Delta J = 3$ for all J. The $1/2 \rightarrow 3/2$ rate is the largest of all.

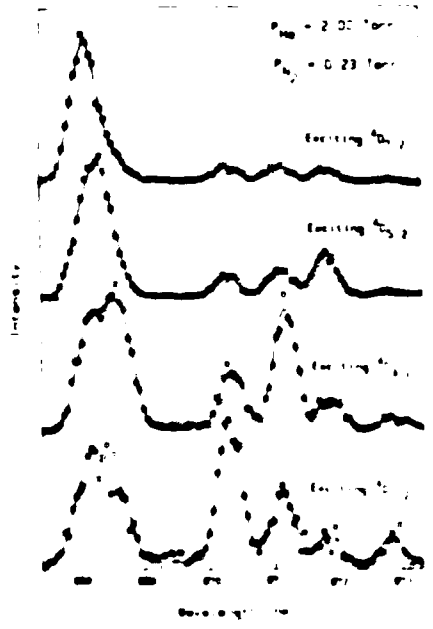

Fig. 1 N atom fluorescence scans.

These preliminary results on N atoms demonstrate how combining initial state selection and final state resolution can reveal the details of state specific collisions.

ACKNOWLEDGMENTS

Research in this area has been supported by NASA [illegible] NAS7-16956, NSF Grant [illegible] and AFOSR [illegible]. We gratefully acknowledge the experimental contributions of Paul Doherty on the flame study and Mark J. Dyer on the [illegible].

REFERENCES

1. R. A. Copeland and D. R. Crosley, [illegible] Phys. [illegible] (1984).
2. R. A. Copeland, M. J. Dyer, and D. R. Crosley, [illegible] Phys. 82, 4022 (1985).
3. P. W. Doherty and D. R. Crosley, Appl. Opt. 21, [illegible].
4. W. R. Bischel, B. E. Perry, and D. R. Crosley, Appl. Opt. 21, 1419 (1982).
5. J. B. Jeffries, R. A. Copeland, and D. R. Crosley, [illegible] published.

High Temperature Materials and Processes, Vol. 7, No. 1, 1986, 41-54

Laser-induced Fluorescence Measurement of Combustion Chemistry Intermediates

David R. Crosley

Molecular Physics Department, SRI International, Menlo Park, California 94025, USA

CONTENTS

ISSN 0334-1704

ABSTRACT

The method of laser-induced fluorescence (LIF) is a highly sensitive and selective way to measure trace species, often free radicals, which are intermediates in the chemistry of combustion. Examples of the molecules detected in flames by LIF are OH, CH, NH, NS and NCO. In this paper we describe the LIF method, using as examples several experiments from our laboratory. Included are experiments designed to develop a quantitative data base for LIF detection, performed in low pressure flow systems and in flames. Also described are measurements in flames where we seek to detect new chemical intermediates to provide insight into the combustion chemistry

INTRODUCTION

As in many technical fields, the introduction of lasers into combustion research has led to information not just new in quality but in entirely different categories than available before. The family of laser spectroscopic probes for combustion [1] includes the methods of spontaneous and coherent Raman scattering, and laser-induced fluorescence (LIF). Each provides information on specific molecular species which are present in the flame system. The Raman techniques are generally applicable to the measurement of parameters of interest to the flow dynamicist: overall density, temperature, and mole fractions of major (> 0.5 mole percent) fuel, oxidant and exhaust gases. LIF is best used for the measurement of trace species present at low concentrations which are intermediates in the combustion chemistry. Through knowledge of those intermediates one can understand the complicated chemical pathways involved in combustion.

The ultimate goal of these LIF experiments is the development of a microscopic understanding of that chemistry at a level which can be used for predictive purposes. Such a detailed picture of the chemistry is not so important for knowledge of, for example, the overall efficiency of combustion, which in practical systems is often controlled by fluid dynamic considerations. Rather the chemical details are crucial to a description of certain important individual processes among these are the formation of pollutants (NO_x, SO_x, soot), ignition phenomena, and flame inhibition.

LIF measurements approach this objective through determination of the trace species which are the carriers of that chemistry. The information can be used in different ways. In a stable laboratory flame, profiles of intermediates can be measured as a function of height above the burner, and compared with detailed computer models of the chemistry of combustion. In principle, one could compare the measurements with such code predictions so as to quantitatively establish the individual steps in the chemical mechanism. In practice, the rate constants for individual chemical reactions within such models are not yet well enough known to make this feasible. However, that situation will continually improve as the appropriate kinetics research continues, its emphasis guided in part by the results of current LIF experiments.

Another way in which LIF profiles can be used to obtain insight into the chemistry is by examination of the relative rates of appearance of certain radical species. For example, both OH and NH radicals are found in flames of CH_4 burning in N_2O. Whether OH precedes NH can address the question of the models and relative rates of breakage of the N-N vs the N-O bond in the N_2O. LIF may be used in an even simpler way in order to demonstrate the existence of some radical species within a flame. Here finding a new radical may pose questions about the flame chemistry which had not been previously considered. Our initial finding [2] of NH in the CH_4-N_2O flames was one example. experiments in which we discovered NS *in flames* will be described in detail below.

In this paper we will describe laser-induced fluorescence spectroscopic measurements in flames using examples from our own laboratory to portray the method. We emphasize that this article is intended to be illustrative and does not constitute a review of the field as a whole. For more comprehensive review papers we refer the reader to the articles cited in Ref. [3] as well as the collection of papers in Ref. [1]. Representative work in both development and applications of LIF can be found within the Diagnostic Sessions at the last International Symposium on Combustion [4].

THE LASER INDUCED FLUORESCENCE TECHNIQUE

In the method of laser-induced fluorescence a laser is tuned so that its wavelength matches that of an absorption line of some species in the flame. The species then absorbs the laser photons, becoming excited to an electronically excited state which then emits a photon (fluoresces). The fluorescent photon, perhaps after spectral filtering, is detected with a photomultiplier whose output forms the LIF signal. Typically the laser is directed into the flame (or other sample system) and

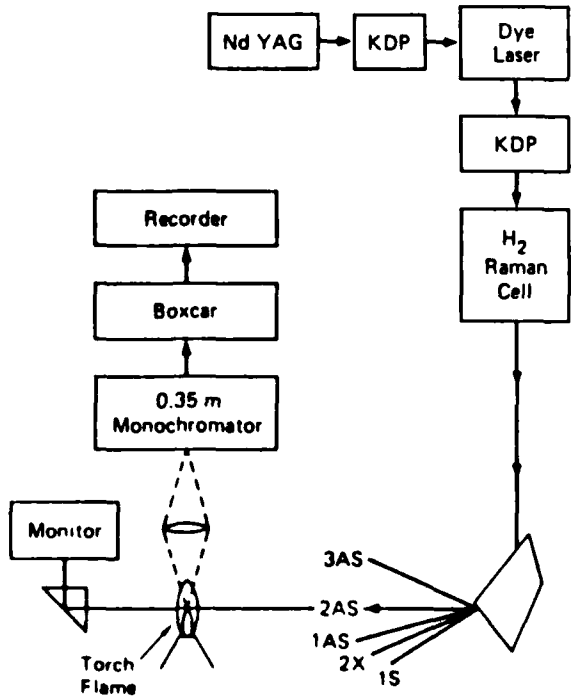

Fig. 1: Schematic illustration of a laser-induced fluorescence experiment in a flame, here shown using wavelengths suitable for excitation of the NS radical. In this case an infrared pump laser (Nd:YAG) at a fixed wavelength of 1.064 μm is frequency doubled in a potassium dihydrogen phosphate (KDP) csrystal to 532nm. This green laser radiation is then used to pump a tuneable dye laser which is operated near 572 nm. This is also frequency doubled, this time into the ultraviolet (286 nm). It in turn undergoes stimulated Raman frequency shifting in H_2 gas, producing a variety of wavelengths. The second antistokes shift near 230 nm is picked off by a prism and directed into the flame. Fluorescence at right angles is filtered through a monochromator and detected with a photomultiplier (not shown). The boxcar integrator is an electronic device whose gated amplifier turns on only when the laser is pulsed, greatly reducing background from the flame. A computer is often used instead of a recorder to acquire the data. [Reprinted from Ref. 19 by permission from the Combustion Institute]

the fluorescence is collected at right angles, as shown in the diagram of Fig. 1.

As the laser is tuned, it goes in and out of resonance with the molecular absorptions, so that the fluorescence signal is produced each time a match occurs. Such a so-called excitation scan is schematically depicted in Fig. 2. In Fig. 3 is shown an experimental excitation scan, here the laser was tuned through part of the absorption spectrum of one particular transition of the CH molecule present in the reaction zone of a CH_4 air flame /5/. One thus obtains a record of the absorption spectrum of the molecule in question, but with a significant difference compared with conventional absorption spectra. In LIF, one detects a positive fluorescence signal against a null background. This contrasts with the small dip in a large transmitted beam that constitutes normal absorption measurements. Thus LIF yields very high sensitivity; total absorptions less than 10^{-6} per cm produce strong LIF signals. Molecular concentrations in the ppb to ppm region can be readily measured.

LIF possess a number of other attributes which make it useful as a combustion probe. The laser can be focussed and the resulting fluorescent signal in turn imaged onto

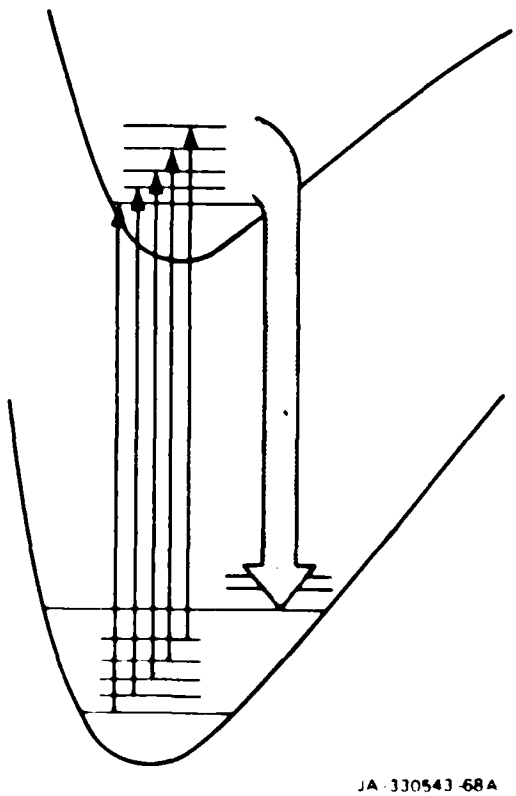

Fig. 2 Diagram indicating an excitation scan for LIF. The laser is scanned across a series of absorptions (upward arrows). Whenever any level in the upper state is excited, fluorescence results (large downward arrow) is collected through with a broad-band filter and detected. Thus the emitted radiation is used to sensitively measure the absorption spectrum and thus detect the ground state of the radical. [Reprinted from Ref. 2a by permission from the Society of Photo-Optical Instrumentation Engineers]

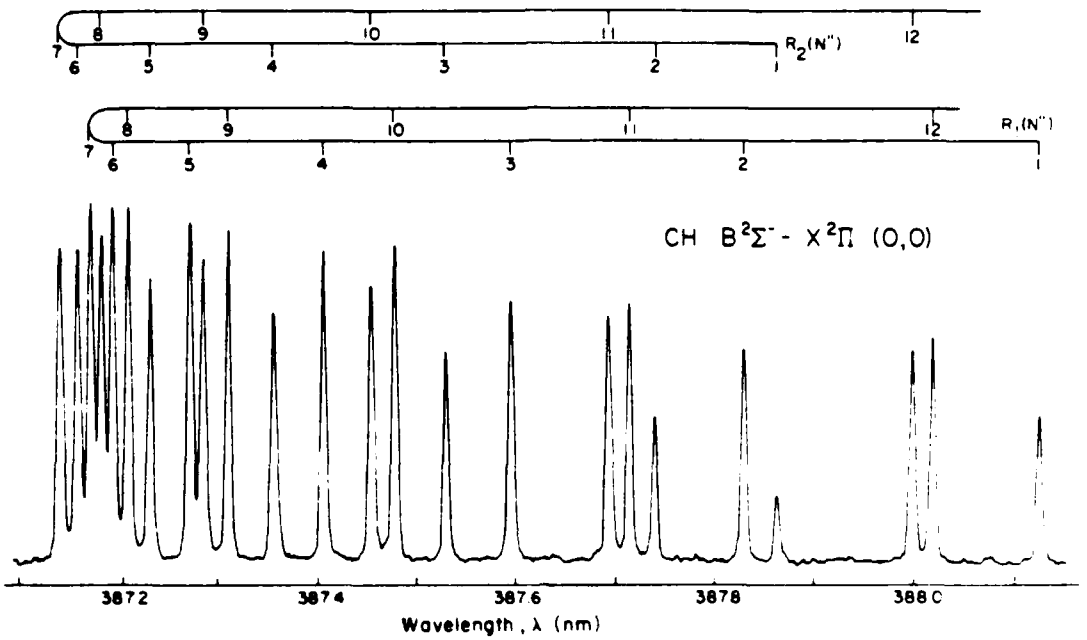

Fig. 3: Excitation scan through a series of rotationally resolved absorption lines of one vibrational band of a particular electronic transition. This is for the CH radical in a methane-air flame. Fluorescence is collected with a monochromator set to view fluorescence emitted by the upper state at a wavelength of 435 nm (reprinted from Ref. 5 by permission of the Optical Society of America).

a slit oriented perpendicular to the beam, thereby providing a high degree of spatial resolution. Sample volumes of $\sim 10^{-3}$ mm^3 are possible although 1 mm^3 is more typical. Most lasers used in LIF studies have pulse lengths of ~ 10 ns; single shot measurements therefore possess this time resolution. These characteristics are important because significant gradients exist over 1 mm spatial scales in atmospheric pressure flames, and, in turbulent flames, conditions change over time periods of the order of a few μs. Additionally, LIF is nonintrusive, that is, it does not perturb the gas flows or the flame chemistry. It can be used in hostile environments where a physical probe such as a sampling nozzle or thermocouple would not survive.

We have already seen that LIF is sensitive, it is also highly selective for small molecules that have well defined spectroscopic characteristics. The typical bandwidth for the pulsed, tunable lasers used for LIF studies is ~ 0.1–0.3 cm^{-1}, comparable to Doppler broadened linewidths in flames. This usually permits ready distinction between different molecular species. However, even if two species present in the flame absorb at the same wavelength, they will generally fluoresce at different wavelengths, permitting discrimination by filtering of the detected emission.

LIF is, in fact, the only measurement method capable of sensitive, fast, spatially resolved measurements on trace chemical intermediate species. However, it is not general as is, for example, mass spectroscopy. Its use is restricted to molecules having absorption transitions at wavelengths accessible to available lasers. With pulsed lasers, one can use nonlinear optical techniques to frequency double, mix, or Raman shift the fundamental tunable dye laser wavelength. In our laboratory we use these methods to perform LIF experiments with tunable radiation over the range 190 to ~ 1000 nm.

Fortunately, many combustion intermediates can be made to fluoresce. A list of many of the free radicals important in combustion chemistry which are detectable with LIF is given in Table I. (Not included are a number of metals, their oxides and halides often found in flames through seeding, nor many larger stable organic reaction intermediates species such as acetone and aldehydes.) The atomic species listed have their longest wavelength absorptions in the vacuum ultraviolet; in flames they are accessible with two-photon absorption, a phenomenon made possible by high laser intensity.

In addition to point measurements of radical species, LIF can be used in one-, two- and three-dimensional

TABLE 1. Molecules (1–4 Atoms) detectable by laser-induced fluorescence which are intermediates in combustion chemistry.

Molecule	Excitation wavelength (nm)	Molecule	Excitation wavelength (nm)
H*	206	NCO*	440
C	280	HCO	615
O*	226	HNO*	640
N	211	NH_2*	598
S	311	C_3	405
OH*	309	C_2O	665
CH*	413	S_2O	340
NH*	336	SO_2*	320
SH*	324	NO_2*	590
CN*	388	HSO	585
CO*	280	CS_2	320
CS	258	CCN	470
NO*	226	HCCO	310
NS*	231	NO_3	570
SO*	267	C_2H_2	238
S_2*	308	CH_2O*	320
C_2*	516		

An asterisk denotes that LIF detection has been performed in a flame

(2D) 8 versions, producing an image of the radical distribution along a line or in a plane through the flame. In the 2D version the laser is focussed into a sheet of radiation, perhaps 0.25 mm thick, using a cylindrical lens. The laser light is passed through the flame; everywhere that the chosen radical exists in the flame, fluorescence results. It is focused at right angles onto a 2D vidicon tube, yielding an instantaneous image of the molecular distribution at the time of occurrence of the 10 ns laser pulse. Such imaging measurements are useful for correlating the distribution in rapidly time-varying systems such as a turbulent flame, where conditions at a given point change rapidly between successive laser pulses.

The LIF signal intensity S is given by

$$S = \ldots BIfN_gA\ldots$$

Here [illegible] represents a collection of apparatus parameters specific to the particular experimental setup. This includes the volume probed by the laser and solid angle viewed by the lens collecting the fluorescence, the filter or monochromator transmission, the photo[illegible] sensitivity and gain, and the [illegible] of the processing electronics such as amplifiers, integrators and recorders. All of these parameters can be calibrated separately and independently. A useful way to calibrate all at once is through the use of Raman scattering of laser light from air above the unlit burner.

The remainder of the terms in Eq. (1) represent fundamental characteristics and behavior of the molecule under study and its flame environment. B is the effective Einstein absorption coefficient (that is, line shape effects are included implicitly) and I the laser intensity, so that BI is the pumping rate from the ground to the excited state in units of s^{-1}. N_g is the ground state concentration in molecules cm^{-3} and f the fraction which resides in the particular absorbing level with internal quantum numbers for vibration (v) and rotation (N), and perhaps molecular fine structure. Thus $BIfN_g$ is the number of excited state molecules produced per cm^3 per second. A is the Einstein emission coefficient (s^{-1}) and ϕ the fluorescence quantum yield.

In general, the electronically excited molecule suffers collisions during the time it resides in the upper state before it radiates at the rate A. Typically, [illegible] each thousand OH molecules excited by a laser in a flame at 1 atm, only one will emit a photon. The rest are collisionally removed to the ground state ("quenched") by collisions. ϕ is this fraction which emits and is given by

$$\phi = A/(A + Q + P)$$

where Q is the collisional quenching rate [illegible] cular flame environment and P is the [illegible] cess such as predissociation [illegible] state in a nonradiative [illegible] B and P are [illegible]

The laser [illegible]

[illegible]

limits of the accuracy attainable with LIF measurements are given by the state of knowledge of the appropriate collisional parameters. A recent assessment [9] of the situation for the diatomic hydrides OH, NH and CH was made. A most promising conclusion was reached for the case of OH, at least in flames of methane and ammonia burning in oxygen. Knowledge of the temperature and initial mixing ratio should furnish enough information to estimate Q to within about 30% in those situations. However, for the other hydrides (and all other molecules given in Table [illegible]) there is available no information on the temperature dependence of the quenching cross sections and very little concerning variation with collision partner. For molecules other than OH, Q for given flame conditions can be estimated to perhaps a factor of three [illegible] simply from general knowledge of molecular collisional phenomena. We shall make use of this [illegible] NS described below.

Fig. 4 [illegible]

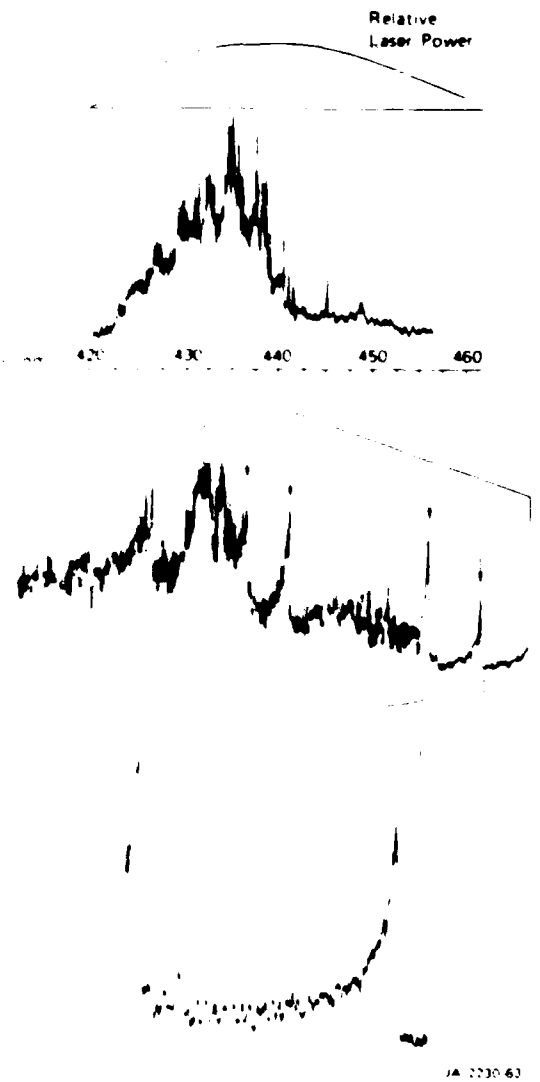

Fig. 5. Excitation scans for the A X electronic transition of NCO in a CH_4/N_2O flame. Fluorescence is collected at 465 nm. The topmost panel shows the relative laser power over the full wavelength range. Top scan: the full excitation over the entire gain region of the dye. Middle: a 4 nm range covering the 000-000 band, whose prominent heads are marked with arrows. Bottom: region between the two heads at longer wavelength, showing the rotationally resolved $^{OP}_{12}$ branch. All of the structure in the top and middle panels comprises lines and bandheads such as seen in the lowest. [Reprinted from Ref. 10 by permission of the Combustion Institute.]

...illustrating the nonthermal nature of ordinary light emission from flames.

As one proceeds to larger molecules the excitation spectra can become much more complex. Fig. 5 shows excitation scans in the NCO molecule in an atmospheric pressure CH_4/N_2O flame /10/. In this case, a spectrometer filter was used to ensure that only fluorescence from NCO was observed; strong excitations of CH, CN and C_2 also occur in this same wavelength region. The upper panel shows data from an excitation scan over the entire gain region of a particular laser dye. A very large number of bands are seen, with considerable blending at this level of resolution. If we scan over a smaller region, as shown in the middle panel, the four heads of the characteristic (000–000) band stand more clearly. The bottom panel shows a yet smaller portion of the spectrum (about 1% of the total range of the top panel) where individual rotational lines (and some noise) are now finally evident. These spectra are considerably more complex than those of diatomics, although NCO represents the next simplest spectroscopic case, that is, a linear triatomic radical. In our study of LIF of this and the NH_2 molecule in flames /10/, we concluded that the most definitive spectra result from excitation in hot bands, that is, those less congested spectral regions to the red where the absorption originates from elevated vibrational levels in the ground electronic state. An example of such a simpler band, with a full rotational analysis, is given in Fig. 6. In this study, we combined the high resolution afforded by the LIF method with the large number of vibrationally and rotationally excited levels accessible in the hot flame. The result was a new quantitative understanding of the vibrational level dependence of the molecular fine structure (spin-orbit splitting) in a linear triatomic radical /11/. Thus, flames can be used to advance laser spectroscopy as well as the converse.

We have noted that it may be necessary to discriminate between two absorbing species on the basis of the fluorescence spectra. A fluorescence spectrum is obtained by tuning the laser to a specific excitation, then keeping its wavelength fixed while scanning a monochromator which views the fluorescence (see Fig. 7). This may be used to look at different emission bands, as indicated in the figure, or to investigate collisional effects (see below).

Figure 8 exhibits fluorescence scans following excitation of NCO near 315 nm (via a different electronic transition than that in Fig. 5). In the lower panel is a fluorescence scan showing emission to various ground state vibrational levels (compare with Fig. 7), performed /12/ in a low pressure discharge flow cell experiment designed to isolate NCO for study. In the top panel is shown a fluorescence scan in an atmospheric pressure CH_4/N_2O flame /13/. Each band in the flame spectrum

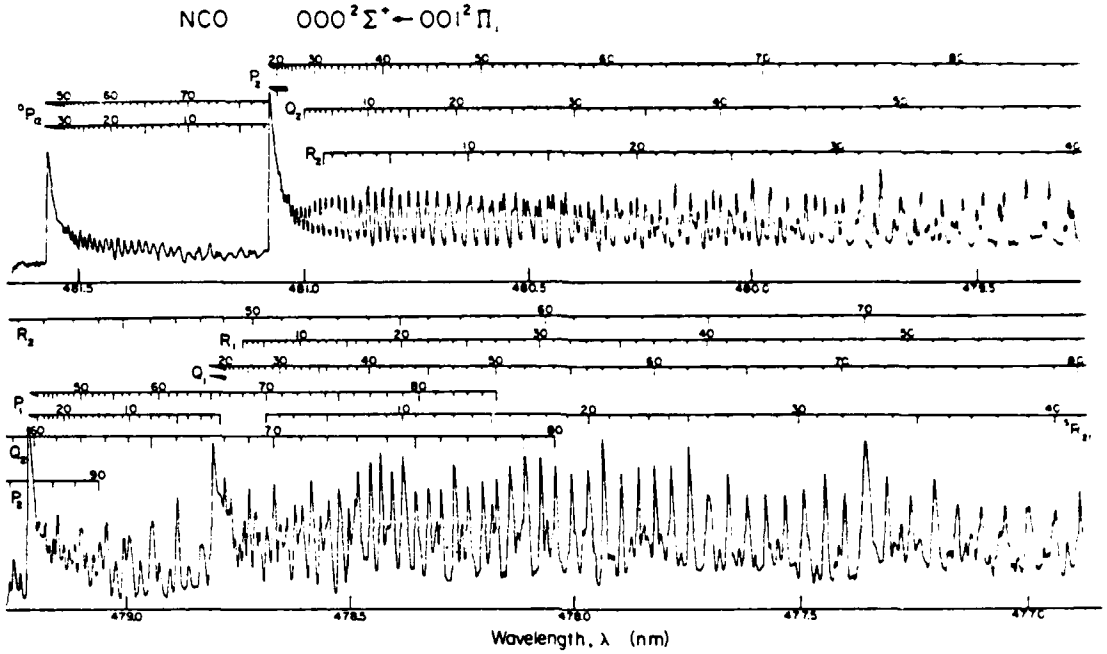

Fig. 6: Fully rotationally resolved, assigned and analyzed band of NCO in the CH_4/N_2O flame. This is a so-called hot band, absorbed by vibrationally excited molecules. It occurs at longer wavelengths than the bands in Fig. 5, and is much freer of congestion from other bands. From the analysis indicated can be determined spectroscopic constants for this linear molecule [Reprinted from Ref. 11 by permission of the National Research Council of Canada].

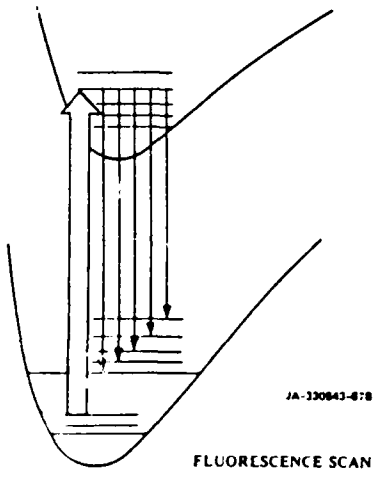

Fig. 7 Diagram depicting a fluorescence scan, in this case for a collision-free situation. Here the laser is set to a specific wavelength (heavy upward arrow) which excites one particular level in the upper state. The monochromator is scanned so that fluorescence at different wavelengths can be viewed (downward arrows). Although it is not shown explicitly on the diagram, the molecule could also undergo collisional energy transfer to one or more of the other upper states. If so, this could also be [illegible] by their fluorescence spectrum. [Reprinted [illegible] by permission of the Society of Photo-[illegible] Engineers]

is broader, due to a different spectral resolution used, but the pattern is clearly recognizable. Also present is fluorescence from OH and CN, excited simultaneously at the same laser wavelength. Obviously, one would wish to look at the 201 or 102 band to obtain the most interference-free spectrum (in actuality, the A-X system shown in Figs. 5 and 6 is generally preferable to NCO detection). Near the excitation used in Fig. 8 lies a region where a single laser wavelength can simultaneously excite /13/ OH, NH, CH and CN; this finding opens the possibility of obtaining simultaneous, instantaneous 2D images of each of these radicals.

A fluorescence scan can also be used to examine the effect of energy transfer collisions upon the molecule while it resides within the electronically excited state. Fig. 9 shows an example, from a study of rotational, vibrational and electronic energy transfer in the CH radical in atmospheric pressure flames /5/. In this case, rotational energy transfer is illustrated. The particular rotational level N = 14 is pumped by the laser. In the spectrally resolved R-branch emission (see Fig. 9), the rotational line emitted by N = 14 is much larger than any others. However, transfer

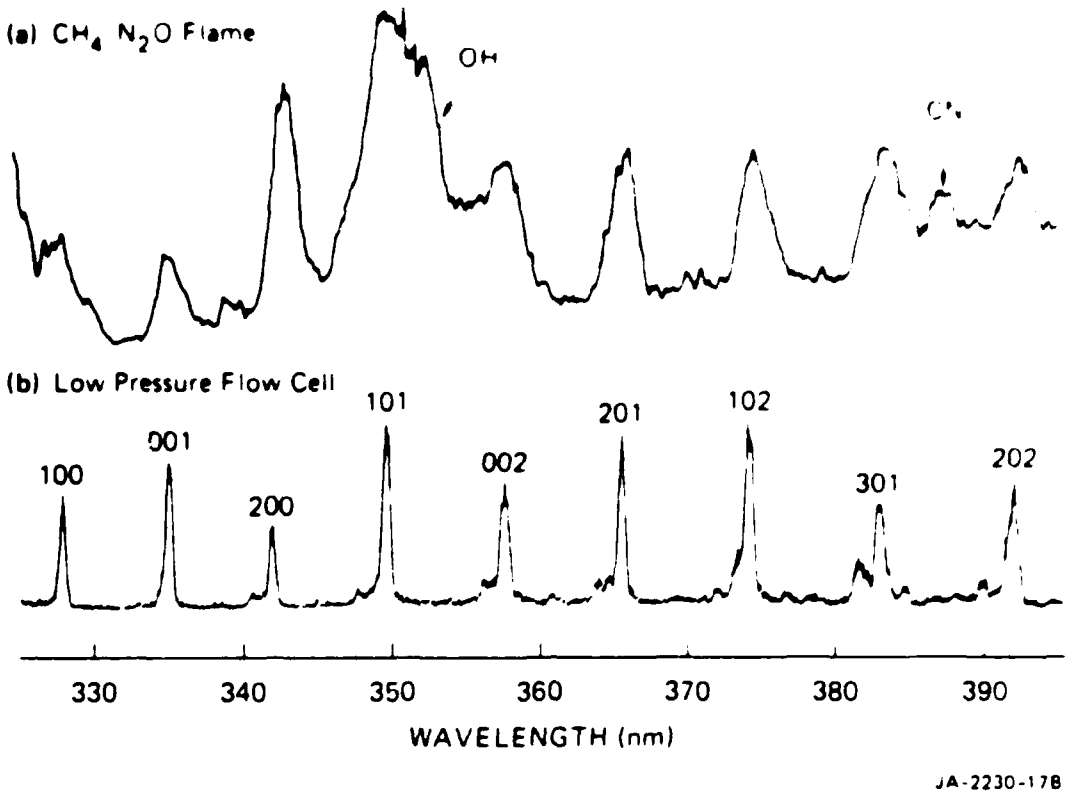

Fig. 8: Fluorescence spectrum of the NCO molecule. Here, one particular level is excited by the laser, and transitions to a series of lower vibrational levels are seen as the monochromator is scanned. Bottom: fluorescence scan in a low-pressure discharge flow system, in which only NCO can be seen. The numbering corresponds to each ground state vibrational level ($v_1v_2v_3$) which is the terminal level of the fluorescence (compared with Fig. 7). Top: fluorescence scan in an atmospheric pressure flame, using the same excitation wavelength. By its characteristic fluorescence pattern NCO can be distinguished even though there are here interferences due to the OH and CN molecules also. The use of the wavelength corresponding to either the 201 or the 102 band appear the best for detecting NCO among these interfering species [Reprinted from Ref. 13 by permission of the Combustion Institute].

has occurred to other rotational levels, as shown by the existence of other R-branch lines. The population distribution in the excited state is neither thermal, nor does it reside exclusively in the laser-pumped level. Rather, the distribution reflects a competition between rotational energy transfer (which drives the distribution toward thermal equilibrium) and quenching (which removes the molecules from the emitting state altogether). Recall also that the emitting CH formed from the chemiluminescent reaction was not describable by a temperature (Fig. 4). This is because the nascent product rotational distribution is in high-N levels, which do not thermalize at the flame gas temperature due to this same competition. In our energy transfer study, we found that rotational transfer in CH occurred about three times as fast as quenching. Such studies are needed for quantitative measurements of LIF and chemiluminescence; they also provide interesting fundamental information on molecular collision dynamics.

LABORATORY STUDIES FOR LIF DEVELOPMENT

Quantitative measurements of combustion reaction intermediates using LIF require knowledge of a large number of spectroscopic and collisional parameters. As we shall see in the next section, crude estimates can in many cases provide very useful information. It is desirable, however, to have as much directly measured information as possible. This is especially true in the case of the more frequently studied, important species such as the OH radical. A large portion of the work in our laboratory is directed at the measurement

of the appropriate parameters needed for quantitative LIF detection in flames. In this section we briefly describe the types of measurements which are necessary.

The first step in establishing LIF detection of some species in a flame is to study under controlled conditions where there do not exist interferences from other molecules. We perform many such measurements in a low-pressure discharge flow system operated typically between 0.01 and 10 torr, depending on the experiment. A microwave discharge is used to produce the radical itself or some precursor which through chemical reaction forms the desired molecule. For example, $H + NO_2 \rightarrow OH + NO$ is an efficient way to produce hydroxyl radicals for study at low pressure. Measurements are also made directly in flames and in our laser-pyrolysis laser fluorescence (LP LF) system [14]. The LP LF facility is a technique which we developed using rapid infrared laser heating of a gaseous sample to provide a controlled environment at elevated temperature (800–1400K). This permits the study of radicals undergoing collisional and reactive processes important in combustion, but without the complexities found in flames due to the occurrence of transport and gas dynamic phenomena.

The first measurements usually made are excitation scan studies, in order to identify the species unambiguously. Here, LIF work relies heavily on previous, classical absorption and emission spectroscopic studies. It is noteworthy that all the combustion intermediates detectable by LIF were first studied by chemists and physicists as part of fundamental spectroscopic studies, not by the user, applications-oriented community. (Hence, it is important to establish a coupling between current and future needs on the one hand and current and likely capabilities on the other).

The excitation scan studies furnish both line positions (e.g., Fig. 6) and intensities, from knowledge of appropriate spectroscopic parameters one can calculate line strengths needed for a reduction of the spectral intensities to populations (Figs. 3 and 4). Because of the existence of numerous hot bands under flame conditions (see Fig. 5 for NCO spectra) it is essential to have the spectroscopic information well established when one begins a search for a given radical under actual combustion conditions.

Fluorescence scans may be needed for identification of the species in the presence of other absorbers as illustrated in the upper panel of Fig. 8. They are also necessary for quantitative measurements; consider this same example. A spectrometer (or filter) would be set to detect only one band of NCO, say the 0_0^0. This represents a small fraction of the total emission; the relative transition probabilities (Franck-Condon factors) for each vibrational band must be determined through fluorescence scans under isolated conditions.

An important set of spectroscopic and collisional parameters can be determined through measurements of the time dependence of the decay of the electronically excited state. Such measurements form an important part of our laboratory studies.

The Einstein emission coefficient A is the reciprocal of the radiative lifetime τ_r,

$$A = 1/\tau_r \tag{3}$$

τ_r may be measured under very-low-pressure conditions in the flow system. A pulsed laser excites the molecule and the direct time-dependent decay of the fluorescence is measured by a fast-response photomultiplier amplifier and data acquisition system. If one adds to the system a known density n_i of some collider gas of species i the effective observed lifetime is shortened due to quenching collisions

$$1/\tau_{eff} = 1/\tau_r + k_{Qi}n_i \tag{4}$$

where k_{Qi} is the quenching rate constant (units $cm^3 s^{-1}$) for collider species i and the radical under study. An example of a series of lifetimes with increasing collider density is given in Fig. 10. These measurements [15] were made at room temperature in a flow system.

In the flame itself, the quenching rate Q is given by a sum of all these bimolecular collision rates and the densities of each species

$$Q = \Sigma_i k_{Qi}n_i \tag{5}$$

To be applicable to flames, one must thus know the temperature dependence of the quenching rate constants. We have considered this by comparison of our room temperature OH results [15] with measurements on the same radical at high temperature using the LP LF apparatus [16].

Several interesting and surprising features have emerged from those OH studies. The first is that the rate constants are large and decrease with increasing temperature, showing that attractive intermolecular forces play a major role in the quenching of OH [15, 16]. Secondly, the k_{Qi} depend markedly on the rotational level of the excited OH, a fact suggestive of some very unusual molecular collision dynamics [15]. We have also made measurements on quenching of

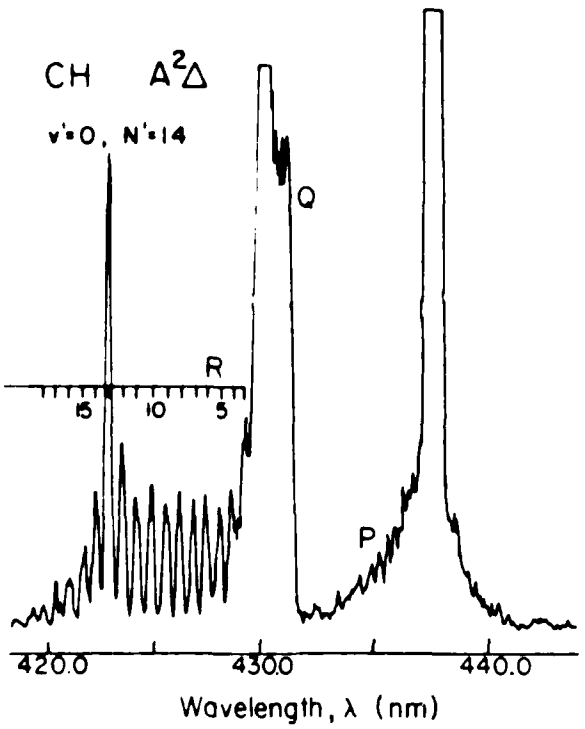

Fig. 9: Fluorescence spectrum of the CH molecule in an atmospheric pressure flame. Here, the N = 14 level of the upper state is pumped. It emits the rotational line R(13) as shown. Other lines are evident as well, corresponding to other rotational levels in the upper state (as in Fig. 7) which have been populated by energy transfer collisions with the flame gases. The upper state is clearly not at thermal equilibrium although some transfer has taken place. Each upper state level also emits in the spectral regions marked Q and P but those branches are not resolved with the monochromator used here [Reprinted from Ref. 5 by permission of the Optical Society of America].

NH /17/ and CH /18/ at elevated temperature. Here, the situation is quite different than for OH; one has neither the correlation with attractive forces seen for OH nor the same kind of temperature dependence. Thus it appears that each molecule must be studied separately; there are at this time too many unknowns to develop simple scaling relationships from one radical to another.

Studies of energy transfer among different levels of the electronically excited state are also of importance in establishing quantitative diagnostics. An example of such a study in CH in flames has already been discussed (Fig. 9); such measurements are also performed in flow systems so as to obtain collider-specific energy transfer rate constants.

LIF DETECTION OF A NEW SPECIES: THE NS RADICAL

For quantitative measurements of radicals using LIF, several spectroscopic and collisional parameters are needed. These are given in Eqs. (1) and (2), and their determination under controlled-environment conditions has been discussed in the preceding section. For the more commonly found radicals such as OH, the measurement of these parameters is necessary and ongoing. However, for nearly all other species in Table 1, much less information is available. We consider here a case in which we needed to estimate many of the needed parameters, but nonetheless were able to draw some very interesting new conclusions concerning detailed combustion chemistry. This study /19/, in which the NS free radical was observed for the first time in flames, represents a different way to use LIF from that in all previous combustion studies.

The NS radical had never before been observed in flames by any means, and had seldom been considered a potential flame intermediate. Its reaction rates have not been measured under any conditions. We wondered whether it may be present in flames of hydrocarbons containing fuel sulfur and fuel nitrogen, which are often combined in various coals. If so, it could be a link between NO_x and SO_x production cycles.

Our studies of the NS radical, which had not previously been detected with LIF under any conditions, began with a series of studies in a flow system /20/ as described in the preceding section. Measurements on several excited states, including the $C^2\Sigma^+$ and $B^2\Pi$, were made, including excitation and fluorescence scans and lifetime studies. An excitation scan through one vibrational band of the C-X transition near 230 nm is shown in the upper panel of Fig. 11. One sees individual rotational lines which can be assigned and analyzed; the four-headed structure is familiar for the type of electronic transition involved.

A small burner was then positioned in place of the flow system and used to burn a CH_4/N_2O mixture seeded with SF_6. The laser was scanned through the same wavelength region. The result is shown in the lower panel of Fig. 11. We can conclude unambiguously that we see here the same molecule examined under controlled conditions in the flow system; the selectivity of LIF is clearly demonstrated in this comparison. There are more individual lines in the flame study because the temperature is higher, leading to a significant population in a larger number of rotational levels.

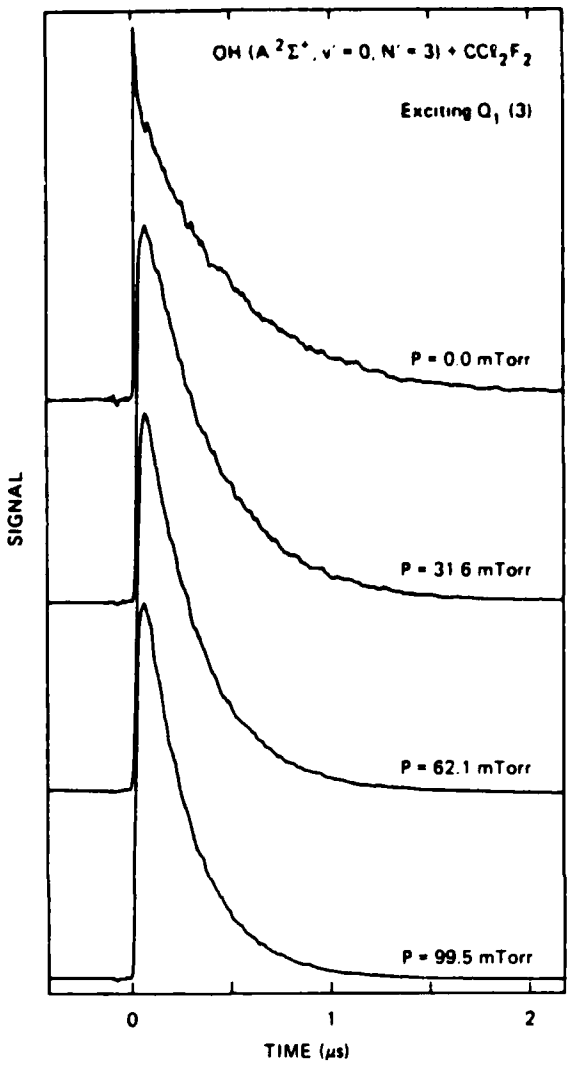

Fig. 10: Fluorescence decay signals of the OH molecule in a room temperature low-pressure discharge flow system experiment. A laser with a pulse length of 10 ns excites the OH. At the end of the laser pulse the OH decays exponentially with a characteristic lifetime. With no added gas, the decay is due entirely to the radiative rate for the transition. As more CCl_2F_2 is added, the decay becomes more and more rapid due to quenching collisions. A plot of the decay rate vs. quencher density would yield the rate constant k_{Qi} as slope and the radiative rate $1/\tau$ as intercept, as indicated in Eq. (4) [Reprinted from Ref. 15 by permission of the American Institute of Physics].

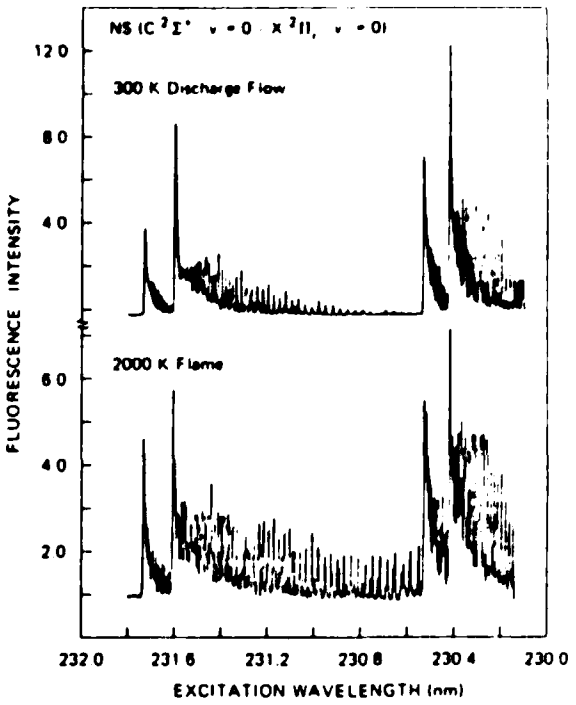

Fig. 11: Excitation scans of the NS molecule. Shown is the 0,0 vibrational band of the $C^2\Sigma^+ - X^2\Pi$ electronic transition near 231 nm. The four prominent band heads are typical for this type of electronic transition; and many individual rotationally resolved lines can be seen. Top panel: excitation scan where the NS is produced in a room temperature, low pressure microwave discharge flow system. Bottom panel: excitation scan in an atmospheric pressure CH_4/N_2O flame, seeded with SF_6. Scans in CH_4/O_2 flames seeded with NH_3 and H_2S appear identical. It is clear that the same molecule is being detected in both cases. In the flame, there exist more individual rotational lines because higher-lying rotational levels contain more population at the high flame temperature [Reprinted from Ref. 19 by permission of the Combustion Institute].

We next moved to a simulated coal flame, for which we used methane burning in oxygen, seeded with NH_3 and H_2S to represent fuel nitrogen and sulfur. The results obtained here were identical to those in the lower part of Fig. 11. Studies were made in a variety of flames with differing amounts of seeding of the fuel nitrogen and fuel sulfur simulants. We even observed NS in a flame of pure natural gas burning in N_2O; here the sulfur came from the methyl mercaptan added by the utility company at 2 ppm concentration, in order to produce a detectable odor in the gas.

Simply finding the NS molecule already raises interesting questions, but conclusions concerning its possible role in NO_x-SO_x interactions might be possible if we had some idea of its absolute concentration in the flame. As indicated by Eqs. (1) and (2), relating the measured signal level S to the desired ground state

concentration N_g requires the knowledge of a large number of spectroscopic and collisional parameters. For NS, it was necessary to draw on those previous measurements which are available, but also make some estimates based on analogy with other molecules. The procedure and our choices are described in detail in Ref. 19. The Einstein A coefficient was taken from a theoretical quantum chemical calculation, it together with our experimental Franck-Condon factors and calculated line strengths furnished an absorption coefficient B. The decay of the $C^2\Sigma^+$ state of NS is governed by predissociation, whose rate P was taken from magnetic depolarization ('Hanle effect') measurements (the effective lifetime, ~ 6 ns, is too fast for direct measurement with our electronics). With A and P, ϕ can be calculated if the quenching rate Q is known. However, quenching of the C-state has never been measured. We estimated individual k_{Qi} by analogy with previous studies on NO and PO, and our measurements on the B-state of NS. A careful consideration of all these factors led to an estimate of an uncertainty of a factor of three in the resulting absolute concentration.

How good is a measurement to within a factor of three? When the molecule has never been seen before in a flame, it can be quite revealing. For example, in some flames, the steady-state NS concentration within the flame zone is as much as 5% of the added sulfur. This means that a very large fraction of the sulfur is being processed through this radical. With this information, and the fact that the NS signal disappeared quickly as the laser was moved into the burnt gases, we deduced that the NS was removed by a reactant present at concentrations of at least a few tenths of a mole percent. It was produced by a reaction between some radical (present at 10 ppm or more) reacting with a stable species present at ~ 0.1% or more.

We concluded that NS may be an important reaction intermediate in the reducing atmosphere of rich hydrocarbon flames containing fuel nitrogen and sulfur, and that it may play a major role in NO_x-SO_x interactions. This observation of its presence does not prove that role, but certainly further studies in flames and direct measurement of its reaction rates are called for. This does demonstrate that, even in the absence of a full set of analytical parameters, LIF can be a powerful tool for bringing new types of insight into combustion chemistry.

CONCLUSION

In this paper we have given a brief review of the method of laser-induced fluorescence as used to understand the chemistry of combustion. LIF is seen to be a very sensitive and selective means of measuring trace chemical reaction intermediates, affording a high degree of spatial and temporal resolution and a nonintrusive nature.

For highly quantitative studies using LIF, a variety of spectroscopic and collisional parameters is needed in the analysis of signal levels. These can be obtained through separate laboratory studies in low pressure flow systems, a laser pyrolysis-laser fluorescence system or in flames themselves. Such measurements are clearly warranted for a number of radicals including the important OH molecule, which is the subject of many LIF combustion measurements.

Even when these parameters are not available, however, LIF can be very useful. The only requirement is that the species in question be unambiguously identifiable in a flame system. An example was given of the first detection of the NS radical in a flame, and important conclusions were reached concerning its participation in coal flames and the interaction between the formation of NO_x and SO_x in such flames. Clearly, both quantitative measurements and semi-quantitative observation of flame radicals using LIF will greatly add to our knowledge of detailed flame chemistry in the future.

ACKNOWLEDGEMENTS

The research described here encompasses many different projects and has been performed by a large number of colleagues, working with whom has been a pleasure. I gratefully acknowledge Richard Copeland, Mark Dyer, Paul Fairchild, Nancy Garland, Jay Jeffries, Gregory Smith and Brian Sullivan for their participation. Funding has been furnished by various agencies for different aspects of the research; I thank the U.S. Army Research Office, the Basic Energy Sciences Division of the Department of Energy, the National Science Foundation, the National Aeronautics and Space Administration, and the Physical Sciences Department of the Gas Research Institute for their support.

REFERENCES

1 CROSLEY, D.R. Laser Probes for Combustion Chemistry. *Amer. Chem. Soc. Symposium Series* **134** (1980)

2 (a) CROSLEY, D.R. *Opt. Engr.* **20**, 511 (1981).
(b) CROSLEY, D.R. *J. Chem. Ed.* **60**, 446 (1982).

3 (a) CROSLEY, D.R. and SMITH, G.P. *Opt. Engr.* **22**, 545 (1983).
(b) BECHTEL, J.H., DASCH, C.J. and TEETS, R. in *Laser Applications*, R.K. Erf and J.F. Ready, eds. Academic, New York (1983).
(c) LUCHT, R.P. in *Laser Spectroscopy and Its Applications*, L.J. Radziemski, R.W. Solarz and J.A. Paisner, eds. Marcel Dekker, New York (1986).

4 Twentieth Symposium (International) on Combustion. The Combustion Institute, Pittsburgh (1985).

5 GARLAND, N.L. and CROSLEY, D.R., *Appl. Opt.* **24**, 4229 (1985).

6 BISCHEL, W.K., PERRY, B.E. and CROSLEY, D.R., *Chem. Phys. Lett.* **82**, 85 (1981). *Appl. Opt.* **21**, 1419 (1982).

7 ALDEN, M., EDNER, H., HOLMSTEDT, G., SVANBERG, S. and HOBERG, T., *Appl. Opt.* **21**, 1236 (1982).

8 (a) DYER, M.J. and CROSLEY, D.R., *Opt. Lett.* **7**, 382 (1982).
(b) KYCHAKOFF, G., HOWE, R.D., HANSON, R.K. and MCDANIEL, J.C., *Appl. Opt.* **21**, 3225 (1982).

9 GARLAND, N.L. and CROSLEY, D.R., Twenty-First Symposium (International) on Combustion, Munich 1986, in press.

10 COPELAND, R.A., CROSLEY, D.R. and SMITH, G.P. Twentieth Symposium (International) on Combustion, The Combustion Institute, Pittsburgh, p. 1195 (1984).

11 COPELAND, R.A. and CROSLEY, D.R. *Opt. J. Ph.* **82**, 1488 (1984).

12 SULLIVAN, B.J., CROSLEY, D.R. and SMITH, G.P. *J. Chem. Phys.*, to be published.

13 JEFFRIES, J.B., COPELAND, R.A., SMITH, G.P. and CROSLEY, D.R. Twenty-First Symposium (International) on Combustion, Munich 1986, in press.

14 SMITH, G.P., FAIRCHILD, P.W., JEFFRIES, J.B. and CROSLEY, D.R. *J. Phys. Chem.* **89**, 269 (1985).

15 COPELAND, R.A., DYER, M.J. and CROSLEY, D.R. *J. Chem. Phys.* **82**, 4022 (1985).

16 (a) FAIRCHILD, P.W., SMITH, G.P. and CROSLEY, D.R. *J. Chem. Phys.* **79**, 1795 (1983).
(b) SMITH, G.P. and CROSLEY, D.R. *J. Chem. Phys.* in press (1986).
(c) JEFFRIES, J.B., COPELAND, R.A. and CROSLEY, D.R. *J. Chem. Phys.* in press (1986).

17 GARLAND, N.L., JEFFRIES, J.B., CROSLEY, D.R., SMITH, G.P. and COPELAND, R.A. *J. Chem. Phys.* **84**, 4970 (1986).

18 GARLAND, N.L. and CROSLEY, D.R., *Chem. Phys. Lett.* to be published.

19 JEFFRIES, J.B. and CROSLEY, D.R., *Comb. Flame* **64**, 55 (1986).

20 (a) JEFFRIES, J.B., SMITH, G.P. and CROSLEY, D.R. *Bull. Amer. Phys. Soc.* **28**, 1320 (1983).
(b) JEFFRIES, J.B., CROSLEY, D.R. and SMITH, G.P. *J. Chem. Phys.*, to be published.

Radiative lifetime and quenching of the $3p\ ^4D^0$ state of atomic nitrogen

Richard A. Copeland, Jay B. Jeffries, Albert P. Hickman, and David R. Crosley
Chemical Physics Laboratory, SRI International, Menlo Park, California 94025

(Received 4 November 1986; accepted 13 January 1987)

The radiative lifetime of nitrogen atoms in the $3p\ ^4D^0$ state is determined to be 43 ± 3 ns, and the total removal rate constants from the excited $3p\ ^4D^0$ state of nitrogen atoms are measured for collisions with He, Ne, Ar, Kr, Xe, and N_2. In a low pressure discharge flow reactor, the $3p\ ^4D^0$ state is prepared by two-photon excitation from the $^4S^0$ ground state of atomic nitrogen. Time-resolved fluorescence from the $3p\ ^4D^0 \rightarrow 3s\ ^4P$ transition monitors the temporal evolution of the population in the $3p\ ^4D^0$ state. As the rare gases become heavier with a more complex electron cloud, the quenching rate constants increase from less than 0.6×10^{-11} $cm^3 s^{-1}$ for He to a value of $66 \pm 12 \times 10^{-11}$ $cm^3 s^{-1}$ for Xe. Collision mechanisms which might account for such a dramatic increase are discussed.

I. INTRODUCTION

Collisional energy transfer involving excited atoms with nonzero spin and orbital angular momentum is a fundamentally interesting and often studied process. The collisions of metastable electronically excited atoms[1] and the collisional deactivation of highly excited Rydberg atoms[2] are two broad areas where a significant amount of data is available. The Rydberg atoms, modeled as one outer electron and an unstructured core, have provided information to test the theories of electronic energy transfer. The quenching of high-lying Rydberg levels is modeled[3] by the interaction of the excited electron with the electron cloud of the collider. The quenching of lower-lying Rydberg levels is better explained by the interaction of the ionic core with the collider.[4]

The quenching cross sections of metastable electronic states of the rare gases are correlated[5] with a mechanism dominated by long-range forces. A similar model was proposed[6] for electronically excited small molecules and applied to the quenching of SO_2. We have successfully applied this long-range forces picture to the variation of the quenching cross section with temperature for the quenching[7-9] of $OH(A\ ^2\Sigma^+)$. This model concentrates on the collision dynamics on the interaction potential of the initial molecular state and does not include the state mixing required for the colliders to move from the initial to final electronic states. On the other hand, state mixing is thought to dominate the deactivation of metastable excited oxygen atoms.[10] This quenching cross section dramatically increases as the colliding rare gas becomes heavier, a result similar to our observations reported here for $N(3p\ ^4D^0)$. This indicates that the quenching process can be quite sensitive to the coupling with available final states.

In this experiment, we measure the radiative lifetime of the $3p\ ^4D^0$ state of nitrogen atoms and the quenching from that state by collisions with rare gas atoms and nitrogen molecules. Here we define quenching as the total collisional removal from the entire fine structure manifold of the $3p\ ^4D^0$ state.[11] The excited nitrogen is prepared by two-photon absorption[12,13]; following excitation, the temporal evolution of the total fluorescence from this state to the $3s\ ^4P$ state is monitored. From the pressure dependence of the fluorescence decay we obtain the collisional quenching rate constant k_Q and extract the thermally averaged cross section, $\sigma_Q \equiv k_Q/\langle v \rangle$, where $\langle v \rangle$ is the average relative collision velocity. The quenching cross section increases by more than a factor of 250 as the rare gas collider is changed from He to Xe. We compare the results with those from other quenching measurements on electronically excited atoms in an attempt to determine the dominant mechanism of the quenching collision. A model which considers only the long range attractive interaction of the collision pair yields reasonable cross sections for Xe and N_2, but cannot explain the large variation in cross section for the five rare gases. Estimates based on a two state excitation transfer mechanism provide cross sections consistent with observations for Ar and Kr colliders. This mechanism refines the collision dynamics on the attractive molecular potential curves by including the coupling between specific initial and final states. In He and Ne energetically accessible excited states are not available and such coupling cannot be the dominant mechanism.

II. EXPERIMENTAL APPROACH

In a low pressure flow reactor, a microwave discharge through either pure N_2 or a rare gas–N_2 mixture generates the nitrogen atoms. The neat nitrogen experiments, used to measure the radiative lifetime and the N_2 collisional quenching rate constant, employ pressures between 0.15 and 1.3 Torr. For the mixed gas experiment, N_2 and rare gas partial pressures vary from 0.05 to 0.2 Torr and 0.3 to 4 Torr, respectively. Total gas pressure, when combined with measurements of mass flow of each species, yields the partial pressures of each component. The average flow velocity for the experiments with N_2, He, and Ar colliders is ~ 3000 cm/s, and for the other rare gas experiments is ~ 200 cm/s. In both conditions, the excitation laser beam intersects the flow ~ 50 cm downstream of the discharge. At this distance and these flow rates any complicating effect of the N atom production method, such as an elevated bulk gas temperature, is insignificant. This assumption is verified by measurements with Ar; the temporal evolution of the fluorescence at constant Ar pressure shows no dependence on the flow velocity between 200 and 3000 cm/s.

References 12 and 13 contain a detailed description of the two-photon laser-induced fluorescence (LIF) technique

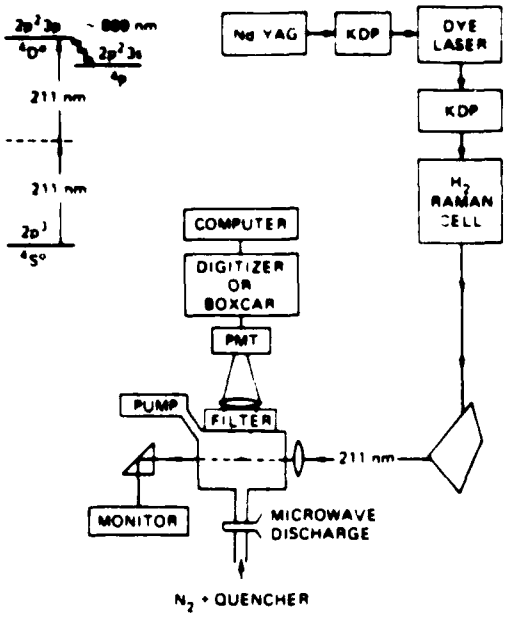

FIG. 1. Schematic diagram of the experiment. Inset denotes the electronic states and wavelengths involved in the detection scheme; fine structure splittings are too small to show on this scale.

as applied to nitrogen atoms, therefore only a brief description follows. A ground state nitrogen atom resonantly absorbs two ultraviolet photons ($\lambda \sim 211$ nm, ~ 10 ns pulse length) which elevate it to the $3p\ ^4D^0$ state. As schematically illustrated in Fig. 1, we obtain this wavelength light by first frequency doubling and then Raman shifting the output of a tunable Nd–YAG pumped dye laser operating near 572 nm. A Pellin–Broca prism separates the desired third anti-Stokes component from the rest of the Raman shifted beam, and a 7.5 cm focal length lens focuses the 211 nm light into the low pressure flow reactor. The spin–orbit interaction splits the $3p\ ^4D^0$ state into four levels with different total angular momentum; the magnitude of this splitting is 111 cm^{-1} between $J = 1/2$ and $J = 7/2$. Thus, we can selectively excite each of the four individual spin orbit levels of the $3p\ ^4D^0$ state by tuning the wavelength of the ultraviolet light.

The population of the excited $N(3p\ ^4D^0)$ is monitored via its near infrared fluorescence (~ 870 nm) to the ^4P state. A red sensitive photomultiplier, either an RCA 31034 or a Hamamatsu R666, detects the fluorescence perpendicular to the laser beam. A long wavelength pass colored glass filter (Schott #RG-830) and an interference filter centered at 870 nm with a 12 nm bandwidth isolate the fluorescence from the other background light. The bandwidth is sufficiently broad that fluorescence is collected from all the spin–orbit levels of the $3p\ ^4D^0$ state, i.e., from the one initially excited and from those populated by collisional energy transfer from the initial level. The fluorescence is time resolved by a 1 GHz transient digitizer (Tektronix R7912) controlled by a PDP 11/10 computer; the data is averaged for 30 to 100 laser shots. Initial results for N_2 as a quencher were obtained with either a 100 MHz transient digitizer (DSP model 2101) or a scanning gate boxcar integrator (Stanford Research Systems SR250); these measurements agree with the results from the 1 GHz digitizer.

A. Fluorescence polarization

The $^4D^0 \rightarrow {}^4P$ fluorescence is polarized, and any effects of the collisonal depolarization on the collisional quenching rate measurements must be avoided. The excitation light has the same linear polarization as the frequency-doubled dye laser because the Raman shifting process does not alter the polarization. Dipole selection rules require the intermediate level of the two-photon excitation to be ^4P, thus, for a given J in the excited state, the population distribution can be calculated for the degenerate sublevels corresponding to different angular momentum projections m_J (the influence of hyperfine coupling is neglected). The $J = 1/2$ level obviously has equal populations in the m_J sublevels; for the $^4S^0$ to $^4D^0$ two-photon excitation, the $J = 3/2$ level also has equal populations in the m_J sublevels. For both the $J = 7/2$ and $5/2$ levels in the $3p\ ^4D^0$ state the initial populations of the m_J sublevels are not equal for excitation with linearly polarized laser light; in fact sublevels with $|m_J| \geq 5/2$ are not populated at all. This anisotropy causes a polarization of the fluorescence of the $3p\ ^4D^0 \rightarrow 3s\ ^4P$ transition near 870 nm.

The $3p\ ^4D^0 \rightarrow 3s\ ^4P$ fluorescence retains most of its initial polarization even after the excited state undergoes collisions. At flow reactor pressures of pure nitrogen above 1.5 Torr and He/N_2 mixtures above 2 Torr, we have observed the retention of substantial fluorescence polarization.[11] Fluorescence polarization means that the spatial distribution of the fluorescence is not isotropic, even in the presence of colliders. Thus, at our specific observation direction, polarization-changing collisions may alter the time dependence of the fluorescence intensity. In order to remove any ambiguities between collisional equilibration of the m_J distributions, we apply a magnetic field of ~ 25 G to randomize the magnetic sublevels and destroy the initial laboratory frame orientation produced by the laser.[14] For magnetic fields above ~ 15 G no polarization of the fluorescence is observed.

III. RESULTS

The bottom panel of Fig. 2 shows the time-resolved fluorescence following excitation of $N(3p\ ^4D^0_{7/2})$ with Xe as a collider. The upper panel exhibits the natural logarithm of this fluorescence data; note that the decay is linear for nearly four decay constants. We fit these time-resolved fluorescence curves to a single exponential between 75% and 5% of the maximum value; Fig. 2 contains such a fit for the sample data. Fits of the decays from 90% to 10% give identical results, further assuring us there is no significant error in the decay constant from collisional relaxation of the initial nonequilibrium m_J distribution in the $J = 7/2$ level.

Because N_2 is required for N atom production, the collisional quenching of $N(3p\ ^4D^0)$ by N_2 must be characterized. As noted above, the temporal evolution of the $3p\ ^4D^0 \rightarrow 3s\ ^4P$ fluorescence was studied vs pressure for a pure nitrogen flow. Decay constants from the fits of the time-resolved fluorescence are plotted vs nitrogen pressure in Fig. 3, where the line is a least-squares fit to this data, weighted by the statistical uncertainty of each decay constant. The slope of the line is the quenching rate constant, $k_Q = 4.6 \pm 0.4 \times 10^{-10}$ $cm^3\ s^{-1}$, and the intercept is the radiative decay

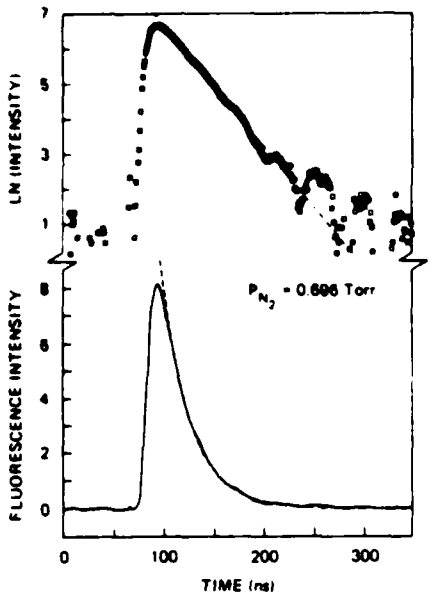

FIG. 2. Temporal evolution of the laser-induced fluorescence from $N(3p\ ^4D^0)$ in linear and logarithmic form. The dashed line is the linear least-squares fit to a single exponential decay.

rate, $k_r = 2.35 \times 10^7\ s^{-1}$, which corresponds to a radiative lifetime of 43 ± 3 ns. The error limits reflect 2-σ uncertainties. Separate experiments were performed exciting each of the four J levels of the $3p\ ^4D^0$ state, and the measured k_Q and k_r are identical for all the J levels. Therefore, within the $\pm$ 10% measurement uncertainty, the radiative lifetime for the $3p\ ^4D^0$ state does not vary with J. Figure 3 contains data from each of the four initial J levels.

The radiative lifetime we determine is slightly faster but still in agreement with the 53 ± 8 ns determination by Richter[15] who made intensity measurements in a nitrogen plasma. It also agrees with the theoretical estimate of 37 ns

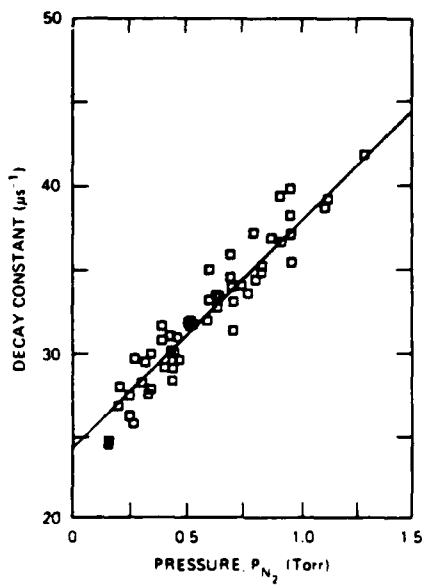

FIG. 3. The pressure dependence of the fluorescence decay constant for collisions with molecular nitrogen.

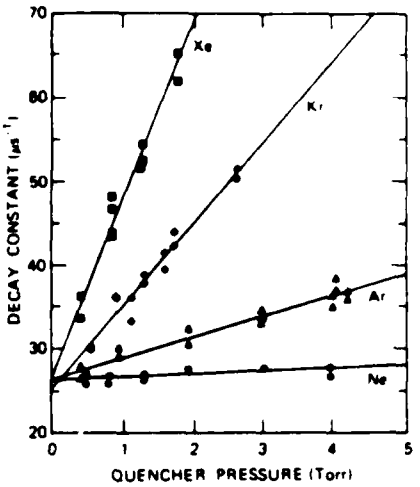

FIG. 4. The pressure dependence of the fluorescence decay constant for the rare gas colliders: Ne (circles), Ar (triangles), Kr (diamonds), and Xe (squares).

from the method of Bates and Damgaard.[16] However, both the lifetime and the quenching rate constant for N_2 disagree with the previously published results from this laboratory by the same two-photon LIF technique; Ref. 12 reports $k_Q = 2.4 \pm 0.6 \times 10^{-10}\ cm^3\ s^{-1}$ and $\tau = 27 \pm 3$ ns. These results, with 1-σ error limits, are from an unweighted fit to data taken at only five different N_2 partial pressures, which is much more scattered than the new data shown in Fig. 3. If we perform a weighted least-squares fit to the five decay constants reported in Ref. 12, we find a quenching rate, $k_Q = 3.4 \pm 2.4 \times 10^{-10}\ cm^3\ s^{-1}$, and a radiative lifetime of 34 ± 12 ns, where these uncertainties are the statistical 2-σ values from the fit. Note that these values differ from those reported in Ref. 12. Within the large statistical uncertainty, the values we calculate from the Ref. 12 data overlap the present results. Also, those measurements were performed without magnetic depolarization and in the presence of 10 Torr of He. Collisional depolarization may have shortened the radiative lifetime observed in this early work.

To measure the rate constants for $N(3p\ ^4D^0_{7/2})$ quenching by each of the rare gases, the partial pressure of nitrogen is held constant and the partial pressure of rare gas is varied from 0.3 to 4 Torr. Because of degeneracy, the signal for $J = 7/2$ is four times bigger than for $J = 1/2$; thus, the statistical precision is best when exciting $J = 7/2$. Because we find no J dependence for either the slope or the intercept of the fluorescence decay data with N_2 collider, for the rare gas colliders only the $J = 7/2$ level is studied. Decay constants from the fits of the time-resolved fluorescence are plotted vs quencher partial pressure in Fig. 4 for Ne, Ar, Kr, and Xe, and again the lines in the figure are from a weighted least-squares fit to the data for each quencher. For the rare gas quenching, the intercept is the sum of the radiative decay rate of the $3p\ ^4D^0$ and the quenching by the residual N_2. All of the intercepts in Fig. 4 are consistent with the nitrogen partial pressure, the measured lifetime, and the nitrogen quenching rate.

Table I shows results for the measurements of the quenching rate constant of $N(3p\ ^4D^0_{7/2})$ by molecular nitro-

TABLE I. $N(3p\ ^4D^0_{7/2})$[a] collisional removal rate constants and cross sections[b]

Quencher	k_Q (10^{-11} cm^3 s^{-1})	α (Å^3)	σ_Q (Å^2) Measured	σ_Q (Å^2) Collision complex[c]
Xe	66 ± 12	4.00	94 ± 17	234
Kr	32 ± 5	2.46	43 ± 7	200
Ar	7.7 ± 1.4	1.63	9.9 ± 1.8	176
Ne	1.1 ± 1.0	0.39	1.3 ± 1.2	110
He	< 0.6	0.20	< 0.4	90
N_2	46 ± 6	1.72	56 ± 7	178

[a] $N(3p\ ^4D^0_{7/2})$ radiative lifetime 43 ± 3 ns.
[b] Error limits are 2-σ uncertainty.
[c] Estimated assuming $P = 1$ [see Eqs. (1) and (3)].

gen and the rare gases He, Ne, Ar, Kr, and Xe. Again, error limits tabulated are 2-σ statistical uncertainties from the decay constant vs partial pressure fit added in quadrature with the estimated uncertainty from all other observables. This estimated systematic error, less than the statistical uncertainty, is dominated by the contribution from the flow determination as measured by calibrated mass flow meters. To examine the differences between collision partners, we remove the velocity dependence of the collision rate by tabulating a thermally averaged quenching cross section, $\sigma_Q \equiv k_Q/\langle v \rangle$. We estimate the upper bound for the quenching rate constant of $N(3p\ ^4D^0)$ by He from a measurement of $k_Q = 1.5 \pm 4.5 \times 10^{-12}$ cm^{-3} s^{-1}. Although the values for the quenching rate constants for He and Ne overlap at the 2-σ level, there is at the 1-σ level a monotonic increase in the rate constant as the rare gas increases in complexity.

There is a dramatic variation in quenching cross section as the rare gas colliders become heavier and have a more complex electron configuration. The quenching cross section increases by nearly a factor of 250 as the collider is changed from helium to xenon. Interestingly, this variation is roughly the same as the increase in the square of the polarizability of the rare gas collider; the polarizability,[17] α, for each rare gas is tabulated in Table I. Such a correlation, together with the large magnitude of the cross section, suggests to us a long-range interaction of either the excited electron or the nitrogen ionic core with the electron cloud of the rare gas collider.

IV. DISCUSSION

A wide variety of physical mechanisms are invoked to explain the data for the nonresonant collisional quenching of electronically excited atoms and small molecules. The large magnitude of the cross section for the collisional deactivation of the excited $N(3p\ ^4D^0)$ and the surprisingly large change in its value among the rare gas colliders will be compared to the predictions of these models, including several possible mechanisms published for other excited atoms. From these comparisons we will conclude that long range attractive interactions are responsible for the large absolute value of the quenching cross section for nitrogen atoms with Ar, Kr, Xe, and N_2. However, a simple attractive forces model must be refined to include the interaction between initial and available final states. For the deactivation of excited atoms by rare gas colliders there are not enough final states for all close collisions to mix the initial states with different electronic final states.

The final electronic states of the colliders after the quenching of the nitrogen $3p\ ^4D^0$ state are unknown, although all of the possible combinations have substantial excess energy to transfer to translation. Nitrogen has seven states, three quartet and four doublet, with energy less than the ~94 800 cm^{-1} of the $3p\ ^4D^0$ state. The level nearest the one excited is the $3p\ ^2S^0$ state, which lies 1200 cm^{-1} below the excited $3p\ ^4D^0$; the nearest level of the same spin is the $3s\ ^4P$, lower in energy by ~11 500 cm^{-1}. Neither helium or neon has excited electronic states with less than the excitation energy of the $3p\ ^4D^0$ nitrogen atom. Thus, these rare gases remain in their ground state and the deactivation of $N(3p\ ^4D^0)$ requires the transfer to translation of at least 1200 cm^{-1} energy. The heavier rare gases all have excited electronic states with less energy than the excited nitrogen atom energy; argon has three, krypton has seven, and xenon has more than 50.[18] Thus, the number of possible final states increases as the rare gases have more complex electron configurations. However, in all cases except xenon there is at least 200 cm^{-1} excess energy which must be transferred to translation of the collision pair. For xenon only the $5p^5 6f$ states are within 100 cm^{-1} of the $N(3p\ ^4D^0_{1/2})$, and these states are more than 100 cm^{-1} from the $3p\ ^4D^0$ state with $J = 5/2$ or $7/2$.

The geometric collision cross section for the excited atom and the collider is the simplest model of electronic quenching, and we apply this model to excited $N(3p\ ^4D^0)$ atoms using Hartree–Fock radii.[19] These geometric cross sections range from 70 Å^2 for Ne to 86 Å^2 for Xe, a variation much smaller than observed. In a simple geometric model, an additional variation with collider might arise from the collision duration. As the collider becomes heavier, thermal collisions will have a longer duration, allowing more time for state mixing. Such an increase is proportional to the square root of the reduced mass, and is only a factor of 2 for the He–N to Xe–N variation. Thus, this simple model is inadequate to describe our data for the quenching of $N(3p\ ^4D^0)$ with the rare gases.

Because the $N(3p\ ^4D^0)$ state has such a large excitation energy, nearly 95 000 cm^{-1}, we first compare its quenching with the collisional removal of highly excited Rydberg levels of atoms. These Rydberg atoms have been modeled[3,4] as an excited electron and a separate ionic core with either the core or the electron acting as a spectator during the interaction with the rare gas collider. The electronic quenching of relatively low-lying Na Rydberg levels with $n \sim 10$ correlates well with the interaction between the ionic core of the excited atom and the perturber rare gas[4]; here the excited electron is a spectator to the interaction. Although a detailed model requires ion/rare gas potential curves the quenching cross sections from such a model should scale like the Langevin cross section,[20] $\sigma \sim \alpha^{1/2}$. This predicted dependence on polarizability is much smaller than the variation observed for N atoms. The collisional quenching of the higher-lying Ryd-

berg levels is thought to occur through the interaction of the excited electron with the rare gas collider[1]: here the ionic core acts as a spectator to the interaction. For example, the electronic quenching of Rb Rydberg states by rare gas collision partners has been studied for both *ns* and *nd* levels.[1,21] In both cases the cross section increases from the measured value for He by about a factor of 100 to the measured value for Xe, however, the minimum cross section is for Ne. These Rb Rydberg cross sections are more than 100 times larger than those measured here for $N(3p\ ^4D^0)$ atoms, although the relative variation with rare gas collider is about the same. These high-lying Rydberg levels are quite closely spaced, and little excess energy is transferred to translational energy. It is difficult to imagine an ionic core which must accept its share of as much as 1200 cm^{-1} translational energy only acting as a spectator to the interaction. Electron–rare gas interaction cross sections typically show a minimum for Ne as observed for Rd Rydberg atom, instead of the $N(3p\ ^4D^0)$ quenching cross sections which show (at the 1-σ level) monotonic increase with rare gas mass, electron number, and polarizability. Thus, the models used for Rydberg level quenching do not appear applicable to the quenching of $N(3p\ ^4D^0)$.

There are similar measurements for the quenching of low-lying valence levels of oxygen and hydrogen atoms by He and Ar.[22] Both $O(3p\ ^1P)$ and $H(n = 3)$ were also prepared by two-photon excitation and observed by far-red laser-induced fluorescence. Collisions with He yielded no observable quenching, while those with Ar showed quite large collisional quenching rate constants: $1 \times 10^{-10}\ cm^{-3}\ s^{-1}$ for $O(3p\ ^3P)$ and $5 \times 10^{-10}\ cm^{-3}\ s^{-1}$ for $H(n = 3)$. Again we see cross sections with large magnitudes for Ar and quite small values for He, however, other rare gas colliders were not studied.

A. Long-range interactions and curve crossings

The rough variation of σ_Q with the square of the polarizability of the rare gas suggests that long-range attractive interactions are involved in the quenching process, at least for Ar, Kr, and Xe. We seek a picture of the quenching collision in those terms. We first examine an approach in which the cross section may be correlated with some parameter describing that attractive interaction. Lin *et al.*[23] derive a linear relationship between the logarithm of σ_Q and the well depth $(\epsilon_{M\text{-}M})^{1/2}$. For the series of rare gases studied here, we find a surprisingly good correlation with the $(\epsilon_{M\text{-}M})^{1/2}$ from Ref. 23 and the results in Table I, including the upper bound for He. However, σ_Q for N_2 is a factor of 6 higher than the rare gas correlation would suggest. On the other hand, the size of the cross section for Ne and the upper bound for He are smaller than one would expect, *a priori*, for a collision governed by attractive forces. Thus we can conclude that attractive forces are likely important for the larger rare gases, and turn to a more dynamical description of the quenching process.

The mechanism can be thought of in three parts: first an approach of the excited nitrogen and its ground state collision partner, then a mixing of the initial and final states, and finally a departure into one or more final state configurations with the N atom now less excited. The collision partners which we have studied fall into three different categories in this regard. For Ar and Kr, there are only a few energetically accessible excited final states of the rare gas, and we regard the process as a curve crossing governed by the difference in the long range potentials for the two configurations. In the cases of Xe and N_2, there are many possible final states energetically allowed, so that the state mixing occurs quite efficiently at nearly any internuclear separation. Here an explicit treatment in terms of curve crossings is difficult to formulate, and we look at the quenching in terms of a single long-range potential involving R^{-6} attraction and a R^{-2} centrifugal barrier. For He and Ne, there are no energetically accessible final states of the rare gas save the initial ground state. Thus, neither the assumption of available final states at all internuclear separations nor the excitation transfer curve crossing is applicable. However, an absence of an available curve crossing indicates that the cross section must necessarily be small.

As we shall see, this approach forms a successful description. The σ_Q values for He and Ne are small, as demanded. For Ar and Kr, the explicit curve crossing calculation, described below, provides results consistent with experiment. For Xe and N_2, the single-potential attractive forces model yields cross sections similar to those measured experimentally. We shall next describe these calculations, considering first the attractive forces picture and then the curve crossing/excitation transfer model.

B. Attractive forces model

The electronic quenching of electronically excited metastable rare gas atoms by a large number of colliders is successfully correlated with a mechanism dominated by long-range forces.[5] A similar model has also been used for the electronically excited small molecules: SO_2[6] and OH.[7–9] In this model the long-range part of the interaction between the excited species A^* and the collider B is the sum of the repulsive centrifugal barrier plus the multipole expansion of the attractive interactions. For collisions at a specific translational energy E, there is a maximum impact parameter b_0 for which a bound complex can be formed. For all impact parameters larger than b_0 the collision partners never surmount the repulsive centrifugal barrier. For all impact parameters smaller than b_0 a close collision occurs and a temporarily bound complex is formed. We assume that if the collision partners experience such a close encounter, quenching will occur with some large probability P. The quenching cross section is

$$\sigma = \pi b_0^{\,2} P. \tag{1}$$

To compare with the measurement this cross section must be averaged over a thermal distribution of collision energies; we denote the thermally averaged quantity σ_Q.

This model has an analytic solution[7] for excited atom–rare gas collisions. The lowest order term which contributes to the interaction potential is the R^{-6} dispersion term,

$$V(R) = Eb^2/R^2 - C/R^6, \tag{2}$$

where b is the impact parameter and C is the van der Waals

coefficient. The analytic solution for the thermally averaged cross section is

$$\sigma_Q = BP\langle \quad \rangle \tag{3}$$

where $B = 3\pi/2$ [illegible] and C can be approximated by the London formula[4]

$$C = \frac{3}{2}\frac{I_A I_B}{I_A + I_B}\alpha_A\alpha_B \tag{4}$$

where I_A (I_B) and α_A (α_B) are the ionization potential and polarizability, respectively, of A and B. The ionization potentials of the two species are known spectroscopically, and the polarizabilities of the ground state species are noted in Table I. We estimate the polarizabilities of $N(3p\,^4D^0)$ and X^* by modeling these atoms as essentially one electron atoms, and then scaling from the known polarizabilities[1,5] of the ground state alkali atoms. We find that α can be reasonably described by the empirical formula

$$\alpha = 9.44(n^*)^6(a_0^3), \tag{5}$$

where $a_0 = 0.529$ Å, n^* is the effective quantum number of the one active electron related to the ionization potential by $I = I_H(n^*)^{-2}$, and I_H is the ionization potential of hydrogen. The $(n^*)^6$ dependence is expected since the units of polarizability are (length)^3 and the unit of length, the radius of a hydrogenic orbital, scales as $(n^*)^2$.

The quenching cross sections calculated from our attractive forces model are presented in Table I. The values calculated for Xe and N_2 are in reasonable agreement with the measured values arbitrarily using a value of $P = 1/2$.[7] For the other rare gases the calculated value is much larger than the measured σ_Q. Such long-range attractive interactions may be important in the determination of a capture cross section, but for excited $N(3p\,^4D^0)$ atoms the variation of the quenching probability P for different rare gas colliders is also important.

We are compelled to reexamine the basic premises of the attractive forces model in the context of these excited atom–rare gas collisions. This physical picture assumes the interaction at long range depends on the relative size of the attractive components of the potential, and the repulsive centrifugal terms. The model does not consider the final states; the model assumes if a close encounter occurs there will be an energetically accessible final state available with facile state mixing. For the case of collisions with Xe and N_2, so many final states are possible that this assumption may be reasonable; however, for He, Ne, Ar, and Kr there are only a few available final states.

C. Excitation transfer

The long-range attractive interaction may induce a potential curve crossing that provides a pathway for excitation transfer. The physical picture of this mechanism is quite simple. At the crossing point, an electron from the outer filled shell of the rare gas collider is captured into the vacancy on the nitrogen ionic core, and the excited valence electron from the nitrogen moves into a Rydberg orbital of the rare gas. Even though exact calculations are not available, we can estimate the asymptotic behavior of candidate final state potential curves and obtain the quenching cross sections that would arise from this mechanism. This picture suggests that the typical situation that leads to effective quenching is an attractive initial state potential curve that crosses one or more final state potential curves at long range. At every curve crossing, the electronic excitation energy of the nitrogen atom may be efficiently transferred to a particular excited state of the collision partner.

The elements of the method are the following: (1) Obtain the asymptotic behavior of the initial and final state potential curves by estimating the appropriate van der Waals coefficients. (2) Locate the crossings between the initial state and plausible final states. For consistency, these must occur at long range, where the approximate potential curves are realistic. (3) Estimate the coupling at each crossing using empirical scaling rules. (4) Depending on the number of crossings identified, apply one of the following methods to obtain the cross section. For single isolated crossings, which occur for Ar and Kr, the Landau–Zener formula is used. When many crossings are possible, as for Xe and N_2, statistical arguments lead to the attractive forces model for the cross section. In the cases of He and Ne, no crossings are identified, and to first order the present model gives a quenching cross section of zero. This prediction is consistent with the observations for He and Ne, and indicates that other, less efficient mechanisms are involved.

A collision of $N(3p\,^4D^0)$ with a rare gas resulting in excitation transfer may be written schematically as

$$N(3p\,^4D^0) + X \rightarrow N(^4S^0) + X^*(n)\,.$$

The excited state of the rare gas X is labeled only by the *principal quantum number n*. Since the collisions take place at thermal energies, we limit our attention to the available final states X^* such that the reaction is exothermic (or at most slightly endothermic). The most probable final state energy levels X^* may be determined from spectroscopic information, as discussed above. We expect that the asymptotic behavior of the molecular potential curves will be $-C_i/R^6$ and $-C_f/R^6$, where C_i and C_f are the van der Waals coefficients for the initial and final molecular states. If the final molecular state lies below the initial state by an energy ΔE, the potential curves will be shown in Fig. 5.

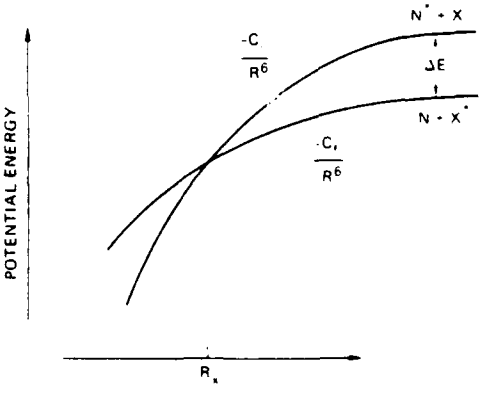

FIG. 5. Illustration of the potential curve crossing for the excitation transfer mechanism. The initial separated atom state, $N(3p\,^4D^0) + X$, and the final state, $N(^4S^0) + X^*$, differ in energy by ΔE; however, the difference in van der Waals coefficients causes a curve crossing at internuclear separation R_x.

The necessary van der Waals coefficients are estimated from the polarizabilities of the interacting species, according to Eq. (4). The polarizabilities of the ground state rare gases are known, and we used Eq. (5) to estimate the polarizabilities of the excited atoms from their ionization potentials. This technique provides a crude estimate of the long-range behavior of the relevant potential curves. We note that the method ignores the possible *p*-like character of the valence orbitals, the interaction would of course depend on whether the *p* orbital was oriented parallel or perpendicular to the internuclear axis. Also, at smaller internuclear distances, the interaction will become repulsive due to overlap of the electron orbitals.

After estimating the potential curves and identifying the crossings, we calculate the matrix element H_{fi} for excitation transfer. We assume that the matrix element is determined essentially by the matrix element for the electron jump from X into the N core. Miller and Morgner[25] have considered excitation transfer from this viewpoint. The matrix element can then be estimated using an empirical formula developed by Olson *et al.*[26] to treat charge exchange. Their formula is

$$H_{fi}(R^*) = 1.044 I_N^{1/2} I_X^{1/2} (R^*/a_0) \exp(-0.857 R^*/a_0) , \tag{6}$$

where $R^* = R(I_N^{1/2} + I_X^{1/2})/(2I_H^{1/2})$, and I_N, I_X, and I_H are the ionization potentials of the ground states of N, the rare gas X, and H, respectively. This scaling formula has a physical basis from the correlation of the overlap of electronic orbitals on different atomic centers, which is expected to fall off exponentially as the interatomic distance increases. Olson *et al.*[26] found their scaling formula to be accurate within a factor of about 3 for a wide range of systems in which values of the coupling matrix element span ten orders of magnitude. We would expect the formula to predict with greater accuracy the relative values of the matrix element for the sequence of similar collision pairs consisting of N* and each of the rare gases.

Given the above estimates of the asymptotic forms of the relevant potential curves and the couplings between these curves, we proceed with the estimation of the cross sections considering each rare gas collision partner separately. For He and Ne, no curve crossing is available. The energy required to reach the lowest excited state of either He or Ne (20.8 and 16.6 eV, respectively) is much larger than the available energy of the $N(3p\,^4D^0)$ (11.8 eV). Excitation transfer to an excited state of He or Ne is energetically forbidden. If we consider collisional deactivation of the excited N, the closest available excited quartet level of N is 1 eV lower, and the nearest doublet level is about 0.15 eV away. Such levels can only be populated if the energy goes to translational energy of the collision partners; the coupling for such a mechanism would arise from the polarizability of the rare gas. Without realistic potential curves, no rigorous calculation of the cross sections can be carried out for this process. However, for such a large energy difference between initial and final states, a very close collision, within the hard sphere radii of the atoms, is required. We expect a small (< 1 Å^2) cross section.

Collisions of excited $N(3p\,^4D^0)$ with Ar and Kr most nearly satisfy the idealized conditions of our excitation transfer model of quenching. In both cases, the number of plausible final states is very small. We assume that the potential curves will be of the form shown in Fig. 5. The initial curve is more attractive because $C_i > C_f$, and it crosses the final curve at the value R_x determined by the condition

$$(C_i - C_f)/R_x^6 = \Delta E .$$

R_x must be sufficiently large that the asymptotic R^{-6} form of the potential is still a reasonable approximation. If this is the case, we can obtain estimates of the total cross section using analytic formulas based on the Landau–Zener formula for the probability of curve crossing.[27] The result, which is obtained analytically by integrating the curve-crossing probability over impact parameter, is

$$\sigma = 4\pi R_x^2 [1 - V_i(R_x)/E] G(\lambda) ,$$

where V_i is the initial state potential, E is the collision energy, and $G(\lambda)$ is a combination of Bessel functions. $G(\lambda) = E$ [illegible]. The parameter λ is given by

$$\lambda = \frac{2\pi H_{fi}^2 R_x}{\Delta F \hbar v} \left[1 + \frac{R_x}{\rho}\right]$$

where ΔF is the absolute [illegible]

TABLE II. Estimates of cross section for excitation transfer.

	ΔE (cm^{-1})	C_i (eV Å^6)	C_f (eV Å^6)	R_x (Å)	Spin-statistical factor
Final state of Ar					
$4s'[0\,1/2]_1$ ($^3P_1$)	241	97	2[illegible]	[illegible]	[illegible]
$4s'[1\,1/2]_2$ ($^3P_2$)	1082	97	2[illegible]	[illegible]	[illegible]
$4s'[1\,1/2]_1$ ($^3P_1$)	[illegible]	[illegible]	[illegible]	[illegible]	[illegible]
Final state of Kr					
$5p[0\,1/2]_1$ P	[illegible]	[illegible]			[illegible]
		[illegible]	[illegible]		
$5p[1\,1/2]_1$ D	[illegible]	[illegible]			
		[illegible]	[illegible]		
$5p[1\,1/2]_2$ P	[illegible]	[illegible]			
		[illegible]	[illegible]		

AD-A184 854 LASER PROBES OF PROPELLANT COMBUSTION CHEMISTRY(U) SRI 2/2
INTERNATIONAL MENLO PARK CA D R CROSLEY ET AL. AUG 87
ARO-21443.7-CH DAAG29-84-K-0092

UNCLASSIFIED F/G 21/2 NL

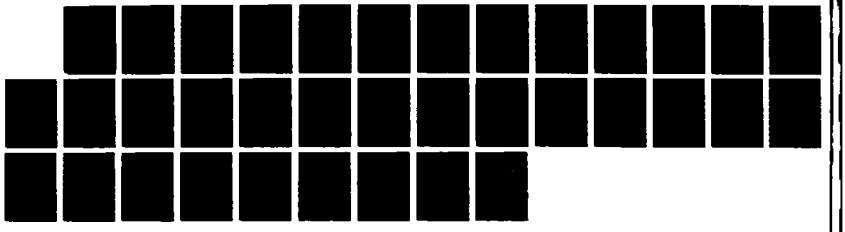

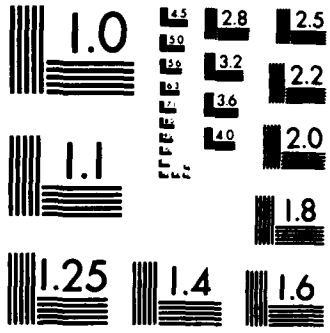

of the initial and final potential curves, and v is the initial relative velocity.

The assumed final states and the van der Waals coefficients used for Ar and Kr are tabulated in Table II. In each case we have listed the values for the initial and the one or two plausible final states. The cross section calculated in Eq. (8) is multiplied by appropriate factors related to spin conservation and the symmetry of the assumed initial and final states. The spin factor arises in those cases when the initial spins are a quartet and a singlet, and the final spins are a quartet and a triplet. By examining the possible values of the total spin quantum numbers S and M_S in the initial and final channels, one obtains the result that only 1/3 of the possible spin pairings in the initial state can lead to a possible final state. The other factor arises from the observation that the electron transfer from the rare gas to the nitrogen core is predominantly between sigma orbitals. (Only sigma orbitals of the rare gas have a projection along the internuclear axis of the collision pair and thus have a favorable overlap with the N^+ core.) The valence orbitals of the initial N* and the final Ar* or Kr* should have the same σ and π character. For the cases we consider, N* is a $3p$ orbital (σ or π), Ar* a $4s(\sigma)$, and Kr* a $5p$ (σ or π). We conclude that a state of Kr* of the appropriate spatial symmetry is always available, and that a state of Ar* is available 1/3 of the time.

The estimates of the cross sections for the excitation transfer to specific states of Ar and Kr are tabulated in Table II. The results are consistent with the experimental measurements. Noting that the initial estimate for Kr was smaller than the measured value, we tried a moderate adjustment of the final state van der Waals coefficient. Arbitrarily reducing C_f by 50% gives cross sections closer to the measured values. The sensitivity of the cross sections to the potentials highlights the difficulties of making estimates when realistic potentials are not known.

We draw the following conclusions from the preceding discussion. The mechanism of excitation transfer clearly depends sensitively on the energy levels available for each particular system. The estimates we have obtained suggest that this mechanism could account for the large dependence of the quenching cross section on the rare gas collision partner. More detailed calculations of the appropriate initial and final state potential curves, and their coupling, would be necessary for a definitive quantitative comparison between experiment and theory.

V. CONCLUDING REMARKS

Experiments on first row atoms like nitrogen offer a rare opportunity to couple experimental results with theoretical predictions. Because of the small number of electrons, *ab initio* potential surface calculations are feasible. Armed with a dynamics calculation on such surfaces and the results of final state selective experiments described below, one can undertake detailed comparisons of the rates and pathways of electronic energy transfer.

The excitation transfer mechanism of excited atom quenching leads to a well-defined excited final state in the rare gas collider; such a prediction can be verified by experiment. The quenching of nitrogen atoms in the $3p\ ^4D^0$ state by Ar and Kr would produce excited rare gas atoms which could be detected via laser-induced fluorescence or ionization with a second probe laser. Detecting these final states of quenching would unambiguously determine the quenching mechanism. Other initial excited states can open or close the energetically allowed rare gas final states. For example, excited $3p\ ^3P$ carbon atoms do not have enough energy for excitation transfer with either Ar or Kr. Thus, if excitation transfer is the dominant mechanism, the quenching cross section for $3p\ ^3P$ carbon atoms should be quite small for Ar and Kr colliders. In addition, the quenching of this state by Xe has only a single available final state, much like the quenching of $3p\ ^4D^0$ nitrogen atoms by Ar. This single example is but one of many possible initial excited atoms which could be studied by two-photon LIF.[13]

The quenching rate constant for the $3p\ ^3P$ state of oxygen by Ar has recently been measured[22] and the thermally averaged cross section for the quenching is 13 Å^2. The excited oxygen state lies below the lowest excited state in Ar; thus, this state cannot be quenched through an excitation transfer mechanism, and the large measured cross section appears to be in disaccord with the mechanism described above. On the other hand, 2000 cm^{-1} below the oxygen $3p\ ^3P$ state lies a $3p\ ^5P$ state. When the $3p\ ^3P$ state is excited in either a "high pressure" flow[22] or a flame,[28,29] radiation from the $3p\ ^5P$ is observed; the result of a collisional spin-changing deactivation. In nitrogen there is no state lying below the $3p\ ^4D^0$ from the same configuration with the same orbital angular momentum. Thus, this particular collisional deactivation pathway is not possible. This example illustrates the importance of considering the final states of both species to understand the physical mechanism of collisional quenching. Experiments with a careful choice of collision systems and final state measurements will provide the detailed rates and pathways required for a comprehensive theory.

To conclude the rate constant for the electronic quenching of $3p\ ^4D^0$ nitrogen atoms by collisions with rare gases and N_2 has been measured. We observe a dramatic variation of the quenching cross section for the different rare gas collision partners. The magnitude of the quenching appears closely related to the number of available final states. In those cases where only a small number of final states are available, we estimate cross sections consistent with experiment using the asymptotic potential curves of the initial and final molecular states of the collision pair. The quenching occurs when isolated curve crossings lead to excitation transfer to a well-defined final state. In those cases where a large number of final states are available, the probability of quenching is approximated by a constant statistical factor, and the attractive forces model provides a reasonable estimate of the cross section.

The radiative lifetime of the N($3p\ ^4D^0$) atoms is measured to be 43 ± 3 ns in agreement with earlier indirect determinations.

ACKNOWLEDGMENTS

We thank Mark J. Dyer for his assistance optimizing the YAG-pumped dye laser, frequency doubling, and Raman shifting optics. We also thank Donald J. Eckstrom for the

loan of a transient digitizer and Jay S. Dickinson for assistance with the digitizer software. We acknowledge numerous fruitful discussions on the mechanisms of energy transfer with David L. Huestis. This research was supported by the United States Army Research Office on Contract No. DAAG-29-84-K-0092. One of us (A.P.H.) was partially supported by SRI Internal Research and Development funds. We also acknowledge the use of a VAX 11/750 computer provided to the Chemical Physics Laboratory by the National Science Foundation on Grant No. PHY-8114611.

[1]For a review, see R. J. Donovan, Prog. React. Kinet. **10**, 253 (1979), and references therein.
[2]For a review, see *Rydberg States of Atoms and Molecules*, edited by R. F. Stebbings and F. B. Dunning (Cambridge University, Cambridge, 1983).
[3]M. Hugon, B. Sayer, P. R. Fournier, and F. Gounand, J. Phys. B **15**, 2391 (1982).
[4]T. F. Gallagher and W. E. Cooke, Phys. Rev. A **19**, 2161 (1979).
[5]J. E. Velazco, J. H. Kolts, and D. W. Setzer, J. Chem. Phys. **69**, 4357 (1978).
[6]D. L. Holtermann, E. K. C. Lee, and R. Nanes, J. Chem. Phys. **77**, 5327 (1982).
[7]P. W. Fairchild, G. P. Smith, and D. R. Crosley, J. Chem. Phys. **79**, 1795 (1983).
[8]R. A. Copeland and D. R. Crosley, J. Chem. Phys. **84**, 3099 (1986).
[9]J. B. Jeffries, R. A. Copeland, and D. R. Crosley, J. Chem. Phys. **85**, 1898 (1986).
[10]R. F. Heidner III and D. Husain, Int. J. Chem. Kinet. **6**, 77 (1974).
[11]Collisional transfer among the fine structure levels of the $^4D^0_J$ state will be separately discussed: J. B. Jeffries, R. A. Copeland, and D. R. Crosley (in preparation).
[12]W. K. Bischel, B. E. Perry, and D. R. Crosley, Chem. Phys. Lett. **82**, 85 (1981).
[13]W. K. Bischel, B. E. Perry, and D. R. Crosley, Appl. Opt. **21**, 1419 (1982).
[14]W. Hanle, Z. Phys. **30**, 93 (1924); applied to energy transfer in OH by R. K. Lengel and D. R. Crosley, J. Chem. Phys. **67**, 2085 (1977).
[15]J Richter, Z. Astrophys. **51**, 177 (1961).
[16]D. R. Bates and A. Damgaard, Philos. Trans. R. Soc. London Ser. A **242**, 101 (1949).
[17]S. C. Chan, B. S. Rabinovitch, J. T. Bryant, L. D. Spicer, T. Fujimoto, Y. N. Lin, and S. P. Pavlou, J. Phys. Chem. **74**, 3160 (1970).
[18]C. E. Moore, Natl. Stand. Ref. Data Ser. Natl. Bur. Stand. **35**, (U. S. GPO, Washington, D. C., 1971).
[19]K. Omidvar, Phys. Rev. A **22**, 1576 (1980); **30**, 2805(E) (1984).
[20]E. W. McDaniel, V. Cermak, A. Dalgarno, E. E. Ferguson, and L. Friedman, *Ion Molecule Reactions* (Wiley-Interscience, New York, 1970).
[21]M. Hugon, F. Gounand, P. R. Fournier, and J Berlande, J. Phys. B **13**, 1585 (1980).
[22]U. Meier, K. Kohse-Höinghaus, and Th. Just, Chem. Phys. Lett. **126**, 567 (1986).
[23]H.-M. Lin, M. Seaver, K. Y. Tang, A. E. W. Knight, and C. S. Parmenter, J. Chem. Phys. **70**, 5442 (1979).
[24]H. Margenau, Rev. Mod. Phys. **11**, 1 (1939).
[25]W. H. Miller and H. Morgner, J. Chem. Phys. **67**, 4923 (1977).
[26]R. E. Olson, F. T. Smith, and E. Bauer, Appl. Opt. **10**, 1848 (1971).
[27]R. E. Olson, Comments At. Mol. Phys. **9**, 231 (1980).
[28]M. Aldén, H. M. Hertz, S. Svanberg, and S. Wallin, Appl. Opt. **23**, 3255 (1984).
[29]A. W. Miziolek and M. A. DeWilde, Opt. Lett. **9**, 390 (1984).

Twenty-First Symposium (International) on Combustion
The Combustion Institute, Pittsburgh, 1987

MULTIPLE SPECIES LASER-INDUCED FLUORESCENCE IN FLAMES

Jay B. Jeffries, Richard A. Copeland, Gregory P. Smith, and David R. Crosley
Chemical Physics Laboratory
SRI International
Menlo Park, California 94025

Abstract

We have observed simultaneous laser excitation of two or more radical species (OH, NH, CH, CN, and NCO) using a single, tunable wavelength in the reaction zone of various atmospheric pressure flames. Individual species are selectively detected by wavelength resolved fluorescence. An overlap among resonant transitions of OH, NH, CH, and CN occurs at 312.22 nm. Using this excitation wavelength, all four radicals may be measured simultaneously in both space and time. Both advantages and limitations are presented. Spectroscopic details on the excitation of $CH(C^2\Sigma^+)$ near 314 nm, $NCO(B^2\Pi_i)$ near 315 nm, and $CN(B^2\Sigma^+)$ near 310 nm and 333 nm are reported. Following laser excitation of $OH(A^2\Sigma^+)$, emission was observed from both $NH(A^3\Pi_i)$ and $CN(B^2\Sigma^+)$. This emission can be attributed to a surprisingly efficient collisional energy tranfer from the excited OH(A) to NH(A) or CN(A). Collisional deactivation of $CH(C^2\Sigma^+)$ to $CH(A^2\Delta)$ and $CH(B^2\Sigma^-)$ was observed and exploited to detect CH LIF in a spectral region free from NH, OH, and CN interference. The diatomic radicals OH, NH, and CN all exhibit a small nonresonant laser excited fluorescence at low (0.05 J/cm^2) power for any laser wavelength in this region.

MP 86-020R
5/21/86

A. Introduction

Laser-induced fluorescence (LIF)[1] is used to detect a wide variety of small free radical molecules which are known or putative reaction intermediates in combustion chemistry. The OH radical has been the subject of most LIF flame experiments. Because the OH concentration peaks in the post-reaction-zone burnt gases, detailed questions about the chemical mechanism require the simultaneous measurement of other intermediates. For comparison with detailed computer models of the flame chemistry, relative concentrations of two or more species in the same region are often more informative than absolute concentrations of just one.

For measurements of more than one radical, the normal approach has been the sequential use of different excitation wavelengths optimized for each species. We address here the possibility of simultaneously exciting more than one radical using a single laser operating at one wavelength. The fluorescent emission could be collected with a single optical system and then dispersed and detected. With such a scheme, the volume probed in the flame is necessarily identical for each species. Thus, the measurements of relative species concentrations are free of the practical problems encountered when overlapping two or more laser pulses in time and space. These problems are difficult because of the variations in beam temporal and spatial profiles not only from shot to shot but also during each pulse itself. Also, in the case of a turbulent flame, different laser beams may not intersect and the same point each shot, due to beam steering. Because of the importance of OH, we have explored multiple-species excitation in the wavelength region where hydroxyl can also be measured.

Historically, this work began on LIF of NCO in flames, comparing its excitation via the B-X system near 315 nm to that using the previously

studied[2] A-X system near 440 nm. We found large laser-excited fluorescence signals from several diatomics, which fluoresce more strongly than NCO because of a smaller partition function, i.e., more molecules per internal quantum level. This led to a search in this region for wavelengths permitting simultaneous excitation of two or three species. Molecules studied near 310 nm were OH, NH, CH, CN, and NCO. A single wavelength absorbed by OH, NH, and CH each of which has a very coarse rotational structure, has been found.

The LIF intensity is greatest for OH, generally present at much higher concentration than the other radicals. Therefore it is important to optimize detection wavelengths and evaluate the level of background signals. We found a very surprising result; exciting OH produces emission from NH and CN in flames which include those radicals. These signals are about one-thousandth of that of OH, and appear to be caused by extremely efficient radical-radical electronic energy transfer.

There have been previous studies in which fluorescence from more than one radical has been resonantly excited in a flame. These include excitation of NH and OH by a Kr^+ laser,[3] and CH, CN and NCO using an Ar^+ laser.[4] In another experiment,[5] two lasers were simultaneously fired to yield linear images of both C_2 and OH. In a cell at atmospheric pressure and room temperature, focussed light at 452 nm was used to simultaneously excite NO_2 via single photon absorption and NO by two photon absorption.[6] The respective visible and ultraviolet fluorescence was filtered to form simultaneous one-dimensional images. An analagous approach for major species has been performed using both spontaneous Raman scattering[7] and CARS.[8] Here, we consider within a single wavelength region optimization of detection of several radicals. Discussed

are new spectroscopic aspects of LIF of CH, NCO, and CN in flames, the energy transfer, and finally laser and fluorescence wavelengths for multiple species measurement.

Electronic states of the radicals observed here are shown in Fig. 1. A 0.07 cm diameter beam from a pulsed tunable dye laser, with 0.03 nm spectral bandwidth and typical pulse energy of 0.2 mJ, was directed into a small flame burned at atmospheric pressure on a glassblowing torch. The flame front was located by maximizing the NH LIF signal. The fluorescence at right angles was polarization scrambled and focussed onto the entrance slit of a small monochromator operated at 1.5 nm resolution; the resulting photomultiplier signal was processed with a gated integrator averaging over 10 to 100 pulses.

B. LIF Spectroscopy

In the region near 315 nm are electronic transitions of several flame intermediates: OH, NH, CH, CN, and NCO. These transitions overlap, permitting the concurrent detection of these species. We consider here spectroscopic details of the excitation in a flame of the C-X system of CH, the B-X system of NCO, and the B-X system of CN. These systems represent important types of electronic transitions: a diatomic having a sparse line structure with overlapping lines only in the bandhead, a triatomic with a very dense rotational and vibrational structure excited in almost any region, and a diatomic with dense rotational structure but significant vibrational spacing.

1. CH

The $C^2\Sigma^+$-$X^2\Pi$ transition of CH has long been known;[9] however, it has been used for LIF flame detection only in one other study.[10] It lies in the region of strong OH excitation, both an advantage and a disadvantage in CH

detection. The diagonal ($\Delta v=0$) bands are the strongest, so most of the fluorescence returns near the excitation wavelength. The off-diagonal ($\Delta v\neq 0$) bands are overlapped with neighboring OH transitions and have only ~1% the intensity of the diagonal bands (see Fig. 3, below). The C-X absorption, however, is very intense with a calculated radiative lifetime ~100 ns[11] (the predissociative lifetime[12] is shorter). The C-state is expected to have a greater fluorescence efficiency than the longer lived $A^2\Delta$ and $B^2\Sigma^-$ states.

There are six important rotational line progressions, two each of P, Q and R. The Q branches are highly overlapped forming the (0,0) head at 314.3 nm, the most prominent feature in the CH spectrum in this region. The P and R branches are a series of closely spaced doublets to either side of this head. Figure 2(a) shows several P-branch doublets along with the strong (0,0) and weaker (1,1) Q heads. This interference-free excitation spectrum was obtained in a flame by monitoring CH that fluoresces in the A-X transition (see below). Figure 2(b) is a fluorescence scan; the excitation wavelength, denoted by an arrow in Fig. 2(a), was selected to avoid excitation of either the nearby NH or OH. Both the B-X and the A-X transitions appear in the fluorescence when the C state is excited. Radiative cascade from the $C^2\Sigma^+$ to either $B^2\Sigma^-$ or $A^2\Delta$ is forbidden. Therefore, the emission from these levels is due to partial collisional deactivation of the the excited C state. Rapid electronic energy transfer then occurs between the A and B states.[13] Measured relative intensities are C-X (0,0): 1000; C-X (0,1): 7; total B-X: 8; and total A-X: 15. Assuming equal quenching rates for each electronic state, and using known radiative rates,[11,14] we conclude that ~10% of the excited C state population is transferred to A and B. Much experimental work on both the quenching and electronic energy transfer still remains to make these emissions quantitative.

The CH C-X excitation overlaps with strong bands of OH and NH. Observation of the A-X fluorescence emission following C-X excitation provides selective detection of CH, free from the strong NH and OH emission. This will be exploited in our search for simultaneous excitation of multiple species.

2. NCO

The rotational structure of the $B^2\Pi_i$-$X^2\Pi_i$ system is complex and has not been unambiguously characterized. Vibrational assignments of absorption spectra were initially made by Dixon[15] and confirmed in a matrix study[16]. Rotational assignments have been made only for the 100-000 ($v_1'v_2'v_3' \leftarrow v_1''v_2''v_3''$) transition.[15] The 000-000 band seems highly perturbed and has not been rotationally characterized. Here we examined the region near the band origin at 315 nm; there are clearly identifiable features which permit unambiguous identification of NCO in the flame environment. The 000 level of the B-state fluoresces to many vibrational levels in the ground state,[17] its spectrum extending from 315 nm far to the red in well separated bands.

Figure 3 shows excitation scans observing at 365 nm (see Fig. 4) for both a low pressure flow tube[17] and a CH_4/N_2O flame. The similarity of the spectra verifies that NCO is the molecule excited in the flame. Several features in the flame spectrum arise from hot band excitation not present at room temperature.

Knowledge of the B(000) fluorescence spectrum is crucial to the detection selectivity for NCO, due to interferences from diatomic molecules. Figure 4 shows a fluorescence spectrum obtained exciting the R_2 bandhead of 000-000. It shows little interference and clearly exhibits the one-to-one correspondence between the bands obtained in the flow cell and in the flame. This type of band structure has both a major advantage and disadvantage. At least one

band should be free of interference from diatomics, but any given band contains only a small fraction of the total fluorescence, therefore reducing the measureable signal intensity. The 000-201 and the 000-102 are generally the best interference-free bands to observe.

The $A^2\Sigma^+$ state of NCO lies below $B^2\Pi_i$ (see Fig. 1); most of the A-X emission is near 440nm. It was not detected in a fluorescence scan at a level <0.003 of the total B-X emission.

NCO absorption of the excitation laser is not limited to the region near the 000-000 bandheads shown, but it persists over a much larger wavelength region with the overlap of many hot bands and rotational lines.

3. CN

We have excited low v' levels of CN in the so called tail band region of the $B^2\Sigma^+$-$X^2\Sigma^+$ system, observing fluorescence in the $\Delta v=0$ bands near 388nm. The hitherto unobserved (3,0) and/or (4,1) band(s) appear with R branches from 309-312 nm and P branches from 312-315 nm, and (2,0) and/or (3,1), also not previously reported, with R between 330-333 nm and P at 333-335nm. Both are discrete sets of about 20 lines per nm. Because the term values for these vibrational levels of both the B and X states of CN are well known, the exact positions can be calculated and assigned easily.[18] The fluorescence intensity of the $\Delta v=2$ band set is ~10% of that in the nearby NH (0,0) lines and about the same as that induced by OH excitation, as described below. That from the $\Delta v=3$ bands is about three times smaller. Although weak, these bands provide the opportunity to resonantly excite CN in the same wavelength region as OH, NH, and CH. For quantitative CN measurements, oscillator strengths for these bands are needed; at present only ab initio calculations[19] exist for these values.

C. Multiple-Species Laser-Induced Fluorescence

When laser light at 315 nm is incident upon the reaction zone of the flame, we see emission caused by a variety of processes. These are fluorescence from the directly excited molecule (i.e., standard LIF), fluorescence from other molecules (NH and CN) when electronically exciting OH, and an underlying continuous background excitation of OH, NH and CN. At high laser intensities multiphoton processes can come into play; under such conditions we see emission from C_2. To design a means for multiple-species excitation in this region, it is necessary to understand the limits posed by the indirect excitation processes. In this section we consider first the NH and CN emission produced by OH excitation, then the wavelengths for multiple-species detection, and conclude briefly with comments on the underlying background.

1. NH and CN Fluorescence Induced by Excited OH

When the laser is tuned to excite only $A^2\Sigma^+$ OH, laser-induced fluorescent emission is produced not only from that molecule but also from $NH(A^3\Pi_i)$ and $CN(B^2\Sigma^+)$. This is a general phenomenon, occuring in $CH_4/NH_3/O_2$ and CH_4/N_2O flames which contain both CN and NH, and for NH in NH_3/O_2 and H_2/N_2O flames. It appears to be caused by electronic-electronic energy transfer between the radicals, an interesting but seldom studied collisional process, and important in flame LIF when exciting in the region of strong OH lines.

Figure 5 illustrates these observations using fluorescence scans; the flame is CH_4/N_2O. In (a), OH is excited via the $P_2(8)$ line of the (0,0) band. In this flame, NH emission in the A-X (0,0) band is present at about 10% of the OH (0,1) band intensity, i.e., about 3×10^{-4} of the total OH fluorescence. The NH signal is absent in the burnt gases. In (b), the OH excitation is $P_1(7)$ of (1,0). Induced emission is also observed in the

diagonal bands of the B-X transition of CN, at about five times the intensity of the OH (1,3) band. Again, moving to the burnt gases eliminates this feature.

There are two possible explanations for such emission. The first is the energy transfer process, and the second is reaction of excited OH with some molecule (NH_2 and HCN) which produces the corresponding radical fragment directly in the emitting state. Several experiments, particularly on NH, were undertaken to distinguish between these possibilities.

Scanning the laser wavelength while monitoring the NH or CN emission exhibits all the expected rotational lines of the (1,0), (0,0) and (1,1) bands of OH, indicating that the efficiency of the process is independent of the v',J' level excited. The intensity is always proportional to the OH LIF signal, that is, to the OH excited state concentration. It does not appear in the burnt gases, where there exists neither NH nor CN as energy transfer partners, but also no NH_2 nor HCN as reactants.

The intensity of NH emission induced by excited OH was measured in a variety of flames expected to have widely different NH_2 concentrations: NH_3/O_2, $CH_4/NH_3/O_2$, H_2/N_2O and CH_4/N_2O. In each case the NH signal caused by OH excitation was proportional to the product [NH][OH], those ground state concentrations measured by resonantly excited LIF. This strongly indicates that the NH emission is produced by OH(A) + NH(A) energy transfer.

The induced NH emission is typically ~0.001 of the directly excited OH fluorescence. Using values[20] of 0.003 for the OH quantum yield and 0.01 for NH, we estimate that the OH(A)+NH(A) transfer accounts for $\sim 3 \times 10^{-4}$ of the total OH quenching. LIF measurements indicate ground state concentrations [NH] ~ 0.03 [OH] ~ 30 ppm, leading to a cross section of ~50Å^2 for this final-state-specific radical-radical energy transfer. The necessary estimates

render this value uncertain by three-fold, but indicate that this process can be quite efficient.

The phenomenon was further studied in laser pyrolysis/laser fluorescence[21] experiments at lower pressure. Here, absorption by SF_6 of pulsed CO_2 laser radiation rapidly heated a mixture containing NH_3 and H_2O_2 to ~1550K. The peroxide decomposed to OH and sufficient F atoms were produced from the SF_6 to form both NH_2 and NH by hydrogen abstraction from NH_3. The OH was excited via A-X (0,0), and NH (0,0) emission was observed to have a fluorescence intensity roughly the same as OH (0,1), ~0.4% of the total OH LIF. This NH emission required the simultaneous presence of NH_3, F-atoms, and excited OH; its temporal profile was a double exponential whose rise time equaled that of the OH(A) decay and whose decay time was the same as that measured directly for NH(A). Upon increasing [NH_3], thus producing more NH_2 at the expense of NH, the NH emission signal rapidly decreased. This again indicates energy transfer, not reaction, is responsible for the NH emission induced via OH excitation.

2. Laser-Induced Fluorescence with Overlapped Resonances

In the region 280-320 nm there are many wavelengths at which two molecules of the set OH,[22] CH,[9] NH,[15,23] and CN[18] absorb within a 0.3 cm^{-1} bandwidth. Near 315 nm NCO is also included. In each case, two radical species can be excited at the same time in the same volume by the same laser pulse, permitting simultaneous LIF without complications of careful alignment of two laser beams or concerns about long term flame stability. Such correlated LIF measurements, yielding concentration ratios, can address important chemical mechanistic questions. Table I lists the overlaps observed.

Of course, with a sufficiently wide laser bandwidth one can readily obtain overlapped transitions. The 0.3 cm^{-1} used here is typical of many lasers used for LIF, and is close to the Doppler width of the absorption lines of the diatomic hydrides at flame temperatures. A larger excitation bandwidth, covering lines which do not overlap within their linewidth, can lead to reduced resonant LIF intensity (of importance in imaging) but the same nonresonant background (see below) and may cause complications in interpretation due to multiple-line excitation of one species.

Near 312.22 nm there exists an overlap of absorptions by the three hydrides OH, NH and CH. Fig. 6 exhibits excitation scans in this region, selectively detecting each of these three species plus CN. In (a), the OH (0,1) band is observed; the largest feature is the same $P_1(7)$ line of (0,0) seen in Fig. 5a. The smaller lines primarily belong to (1,1) and are observed through v'=1→0 energy transfer[24]. This is evident in (b) where the OH (1,2) band is detected.

In (c), the diagonal bands of CN B-X are detected. The signal tracks that of the OH excitations, illustrating the lack of dependence of the energy transfer on internal OH level. An unassigned resonant transition of either (4,1) or (3,0) of CN is partially overlapped with this coincident resonant excitation of the three hydrides. The resonantly excited CN radiates primarily in (4,4) at 385.1 nm or (3,3) at 385.5 nm, both shorter wavelengths than those of the (0,0) at 388.3 nm and (1,1) at 387.1 nm. Following excitation of v'= 3 or 4 there is little vibrational relaxation of the CN, an observation consistent with earlier work.[25] Therefore, the resonantly excited CN is not seen in Fig. 6c where the monochromator detects only fluorescence emitted by v'=0 and 1, populated via excited OH.

In (d), the NH A-X diagonal band region of the A-X system is selectively detected. The prominent excitation is the P_1, P_2, P_3 triplet for N"=12 in the (2,1) band. Also evident are OH lines, seen here through the energy transfer as discussed above. Panel (e) shows an excitation scan of CH C-X, observed via energy transfer to $A^2\Delta$. The doublet features are the R_1 and R_2 branches for N"=7 in (0,0), and the weaker lines are part of the (1,1) band.

At the wavelength of 312.22 nm, (as indicated by the arrow in the bottom panel of Fig. 6) all four of OH, NH, CH, and CN are resonantly excited, as seen in the fluorescence scan of Fig. 7. In the peaks labelled CN, the resonant excitation appears as the feature at shorter wavelength, while the taller peak at longer wavelength is the OH-induced (0,0) and (1,1) emission. Scanning onto non-overlapping OH lines was used to measure the energy transfer component. Approximately 5% of the NH emission at the overlap wavelength occurs by energy transfer from A-state OH.

3. Other Observations

Underlying all excitation scans at relatively low laser power (typically 0.05 J/cm^2) is an apparently continuous or nearly continuous background. This is observed at the characteristic fluorescence wavelengths of each of the diatomics. It is ~ 20% of the weakest signals discussed above; see, for example, the excitation scan of CH C-X (observing the weak A-X emission) in Fig. 6(e). These background signals are linear in laser power and persist to very low levels, so they are not likely multiphoton processes. They can complicate interpretation of LIF signals, especially under conditions where one does not scan the laser off a line to establish the local spectral baseline. At higher power density, new effects come into play. When the laser intensity was increased to >1J/cm^2, fluorescence from C_2 was also observed.

Both high power effects and the background nonresonant excitation at low intensities need be explored more thoroughly in the future.

D. Summary

We have described several LIF spectroscopic experiments near 315 nm, performed in different flames. Here absorptions exist belonging to several molecular free radicals (OH, NH, CH, CN and NCO) important in combustion chemistry. The use of a tunable laser for excitation and a tunable spectrometer for selective detection has revealed new aspects of LIF in flames.

The overlap of resonant transitions pumping two or more of these species simultaneously, using a single laser beam, has been explored. Several two-species overlaps have been found, and there is one wavelength at which OH, NH and CH all absorb. These spectroscopic coincidences will permit instantaneous correlation measurements between different species in pointwise or imaging experiments, without the added complications of alignment of two distinct laser beams with the accompanying variation in spatial and temporal profiles of each pulse. Such simultaneous measurements could be made by collecting the fluorescence with a single optical system. Beam splitters and appropriate filters would be used to direct the fluorescent light for each species to a separate detector.

During this search, we found several unanticipated energy transfer processes. The first is emission from the A and B states of CH following excitation of the higher-lying C-state, a phenomenon which was exploited as an simultaneous but interference-free way to detect CH in the presence of NH and OH. Second, excitation of OH led to emission from NH and CN (but not CH), apparently due to electronic-electronic energy transfer in radical-radical collisions. This is an interesting but little-known process warranting further study; in flames it places limits on the concentrations for which other radicals can be measured simultaneously with OH. Finally, an even lower background signal due to nonresonant excitation of all radicals at low laser

power, and multiphoton processes at higher intensity, will set further ultimate detection limits.

These interesting spectroscopic aspects and collisional processes deserve additional investigation, placing simultaneous, multispecies detection on a more quantitative basis. This work nonetheless demonstrates how these excitations can increase our understanding of flame chemistry through knowledge of flame radical concentrations.

Acknowledgement

We thank Nancy L. Garland for critical comments on this manuscript. This study was supported by the U.S. Army Research Office, on Contract DAAG29-84-K-0092.

REFERENCES

1. Crosley, D. R., ed.: Laser Probes of Combustion Chemistry, Amer. Chem. Soc. Symp. Series, Vol. 134, 1980; Crosley, D. R. and Smith, G. P.: Opt. Engr. 22, 545 (1983); Bechtel, J. H., Dasch, C. J., Teets, R., in Laser Applications (R. K. Erf and J. F. Ready, Eds.), Academic Press, New York, 1983; Lucht, R. P.: in Laser Spectroscopy and Its Applications (L. J. Radziemski, R. W. Solarz and J. A. Paisner, Eds.), Marcel Dekker, New York, 1986.
2. Copeland, R. A., Crosley, D. R., and Smith, G. P.: Twentieth Symposium (International) on Combustion, The Combustion Institute, Pittsburgh, 1985, p. 1195; Copeland, R. A., and Crosley, D. R.: Can. J. Phys. 62, 1488 (1984).
3. Vanderhoff, J. A., Anderson, W. R., Kotlar, A. J., and Beyer, R. A.: Twentieth Symposium (International) on Combustion, The Combustion Institute, Pittsburgh, 1985, p. 1299, 1984.
4. Anderson, W. R., Vanderhoff, J. A., Kotlar, A. J., Dewilde, M. A., and Beyer, R. A.: J. Chem. Phys. 77, 1677 (1982).
5. Alden, M., Edner, H., and Svanberg, S.: J. Appl. Opt. B 29, 93 (1982).
6. Alden, M., Edner, H., and Wallin, S.: Opt. Lett. 10, 529 (1985).
7. Sochet, L. R., Lucquin, M., Bridoux, M.,Crunelle-Cras, M., Grase, F., and Delhaye, M.: Comb. Flame 36, 109 (1979); Drake, M. C., Lapp, M., Penney, C. M., Warshaw, S., and Gerhold, B. W.: Eighteenth Symposium (International) on Combustion, The Combustion Institute, Pittsburgh, 1981, p. 1521.
8. Eckbreth, A. C., and Anderson, T. J.: Appl. Opt. 24, 2731 (1985).

9. Tori, H.: Nature 124, 480 (1929); Gero, L.: Z. Physik 117, 709 (1941); Moore, C. E., and Broida, H. P.: J. Res. Nat. Bur. Stand. 63A, 19 (1959).

10. Chou, M.-S., and Dean, A. M.: Int. J. Chem. Kinetics 17, 1103 (1985).

11. Hinze, J., Lie, G. C., and Liu, B.: Astrophys. J. 196, 621 (1975).

12. Brzozowski, J., Bunker, P., Elander, N., and Erman, P.: Astrophys. J. 207, 414 (1976).

13. Garland, N. L., and Crosley, D. R.: Appl. Opt. 24, 229 (1985).

14. Garland, N. L., and Crosley, D. R.: J. Quant. Spectros. Radiat. Transfer 33, 591 (1985).

15. Dixon, R. N.: Can. J. Phys. 38, 10 (1960).

16. Milligan, D. E., and Jacox, M. E.: J. Chem. Phys. 47, 5157 (1967).

17. Sullivan, B. J. Crosley, D. R., and Smith, G. P.: to be published.

18. Huber, K. P., and Herzberg, G.: Molecular Spectra and Molecular Structure IV: Constants of Diatomic Molecules, Van Nostrand Reinhold, New York, 1979.

19. Lavendy, H., Gandana, G., and Robbe, J. M.: J. Molec. Spect. 106, 395 (1984).

20. Garland, N. L., and Crosley, D. R.: Twenty-First Symposium (International) on Combustion, in press.

21. Smith, G. P., Fairchild, P. W., Jeffries, J. B., and Crosley, D. R.: J. Phys. Chem. 89, 1269 (1985).

22. Dieke, G. H., and Crosswhite, H. M.: J. Quant. Spectros. Radiat. Transfer, 2, 97 (1962).

23. Malicet, J., Brion, J., and Guenebaut, H.: J. Chim. Phys. 67, 5 (1970).

24. Smith, G. P., and Crosley, D. R.: Appl. Opt. 22, 1428 (1983).

25. Vanderhoff, J. A., Beyer, R. A., Kotlar, A. J., and Anderson, W. R.: Combu. Flame 49, 197 (1983).

FIGURE CAPTIONS

Fig. 1. Electronic term energies for OH, NH, CH, C_2, CN, and NCO up to 35,000 cm^{-1} above the ground state of each molecule. Vibrational and rotational energy is not included. States observed in this study are shown as solid lines while unobserved states are denoted by dashed lines.

Fig. 2. (a) Excitation spectra of the C-X system of CH, in a CH_4/O_2 flame, detected via fluorescence in the A-X system at 431 nm. The Q branches of both the (0,0) and (1,1) bands form unresolved band heads. The resolved P branch lines are assigned.

(b) Fluorescence spectrum exciting the $C^2\Sigma^+$, v'=0 level at the (0,0) Q band head, as denoted by an arrow in (a). The inset below the C-X (0-0) fluorescence shows the contribution of scattered laser light. Fluorescence from the C-X (0,1) band and the diagonal bands of the B-X and the A-X systems form the labeled features on top of a broad, unresolved laser induced fluorescence background.

Fig. 3. Excitation spectra of the NCO radical in the B(000)-X(000) band, detected with a monochromator viewing B-X fluorescence in the 000-201 band at 365 nm with a 1 nm bandwidth. The upper trace is from a flame and the lower trace in a room temperature, low pressure flow cell (Ref. 17).

Fig. 4. NCO fluorescence spectra when exciting the R_2 head of the B(0,0,0)-X(0,0,0) band. The lower spectrum was obtained in a room temperature low pressure flow cell in Ref. 17. The upper spectrum

was taken in a CH_4/N_2O flame by scanning a monochromator with 2 nm resolution. The corresponding peaks in the two spectra verify the identity of NCO in the flame. The numbers above the peaks in the lower spectrum refer to the ground state vibrational level on which the fluorescence terminates. Interference from OH and CN, from both flame emission and laser-induced processes, appears in the upper trace.

Fig. 5. (a) Fluorescence spectra in the flame front and burnt gases of a CH_4/N_2O flame when exciting OH $A^2\Sigma^+$ via the $P_2(8)$ line in the (0,0) band. The NH A-X (0,0) band emission results from OH excitation. The excitation wavelength does not overlap with any resonant transitions in NH.

(b) Fluorescence spectra for the same flame when the OH is excited by the $P_1(7)$ transition in the (1,0) band. The fluorescence from the CN B-X system is induced OH excitation. There is no significant resonant CN excitation at this wavelength.

Fig. 6. Excitation spectra at various fluorescence wavelengths in the flame front of a CH_4/N_2O flame. (The arrow in the lowest panel denotes the excitation wavelength used for the fluorescence spectrum shown in fig. 7.)

(a) Monochromator wavelength, λ_0 = 348 nm to observe fluorescence from the (0,1) band of the A-X system of OH.

(b) λ_0 = 353 nm to observe the (1,2) band of the OH A-X system.

(c) λ_0 = 388 nm to observe the (0,0) and (1,1) bands of the CN B-X system. All the major features follow OH excitations and are energy transfer or chemiluminescent reaction. The tiny lines

between 312.1 and 312.15 nm are direct resonant excitation of the $\Delta v=3$ bands of the B-X system of CN.

(d) λ_0 = 337 nm to observe the (0,0), (1,1), and (2,2) bands of the NH A-X system. The three largest lines are the P(12) triplet of the (2,1) band. The other large features are OH excitation which induces NH fluorescence.

(e) λ_0 = 431 nm to observe the A-X system of CH. The doublet feature is the R(7) pair of the C-X (0,0) band. The doublet just to the red of R(7) is the R(15) doublet in the (1,1) band.

Fig. 7. Wavelength dependence of the fluorescent emission following excitation at 312.22nm (as denoted by the arrow in fig. 6e). The spectrum shows resonant LIF from four species: OH, NH, CH, and CN. The large CN feature has two peaks: that at shorter wavelength is (3,3) and/or (4,4) band resonant LIF, and the emission at 388nm is that induced following OH excitation as discussed in the text.

Table I

COINCIDENT RESONANT EXCITATION WAVELENGTHS

Excitation Wavelength	Radical Species	Transition			Energy[a] cm^{-1}
334.09	NH	A-X	(0,0)	$R_3(4)$	29932.71
	CN	B-X	unknown	$\Delta v=2$	-
315.10	OH	A-X	(0,0)	$P_1(13)$	31726.79
	NCO	B-X	000-000	unknown	-
314.85	OH	A-X	(1,1)	$Q_2(5)$	31752.72
	NH	A-X	(2,1)	P(17)	-
	NCO	B-X	000-000	R_1 head	-
314.66	OH	A-X	(1,1)	O_2 head	-
	NH	A-X	(1,0)	P(22)	-
314.44	OH	A-X	(0,0)	$P_1(12)$	31799.49
	CH	C-X	(0,0)	$Q_2(10)$	31799.4
				$Q_1(11)$	31799.6
312.22	OH	A-X	(0,0)	$O_2'(15)$[b]	32019.34
			(1,1)	$R_1(6)$	
	NH	A-X	(2,1)	$P_1(12)$	32019.38
	CH	C-X	(0,0)	$R_1(7)$	32019.32
	CN	B-X	unknown	$\Delta v=3$	-

[a]Transition energies are taken from Refs. 9, 15, 22, and 23.
[b]Notation from Ref. 22.

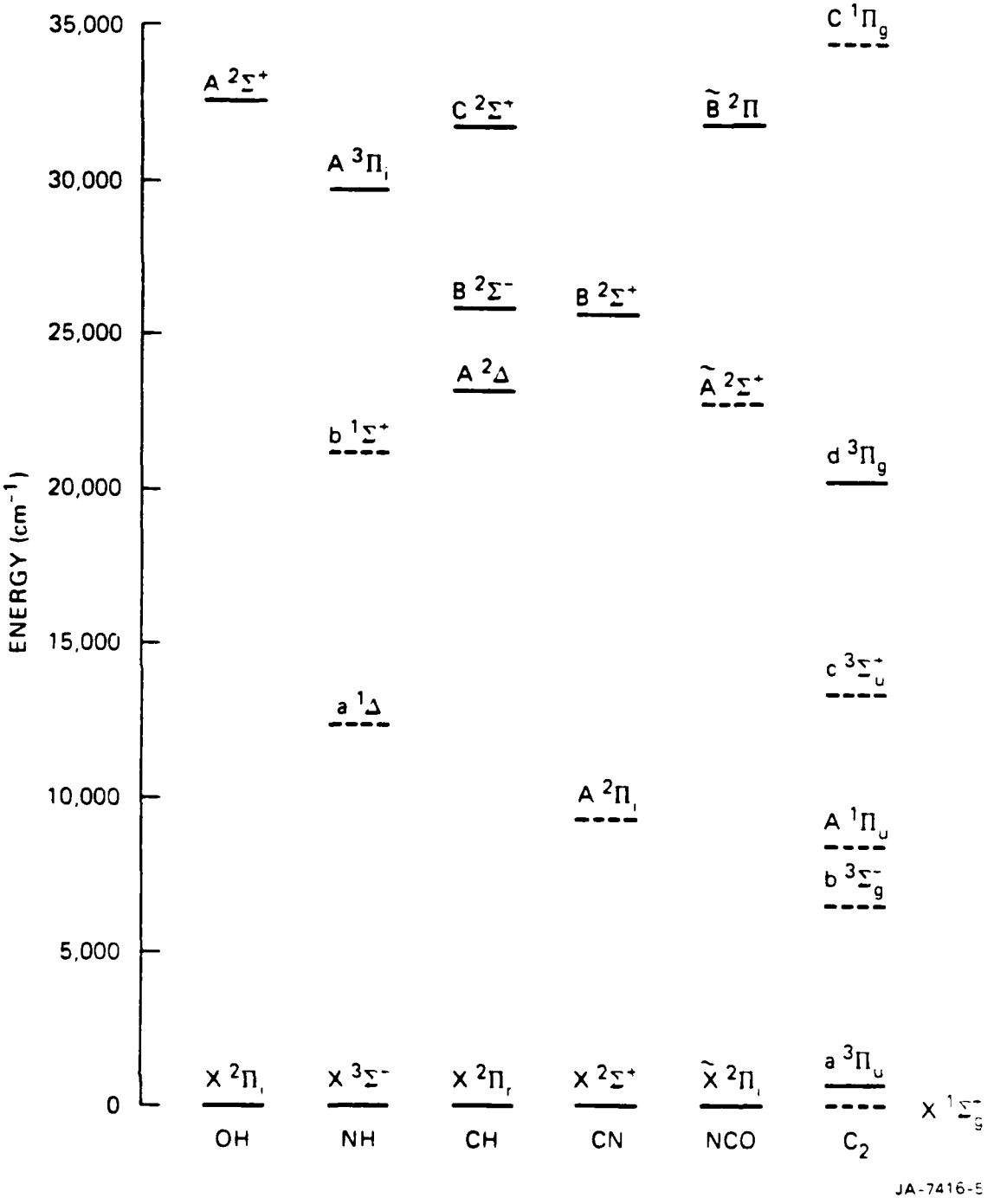
35,000
30,000
25,000
20,000
15,000
10,000
5,000
0
ENERGY (cm⁻¹)
A ²Σ⁺
A ³Π
b ¹Σ⁺
a ¹Δ
X ²Π
X ³Σ⁻
X ²Π
C ²Σ⁺
B ²Σ⁻
A ²Δ
X ²Σ⁺
B ²Σ⁺
A ²Π
X̃ ²Π
Ã ²Σ⁺
B̃ ²Π
C ¹Π
d ³Π
c ³Σ⁺
A ¹Π
b ³Σ⁻
a ³Π
X ¹Σ⁺
OH
NH
CH
CN
NCO
C₂
JA-7416-5

Figure 1

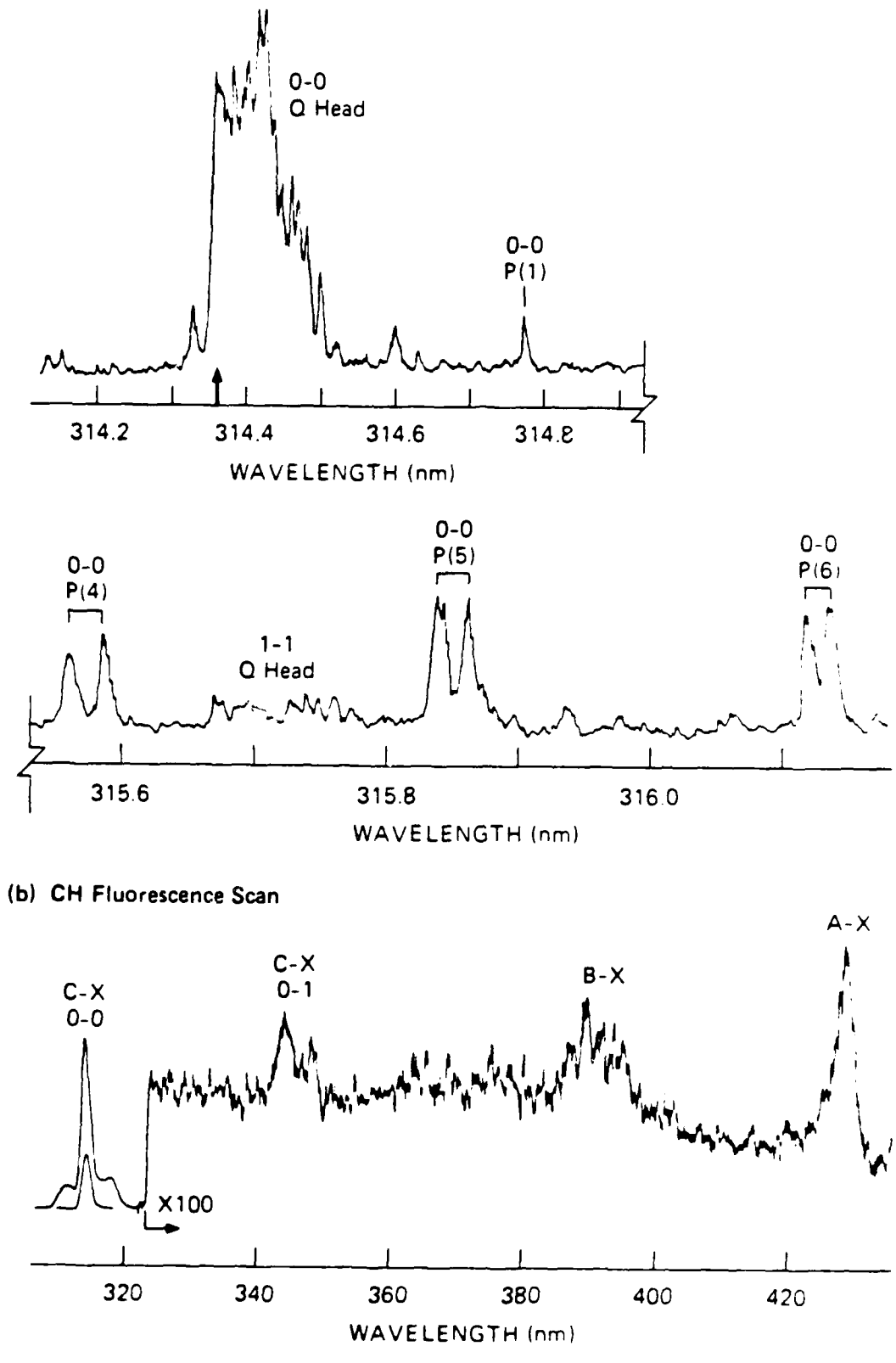
(a) CH Excitation Scans (C-X)
0-0
Q Head
0-0
P(1)
314.2
314.4
314.6
314.8
WAVELENGTH (nm)
0-0
P(4)
1-1
Q Head
0-0
P(5)
0-0
P(6)
315.6
315.8
316.0
WAVELENGTH (nm)
(b) CH Fluorescence Scan
C-X
0-0
C-X
0-1
B-X
A-X
X100
320
340
360
380
400
420
WAVELENGTH (nm)
JA-7416-7

Figure 2

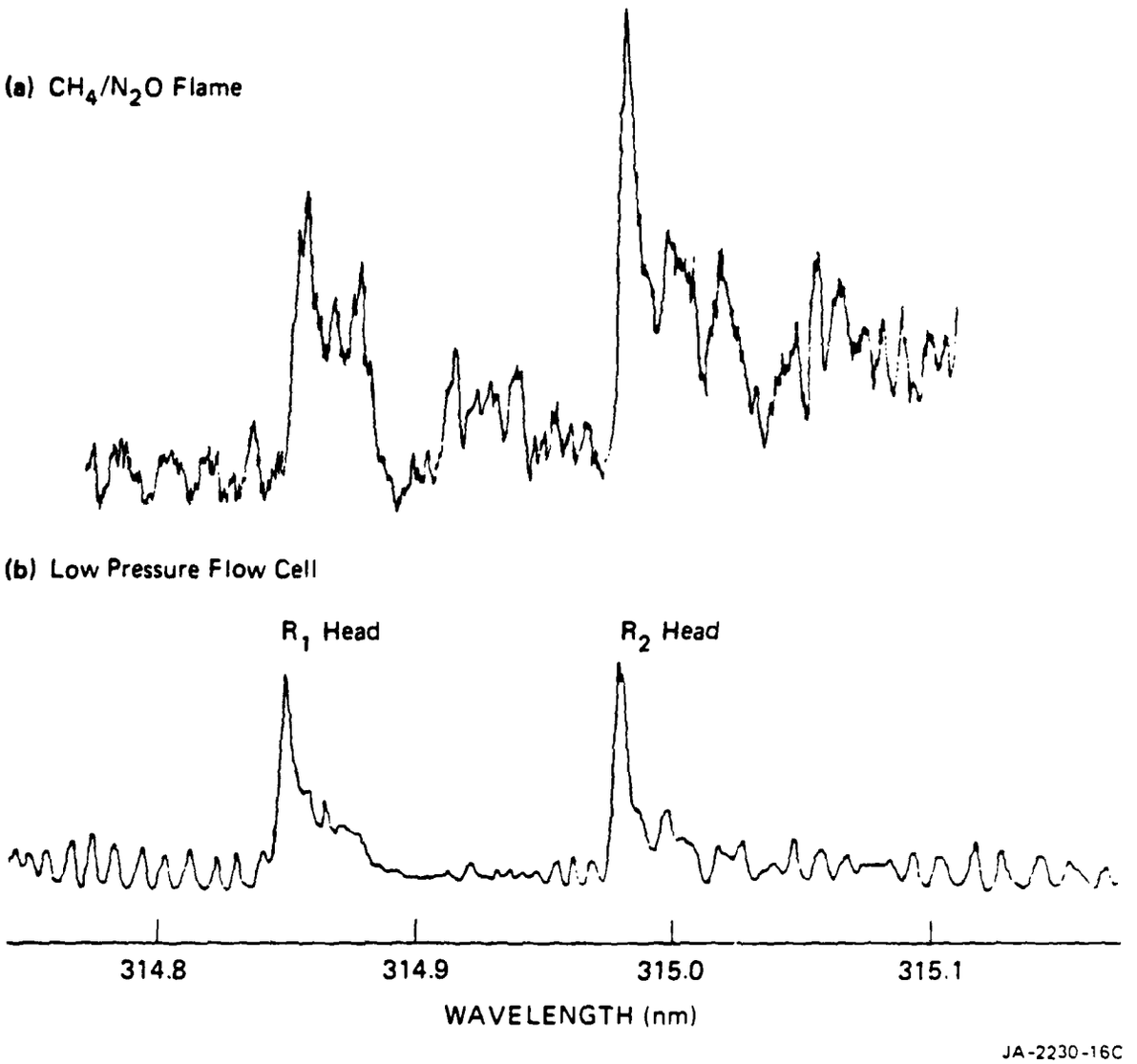
(a) CH_4/N_2O Flame
(b) Low Pressure Flow Cell
R_1 Head
R_2 Head
314.8
314.9
315.0
315.1
WAVELENGTH (nm)
JA-2230-16C

Figure 3

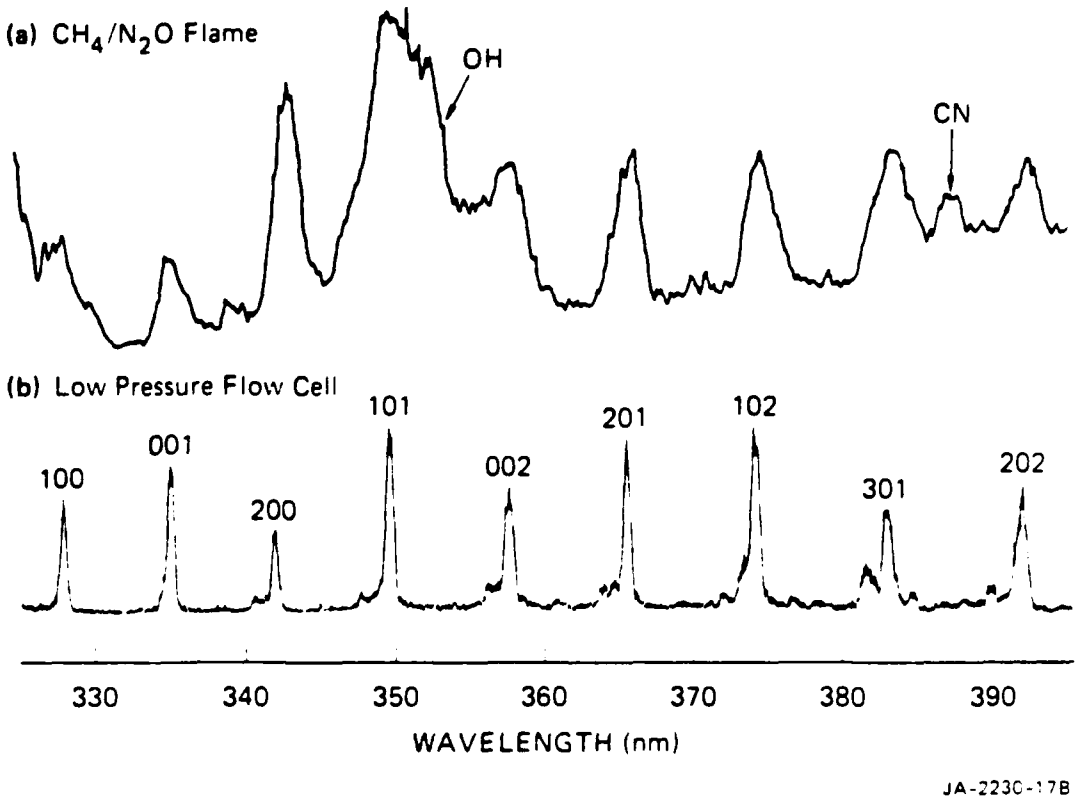
(a) CH_4/N_2O Flame
OH
CN
(b) Low Pressure Flow Cell
100
001
200
101
002
201
102
301
202
330
340
350
360
370
380
390
WAVELENGTH (nm)
JA-2230-17B

Figure 4

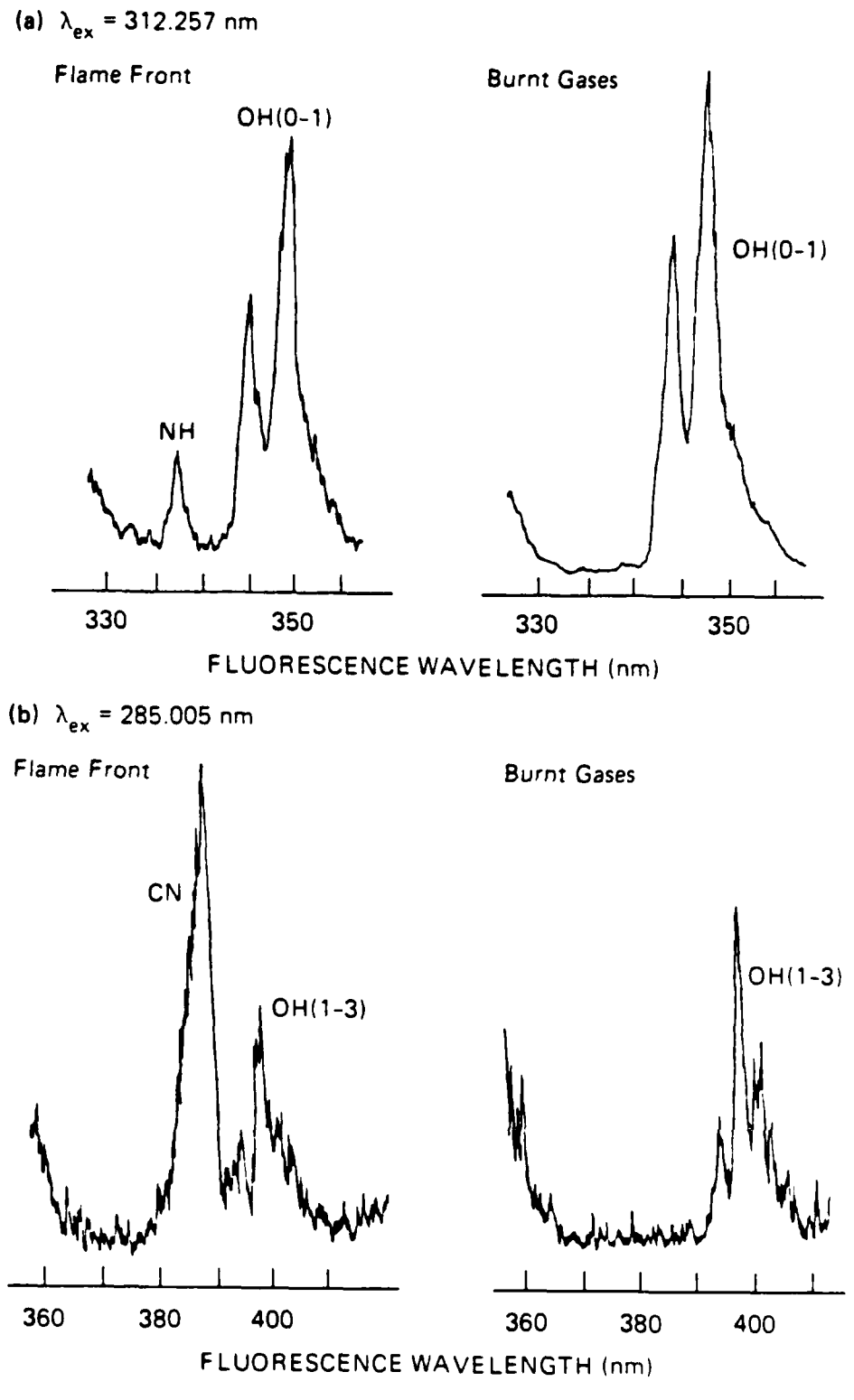
(a) λ_{ex} = 312.257 nm
Flame Front
Burnt Gases
OH(0-1)
NH
OH(0-1)
330
350
330
350
FLUORESCENCE WAVELENGTH (nm)
(b) λ_{ex} = 285.005 nm
Flame Front
Burnt Gases
CN
OH(1-3)
OH(1-3)
360
380
400
360
380
400
FLUORESCENCE WAVELENGTH (nm)
JA-7416-9

Figure 5

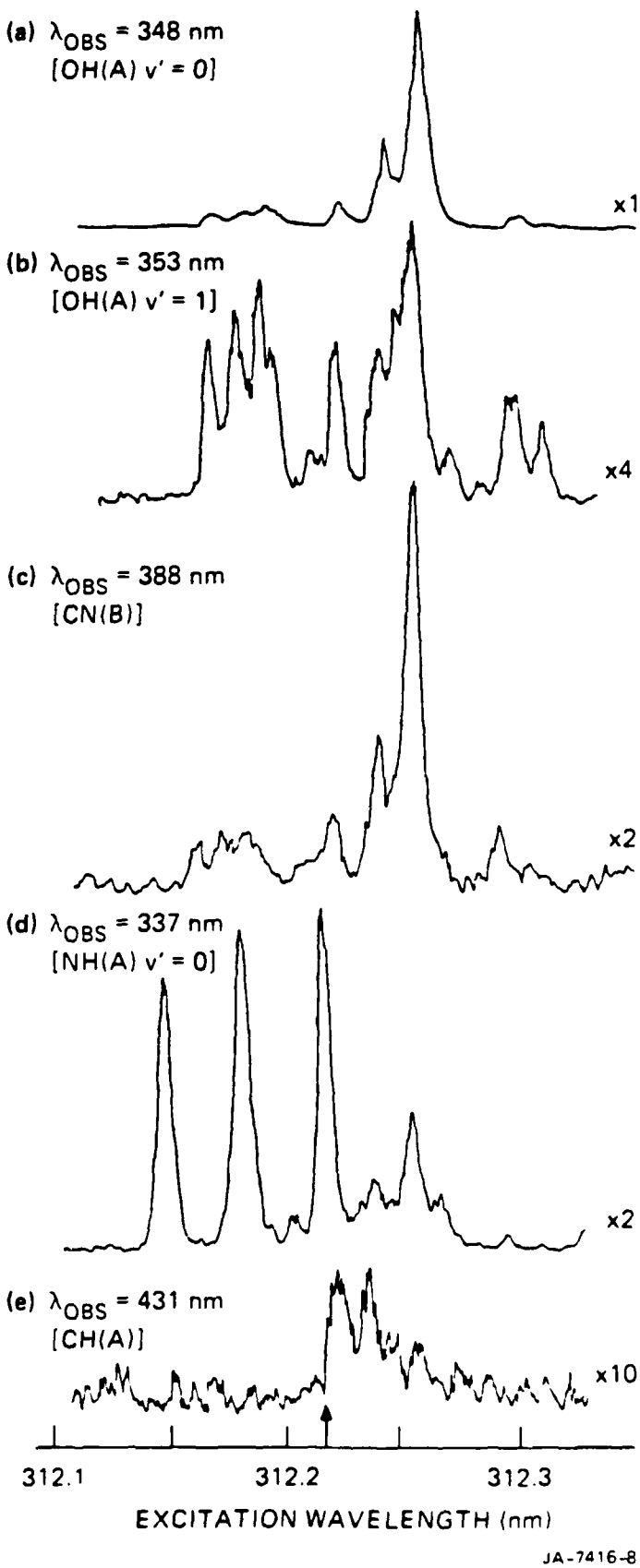
(a) λ_{OBS} = 348 nm
[OH(A) v' = 0]
x1
(b) λ_{OBS} = 353 nm
[OH(A) v' = 1]
x4
(c) λ_{OBS} = 388 nm
[CN(B)]
x2
(d) λ_{OBS} = 337 nm
[NH(A) v' = 0]
x2
(e) λ_{OBS} = 431 nm
[CH(A)]
x10
312.1
312.2
312.3
EXCITATION WAVELENGTH (nm)
JA-7416-8

Figure 6

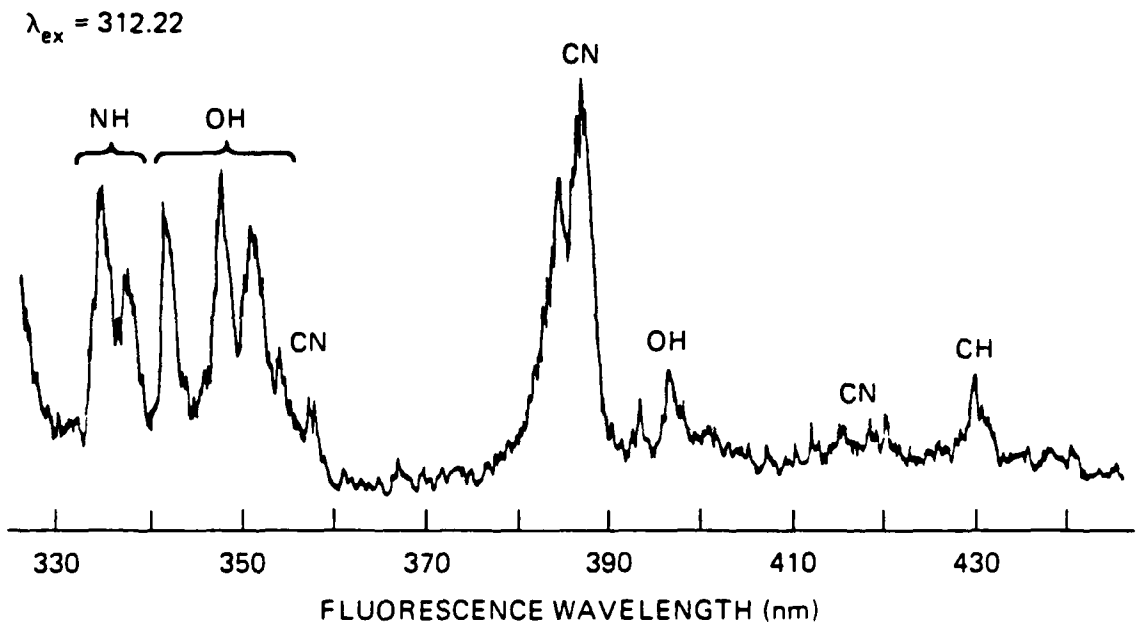
λ_{ex} = 312.22
NH
OH
CN
CN
OH
CN
CH
330
350
370
390
410
430
FLUORESCENCE WAVELENGTH (nm)
JA-7416-6

Figure 7

VI REFERENCES

1. R. A. Beyer and M. A. DeWilde, "Convective Heating of Energetic Materials," Ballistic Research Laboratory Report BRL-TR-2701, December 1985.

2. A. Birk, L. H. Caveny and W. A. Sirignano, Eastern Sectional Meeting of the Combustion Institute, Providence, Rhode Island, November 1983.

3. T. Parr and D. Hanson-Parr, Paer 87-8, Western Sectional Meeting of the Combustion Institute, Provo, Utah, April 1987.

4. M. A. Schroeder, "Critical Analysis of Nitramine Decomposition Data: Product Distributions from HMX and RDX Decomposition," Ballistic Research Laboratory Report BRL-TR-2659, June 1985.

5. R. A. Beyer, Eastern Sectional Meeting of the Combustion Institute, East Hartford, Connecticut, November 1977.

6. B. B. Goshgarian, "The Thermal Decomposition of Cyclotrimethylene-trinitramine (RDX) and Cyclotetramethylenetetranitramine (HMX)," Air Force Rocket Propulsion Laboratory Report AFRPL-TR-78-76, October 1978.

7. R. A. Beyer, M. A. DeWilde and W. J. Scott, Eastern Sectional Meeting of the Combustion Institute, Providence, Rhode Island, November 1983.

8. K. Aron and L. E. Harris, Chem. Phys. Lett. 105, 413 (1984); L. E. Harris, "CARS Spectroscopy of the Reaction Zone of Methane-Nitrous Oxide and RDX Propellant Flames," Armament Research and Development Center Report ARAED-TR-85007, January 1986.

9. T. Parr, in "Combustion Probes for Solid Nitramines," Army Research Office Workshop Report by R. W. Shaw, Jr., S. C. Johnston and G. F. Adams, June 1986.

10. D. F. McMillen, J. R. Barker, K. E. Lewis, P. L. Trevor and D. M. Golden, "Mechanisms of Nitramine Decomposition: Very Low-Pressure Pyrolysis of HMX and Dimethylnitramine," Final Report, SRI Project 5787, June 1979.

11. D. F. McMillen, S. E. Nigenda, A. C. Gonzalez and D. M. Golden, in "Combustion Probes for Solid Nitramines," Army Research Office Workshop Report by R. W. Shaw, Jr., S. C. Johnston and G. F. Adams, June 1986.

12. M. C. Branch, A. Alfarayedhi and M. Sadeqi, Paper 87-20, Western Sectional Meeting of the Combustion Institute, Provo, Utah, April 1987.

13. S. Hulsizer, D. H. Campbell and T. Edwards, Paper 5-6A, Central Sectional Meeting of the Combustion Institute, San Antonio, Texas, April 1985; D. P. Weaver and D. H. Campbell, private communication, November 1986.

14. M. A. DeWilde, L. J. Decker and D. R. Crosley, unpublished results, 1979.

15. D. R. Crosley, Opt. Engr. 20, 511 (1981).

16. J. A. Vanderhoff, W. R. Anderson, A. J. Kotlar and R. A. Beyer, Twentieth Symposium (International) on Combustion, The Combustion Institute, Pittsburgh, 1984, p. 1299.

17. B. J. Sullivan, G. P. Smith and D. R. Crosley, Chem. Phys. Lett. 96, 307 (1983).

18. W. K. Bischel, B. E. Perry and D. R. Crosley, Chem. Phys. Lett. 82, 85 (1981); Appl. Opt. 21, 1419 (1982).

19. A. W. Miziolek, B. E. Forch and R. C. Sausa, Amer. Inst. Phys. Conf. Proc. 146, 628 (1986).

20. P. W. Fairchild, G. P. Smith and D. R. Crosley, J. Chem. Phys. 79, 1795 (1983).

21. C. W. Larson and D. M. Golden, Paper 83-70, Western Sectional Meeting of the Combustion Institute, Los Angeles, California, October 1983.

22. R. A. Copeland, D. R. Crosley and G. P. Smith, Twentieth Symposium (International) on Combustion, The Combustion Institute, Pittsburgh, 1984, p. 1195.

23. N. L. Garland and D. R. Crosley, J. Quant. Spectros. Radiat. Transfer 31, 591 (1985).

24. R. A. Copeland and D. R. Crosley, Can. J. Phys. 62, 1488 (1984).

25. J. B. Jeffries, R. A. Copeland, G. P. Smith and D. R. Crosley, Twenty-First Symposium (International) on Combustion, The Combustion Institute, Pittsburgh, 1987, in press.

26. R. A. Copeland, J. B. Jeffries, A. P. Hickman and D. R. Crosley, J. Chem. Phys. 86, 4876 (1987).

27. G. P. Smith, R. A. Copeland and D. R. Crosley, Third International Laser Science Conference, Atlantic City, New Jersey, November 1987; to be published.

28. C. W. Larson, R. Patrick and D. M. Golden, Comb. Flame 58, 229 (1984).

29. D. M. Golden and C. W. Larson, Twentieth Symposium (International) on Combustion, The Combustion Institute, Pittsburgh, 1984, p. 595.

END

11-87

DTIC